

Synthesis and Reactivity of a Bulky Indium Anion

by

Sophie Grace Unsworth

Supervised by Dr Mathew D. Anker

A thesis submitted to the Victoria University of Wellington in partial fulfilment
of the requirements for the degree of Master of Science in Chemistry

Te Herenga Waka — Victoria University of Wellington

2024



VICTORIA UNIVERSITY OF
WELLINGTON
TE HERENGA WAKA

Acknowledgements

Mat, as my supervisor, your dedication to inorganic chemistry and commitment to my growth have been exceptional. I'm grateful for the significant time we've spent together, both inside and outside the lab. Your guidance and support throughout my academic journey has been invaluable. You've imparted knowledge with clarity, deepened my understanding, and fuelled my passion for chemistry. Your patience and willingness to answer my questions have shaped my scientific thinking and experimental skills. Your encouragement and constructive feedback have motivated me to strive for excellence. I appreciate the nurturing environment you've created, allowing me to flourish as a chemist. Working alongside you has been an honour, and I'm forever grateful for your contributions to my growth.

Thank you to the members of the Anker and Fulton–Cole research groups. Your assistance and genuine friendship have made a significant impact on my overall experience. Building such strong connections with individuals who share similar research goals has made this experience all that more enjoyable. I am grateful for the camaraderie we have built and the memories we have created together. Thank you all for being a part of this journey.

Jan, I wanted to express my sincere gratitude for the invaluable assistance you have provided me with during our NMR experiments. I am truly grateful for the time and effort you have invested in supporting our work.

Scott, I want to extend my gratitude for your exceptional expertise in modelling the complex X-ray data we have produced over the last two years. Your commitment to solving our X-ray structures have played a crucial role not only in this thesis but in many others too.

I would like to take this opportunity to express my appreciation to the mentors who have significantly influenced my passion for chemistry throughout my academic journey. Starting from my high school teachers to the esteemed academics at Victoria University of Wellington, I am sincerely grateful for your unwavering guidance, attention, and help throughout the years.

I would like to express my gratitude to the funding sources that have played a pivotal role in facilitating the research presented in this thesis. I extend my appreciation to Victoria

University of Wellington for granting me the invaluable opportunity to pursue my undergraduate and master's studies. Additionally, I am immensely thankful to the Curtis–Gordon Scholarship Committee for their financial support.

To my family and friends, I want to express my gratitude for the continuous inspiration you have provided me throughout my life, always encouraging me to pursue my goals. The invaluable attributes you have instilled in me are now an integral part of my daily life. Despite the complexities of my research that may have been challenging to grasp, your unwavering support has remained. Your genuine interest in my pursuits, celebrating both my triumphs and misadventures, has meant the world to me.

Abstract

The research presented in this master's thesis focuses on the synthesis and reactivity of *N*-heterocyclic indium anions – indyl anions, specifically $[\text{In}(\text{xNON}^{\text{TCHP}})]^-$, (xNON = 4,5-bis(2,6-diisopropylanilido)-2,7-di-*tert*-butyl-9,9-dimethylxanthene, TCHP = 2,4,6-tricyclohexyl phenyl). These indyl anions, which feature the xNON ligand with *N*-substituents bearing the TCHP group are charge balanced with a potassium cation. The study of anionic indium(I) complexes has gained significant attention in the past five years due to their nucleophilic properties and versatile reactivity patterns. This research contributes to the rapidly developing field of anionic indium chemistry, exploring the synthesis and reactivity of new indyl anions.

Chapter One provides a literature review on the synthesis of the first low-valent group 13 complexes, followed by a detailed review of the first anionic group 13 complexes with a considerable focus on the heavier analogues. We discuss the synthetic strategies employed to obtain these anionic complexes, highlighting the ligand systems and reducing agents used in their preparation. The review also discusses their structural features, including bond lengths, angles, and coordination geometries, as determined by single crystal X-ray crystallography.

Chapter Two broadens the scope of the xNON ligand system, which has been previously synthesised using Dipp *N*-substituents, by introducing a bulky TCHP substituent. The aim is to enhance the steric properties of the ligand and investigate the impact they will have on the properties of the resulting indyl anion complexes.

Chapter Three expands the existing literature on the chemistry of indium(I) complexes by introducing a new bulky indyl anion. This chapter presents three different synthetic routes that have been developed to obtain three distinct TCHP indyl anions. We discuss how these different indyl anions may differ in stability and reactivity compared to previous literature examples.

Chapter Four focuses on the reactivity studies conducted on the three synthesised TCHP indyl anions. This chapter aims to investigate the reactivity patterns of the indyl anions and evaluate the success of different reactions attempted, as well as any unexpected or interesting findings. The limitations and challenges encountered during the reactivity studies are addressed, highlighting the reactions that did not yield the desired outcomes. The reasons for unsuccessful reactions are analysed, and possible strategies for addressing these challenges in the future are discussed.

List of Abbreviations

2,2,2-crypt	N[(CH ₂ CH ₂ O) ₂ CH ₂ CH ₂] ₃ N
2D	2 Dimensional
18-c-6	18-crown-6
δ	Chemical shift
Å	Angstrom
Ar*	((4-methyl-2,6-phenylene)bis(methanetriyl))tetrabenzene
BDI	β-Diketiminate – CH[C(CH ₃)NH] ₂
C ₆ D ₆	Deuterated benzene
CDP	Contact dimeric pair
Cp	Cyclopentadienyl
Cp*	Pentamethyl cyclopentadiene
Cp ^{4*}	1,2,3,4-tetramethyl cyclopentadiene
DCM	Dichloromethane
DEPhos	(Oxydi-2,1-phenylene)bis(diphenylphosphine)
DMP-NC	2,6-dimethylphenyl isocyanide
Dipp	2,6-Diisopropylphenyl – 2,6-(ⁱ Pr) ₂ C ₆ H ₃
Et ₂ O	Diethyl ether
HMBC	Heteronuclear Multiple Bond Correlation
HMDS	Bis(trimethylsilyl)amide – N[Si(CH ₃) ₃] ₂
HSQC	Heteronuclear Single Quantum Coherence Spectroscopy
ⁱ Pr	<i>iso</i> Propyl – CH(CH ₃) ₂
KC ₈	Potassium graphite
IR	Infrared
MALDI TOF	Matrix-Assisted Laser Desorption/Ionization–Time of Flight

Me	Methyl	– CH ₃
Mes	2,4,6-Trimethylphenyl	– 2,4,6-(CH ₃) ₃ C ₆ H ₂
MIP	Monomeric ion pair	
NHC	<i>N</i> -heterocyclic carbene	
NMR	Nuclear magnetic resonance	
NON	bis(amidodimethyl)disiloxane	– [O(SiMe ₂ N) ₂] ²⁻
RT	Room temperature	
ppm	Parts per million	
SIP	Separated ion pair	
^t Bu	<i>Tert</i> Butyl	– C(CH ₃) ₃
TCHP	2,4,6-tricyclohexyl phenyl	
Ter	[2,6-trip ₂ -3,5- ⁱ Pr ₂ C ₆ H] ⁻	
THF	Tetrahydrofuran	
Tol	Toluene	
xNON	4,5-bis(2,6-diisopropylanilido)-2,7-di- <i>tert</i> -butyl-9,9-dimethylxanthene	

Table of Contents

Acknowledgements	II
Abstract	IV
List of Abbreviations.....	V
Chapter 1. Introduction	1
1.1 Group 13 Elements	1
1.2 Neutral Group 13 (I) Complexes	3
1.3 <i>N</i> -Heterocyclic Carbenes.....	6
1.4 Anionic <i>N</i> -Heterocyclic Group 13 Analogues	9
1.4.1 The Gallyl Anion.....	9
1.4.2 The Boryl Anion.....	11
1.4.3 The Indyl Anion.....	12
1.4.4 The Aluminyl Anion.....	17
1.4.5 Reactivity of Aluminyl Anions.....	21
1.5 Overview of Literature Review	25
1.6 Project Outline and Research Aims	26
Chapter 2. Ligand Development	27
2.1 Introduction	27
2.2 Ligand Selection	28
2.3 Synthesis of TCHP Amine	28
2.4 $x\text{NON}^{\text{TCHP}}$ Ligand Synthesis	29
Chapter 3. Synthesis of $x\text{NON}^{\text{TCHP}}$ Indyl Anions.....	33
3.1 Synthesis of $(x\text{NON}^{\text{TCHP}})\text{K}_2$ (38).....	33
3.2 Synthesis of $(x\text{NON}^{\text{TCHP}})$ Indyl Anions	34
3.2.1 Synthesis of $(x\text{NON}^{\text{TCHP}})\text{InK}(\text{Et}_2\text{O})(\text{THF})_2$ (40).....	34
3.2.2 Synthesis of $(x\text{NON}^{\text{TCHP}})\text{InK}(\text{Cp}^{4*})\text{K}$ (46).....	39
3.2.3 Synthesis of $(x\text{NON}^{\text{TCHP}})\text{InK}(\text{tol})$ (47).....	42
3.2.4 Comparison of $(x\text{NON}^{\text{TCHP}})$ Indyl Anions	44
Chapter 4. Reactivity of $(x\text{NON}^{\text{TCHP}})$ Indyl Anions	46
4.1 Stability of $(x\text{NON}^{\text{TCHP}})\text{InK}(\text{Et}_2\text{O})_2(\text{THF})_2$ (40)	46
4.2 Reactions With 18-crown-6	47
4.3 Initial Reactivity Studies of the Indyl Anion.....	54
4.3.1 Reactivity With SnCl_2	54
4.3.2 Reactivity With 2,6-dimethylphenyl Isocyanide	59
4.4 Unsuccessful Reactivity of $x\text{NON}^{\text{TCHP}}$ Indyl Anions.....	61
4.5 Conclusion and Future Work.....	64

Chapter 5. Experimental.....	66
5.1 General Experimental	66
5.2 Characterisation Techniques.....	66
5.2.1 Nuclear Magnetic Resonance Spectroscopy (NMR).....	66
5.2.2 Single Crystal X-Ray Diffraction	67
5.3 Synthetic Procedures	68
5.3.1 Preparation of $(x\text{NON}^{\text{TCHP}})\text{H}_2$, 37	68
5.3.2 Preparation of $(x\text{NON}^{\text{TCHP}})\text{K}_2$, 38	69
5.3.3 Preparation of $(x\text{NON}^{\text{TCHP}})\text{InI}_2\text{K}$, 39	69
5.3.4 Preparation of $(x\text{NON}^{\text{TCHP}})\text{InK}(\text{Et}_2\text{O})_2(\text{THF})_2$, 40	70
5.3.5 Preparation of $(x\text{NON}^{\text{TCHP}})\text{InK}(\text{Cp}^{4*})\text{K}$, 46	70
5.3.6 Preparation of $(x\text{NON}^{\text{TCHP}})\text{InK}(\text{Tol})$, 47	71
5.3.7 Preparation of $(x\text{NON}^{\text{TCHP}})\text{K}(18\text{-c-6})\text{K}$, 48	71
5.3.8 Preparation of $(x\text{NON}^{\text{TCHP}})\text{InI}_2(18\text{-c-6})\text{K}$, 49	72
5.3.9 Preparation of $(x\text{NON}^{\text{TCHP}})\text{In}(18\text{-c-6})\text{K}$, 50.....	72
5.3.10 Preparation of $[(x\text{NON}^{\text{TCHP}})\text{InCl}_2\text{K}]_2$, 52	73
5.3.11 Preparation of $(x\text{NON}^{\text{TCHP}})\text{InCl}_2\text{K}(\text{THF})_4$, 53	73
5.3.12 Preparation of $(x\text{NON}^{\text{TCHP}})\text{InI}(\text{DMP-NC})$, 55	73
References.....	75

Chapter 1. Introduction

1.1 Group 13 Elements

The group 13 elements are located within the *p*-block main-group elements. These elements include boron, aluminium, gallium, indium, and thallium (Table 1). This group was the first group discovered in the periodic table to contain both metals and non-metals.¹ Boron is a metalloid, and therefore, it has different properties to the rest of the metallic elements in group 13. Research into the group 13 elements commenced in the 1800s after each element was identified. Initially research into the group 13 elements was hindered since these elements were not readily found in their free state, apart from aluminium. While less frequent, boron can also be found in a variety of minerals called borates. Elemental boron and aluminium were initially obtained by reducing $\text{Na}_2\text{O} \cdot 2\text{B}_2\text{O} \cdot 5\text{H}_2\text{O}$ (borax) and AlCl_3 respectively, with a group 1 metal.²⁻

3

Table 1. Group 13 Elements.

Element	Discovered date	Obtained	State
B	1808	Reducing borax	Dark amorphous powder
Al	1825	Reducing AlCl_3	Soft, silvery-white metal
Ga	1875	Spectrum of zinc blende ore	Soft, silvery-white metal
In	1863	Spectrum of sphalerite	Soft, silvery metal
Tl	1861	Spectrum of uranium	Soft, silvery-white metal

Aluminium, being the most abundant metal in the earth's crust, can be found in numerous minerals, such as alunite and aluminite.^{4,5} The versatile nature of aluminium and its numerous chemical derivatives make it valuable in organic and organometallic synthesis,⁶ due to its wide range of applications including catalysis, materials science, coordination chemistry, and medicinal chemicals.^{7,8} The reactivity and properties of aluminium compounds have been explored to develop new synthetic methodologies and understand their potential applications in different fields. Gallium and indium, in comparison, are impurities in other minerals and therefore they are less abundant.⁹ In 1860s, indium and thallium were discovered following the invention of the spectroscope, a device used to measure the spectrum of light. Thallium was discovered through its presence in the spectrum of uranium. Utilising the spectroscope, Reich

and Richter observed distinct lines in the spectra, among these observations was the identification of a violet line, which is associated with indium.¹⁰ Acknowledging that thallium is classified as a cumulative poison capable of causing detrimental health effects and degenerative changes in multiple organs is crucial.^{11, 12} Therefore, comparably fewer reports on the reaction chemistry of its organometallic complexes have been conducted compared to the lighter group 13 elements, and it will not be discussed further. Finally, gallium was identified spectroscopically in 1875 from a new violet line present in a zinc blend of sphalerite.¹³

Since the 19th century, extensive research has been conducted to understand the properties and reactivity of group 13 compounds.^{14, 15} These elements possess three valence electrons and display the flexibility to exist in either the +3 or +1 oxidation states (Table 2). Boron exhibits unique properties due to its small size and electron configuration ([He]2s²2p¹). As a metalloid, it shares some potential applications with carbon, such as in the development of superhard materials and biological compounds.^{16, 17} However, despite these similarities, boron displays a diverse range of structural configurations and when combined with other materials, it exhibits further structural changes. This unpredictability offers several applications, such as in 2D heterostructures or utilising its metallic character for building components.¹⁸

Table 2. Oxidation states of group 13.

Group	13
General electronic configuration	ns ² np ¹
Group oxidation state	+3
Other oxidation state	+1

The remaining group 13 elements from aluminium to indium exhibit metallic properties and demonstrate consistent trends for several characteristics, including boiling point, lattice energy, conductivity, as well as others.¹⁹ These similarities among aluminium, gallium and indium set them apart from boron. Descending group 13 from boron to indium, the valance s electrons experience an increase in nucleus attraction, leading to diminished reactivity and reduced bonding for these valance s electrons. Therefore, the heavier analogues of group 13 tend to prefer the +1 oxidation state – this is referred to as the inert pair effect.²⁰ The chemistry of group 13 elements in this low-valent +1 oxidation state has attracted significant attention in recent years, leading to the rapid development in the understanding of the reactivity of these complexes both experimentally and theoretically.²¹⁻²³ Compounds featuring low oxidation

states often display unique structural characteristics, bonding modes and chemical behaviours compared to compounds in their more common higher oxidation state.²⁴ These low oxidation state compounds often offer intriguing opportunities for exploring novel bonding motifs, unusual coordination environments, and unconventional chemical transformations. The study of compounds in the lower oxidation states of group 13 elements contributes to a deeper understanding of the fundamental principles governing element–element interactions and broadens the scope of main–group chemistry, which could have applications for nanosized materials, catalysis, and small–molecule activation.^{25–27}

1.2 Neutral Group 13 (I) Complexes

To achieve a neutral complex with the group 13 metal in the +1 oxidation state, a monoanionic ligand system must be utilised. This ligand system must possess a –1 charge, which effectively balances the +1 charge on the metal centre, resulting in a neutral complex. Experimental and Density Functional Theory (DFT) calculations have been conducted on the reactions of group 13 elements with multidentate ligands, which have highlighted these requirements for stabilisation and how ligand environments can influence reactivity.²⁸ These ligand systems play a crucial role in stabilising the metal centre and enabling further reactivity. Despite boron’s classification as a metalloid, displaying both metallic and non–metallic properties, there are yet to be any low–valent neutral B(I) complexes reported to date.

Among the heavier group 13 elements, examples of monomeric M^I ($M^I = \text{Al, Ga or In}$) carbenoid compounds have been reported (Figure 1). While carbenoid compounds of aluminium and gallium have been reported for all three ligands, namely MCp^* ($\text{Cp}^* = \text{pentamethyl cyclopentadiene}$), $\text{M}(\text{Ter})$ ($\text{Ter} = [2,6\text{-trip}_2\text{-}3,5\text{-}^i\text{Pr}_2\text{C}_6\text{H}]^-$, $\text{trip} = 2,4,6\text{-}^i\text{Pr}_3\text{C}_6\text{H}_2$, $^i\text{Pr} = \text{isopropyl}$) and $\text{M}(\text{BDI}^{\text{Dipp}})$ ($\text{BDI}^{\text{Dipp}} = \text{CH}[\text{C}(\text{CH}_3)\text{N-Dipp}]_2$, $\text{Dipp} = 2,6\text{-}^i\text{Pr}_2\text{C}_6\text{H}_3$), neutral indium(I) has only been reported for MCp^* and $\text{M}(\text{BDI}^{\text{Dipp}})$ complexes.

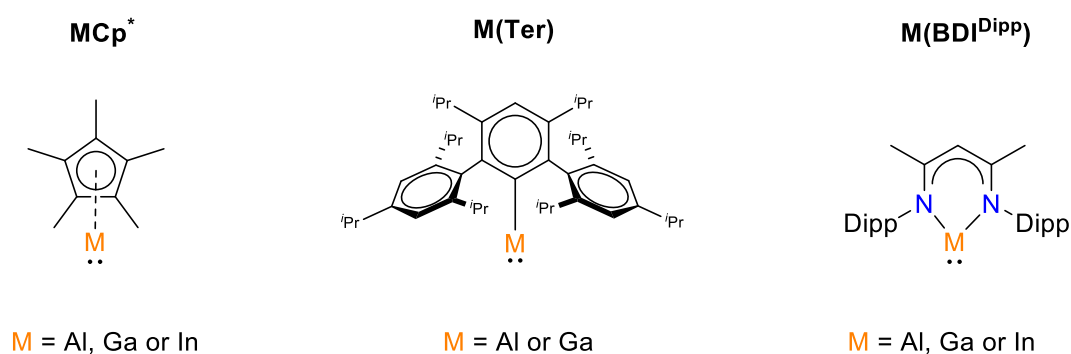
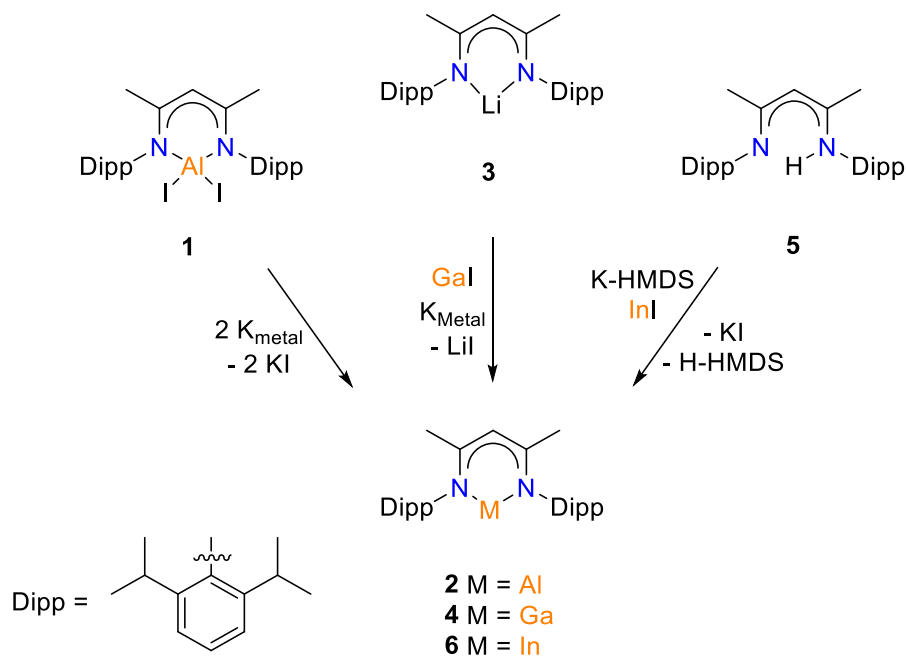


Figure 1. Low–valent neutral group 13 complexes. ^iPr groups have been decreased in size for clarity.

Crystallographic data reveals that the MCp^* complexes of aluminium, gallium and indium are found in varying cluster arrangements. The aluminium complex (AlCp^*) forms a regular tetrahedron cluster, with four aluminium atoms,²⁹ GaCp^* is present in a hexameric cluster with six Ga^{1+} ions and six Cp^* ligands within the cluster,³⁰ while InCp^* adopts an octahedral cluster conformation.³¹ A significant advancement in low-valent group 13 chemistry came with the synthesis of $\text{Al}(\text{Ter})$, a monomeric alkyl-based Al^{I} carbenoid complex that effectively prevents dimerisation or tetramerisation of the metal centre.³² The $\text{Ga}(\text{Ter})$ complex does dimerise, which limited its impact as a solely monomeric alkyl based Ga^{I} carbenoid complex.³³ In contrast, the $\text{M}(\text{BDI}^{\text{Dipp}})$ systems offers a bidentate ligand scaffold that provides excellent support for the group 13(I) metal centre. This ligand framework has been extensively studied for group 13 metals, primarily focussing on aluminium through to indium (the thallium analogue has been synthesised but will not be discussed).³⁴ The BDI^{Dipp} complexes utilise a rigid bidentate ligand system that takes advantage of the ambiphilic reactivity of group 13 elements. These complexes utilise a nucleophilic lone-pair and vacant p -orbital on the metal centre, which allow for diverse coordination modes. The BDI heterocycle system was initially utilised for the synthesis and characterisation of the first N -heterocyclic monomeric $\text{Al}(\text{I})$ compound. This synthesis was conducted by Cui *et al*, where they found that the reaction of $(\text{BDI}^{\text{Dipp}})\text{AlI}_2$ (**1**), with two equivalents of potassium metal, formed the monomeric $\text{Al}(\text{I})$ compound, **2**, $(\text{BDI}^{\text{Dipp}})\text{Al}$ (Scheme 1).³⁵



Scheme 1. Synthesis of low-valent neutral group 13 complexes.

A single crystal X-ray crystallographic experiment was used to analyse **2** for structural characterisation, which demonstrated the average bond distance between Al–N in compound **2** is 1.957(2) Å. The increased bond length between Al–N in compound **2** compared to Al(III) compounds reported, indicates that **2** is an Al(I) complex with a higher degree of covalency in the Al–N bond.³⁶ The larger ionic radii of Al(I) compared to Al(III) accounts for the longer Al–N bond distance in **2**. The N–Al–N bond angle was determined to be 89.86°, suggesting the 3p orbitals of the aluminium centre are involved in the bonding with the two *N*-substituents in the ligand system. Additionally, the data obtained from the single crystal X-ray crystallographic experiment confirmed that the heterocyclic backbone in **2** is planar, which is consistent with the characteristics of the related *N*-heterocyclic carbenes (NHCs).³⁷ While three- and four-coordinate aluminium complexes have been explored and synthesised before, the successful isolation of a stable two-coordinate aluminium(I) complex is a landmark achievement that opens new avenues for further research to explore the reactivity of neutral Al(I) complexes and find potential applications.³⁸

Following the report on the first neutral *N*-heterocyclic Al(I) complex (**2**), in 2000 Power successfully synthesised the first neutral *N*-heterocyclic Ga(I) complex.³⁹ This synthesis involved the addition of (BDI^{Dipp})Li (**3**), GaI and K_{metal} resulting in the formation of yellow crystals of (BDI^{Dipp})Ga, **4** (Scheme 1). Utilising UV–Vis, IR and both ¹H and ¹³C{¹H} NMR spectroscopies and crystallography, compound **4**'s molecular structure and functional groups were investigated. The single crystal X-ray crystallographic data of compound **4** reveals the BDI backbone to be planar, and the Dipp substituents attached to the BDI backbone are oriented at angles of 88.2° and 89.2°, compared to the plane of the BDI backbone. This arrangement of the substituents contributes to the overall three-dimensional structure of **4**. The bond lengths of Ga–N in **4** are reported as 2.0528(14) and 2.0560(13) Å. These bond lengths are slightly longer than the corresponding aluminium compound, **2**, mentioned earlier. The difference in bond lengths arises from the different ionic radii for the two compared metals, aluminium, and gallium. Furthermore, the bond angle of N–Ga–N in compound **4** is reported as 87.53(5)°, which is a smaller angle than the aluminium analogue. This further confirms the difference in structural features of gallium and aluminium. Compound **4** has undergone extensive reactivity studies since its initial synthesis, forming metal–metal bonds with various metals, Ga–N double bonds with azide derivatives, and reacting with small gas molecules like CO.^{40–42}

Descending group 13, Hill and Hitchcock accomplished the synthesis of the first neutral *N*-heterocyclic In(I) complex, demonstrating a novel two-coordinate neutral In(I) analogue through a ‘one pot’ reaction.⁴³ This was achieved *via* the combination of (BDI^{Dipp})H (**5**), InI and K-HMDS (K-HMDS = potassium bis(trimethylsilyl)amide) (Scheme 1). (BDI^{Dipp})H is deprotonated by K-HMDS, which then reacts with InI to give In(BDI^{Dipp}) (**6**) and KI. By conducting the reaction in a single step, a neutral two-coordinate indium(I) complex **6**, was formed. Both ¹H and ¹³C{¹H} NMR spectroscopy, as well as single crystal X-ray crystallography and elemental analysis, have been used to characterise **6**. The single crystal X-ray crystallography experiment analysis revealed that the heterocycle in **6** has an almost planar ring structure, comparable to the lighter group 13 analogues. The In–N bond lengths measured are 2.268(3) and 2.276(3) Å, which are longer in contrast to **2** and **4**. Additionally, the bond angle of N–In–N is 81.12°, indicating a more acute angle compared to the lighter analogues. The presence of the BDI ligand in **6** stabilises the In(I) centre against disproportionation to In(0) and In(III). These literature examples of the first neutral group 13 low-valent *N*-heterocyclic complexes show that the Al(I), Ga(I) and In(I) derivatives are all isostructural to each other, suggesting that they share similar structural features and bonding characteristics. Due to the *N*-heterocyclic ligand used to support these group 13(I) complexes and the lone pair of electrons located on the group 13 centre, comparisons have been drawn between these complexes and *N*-heterocyclic carbenes (NHCs).⁴⁴ Therefore I will briefly cover the characteristics of carbenes.

1.3 *N*-Heterocyclic Carbenes

Carbenes are divalent neutral carbon compounds with six valance electrons located on the carbon atom.⁴⁵ In the early 1990s, a pioneering study of carbenes was conducted and published on the first stable crystalline *N*-heterocyclic carbene (NHC) by Arduengo *et al.*³⁷ After this breakthrough, many publications followed which report on the synthesis and analysis of other new NHCs. Compared to traditional carbenes, NHCs are electron-rich due to their resonance structures (Figure 2).

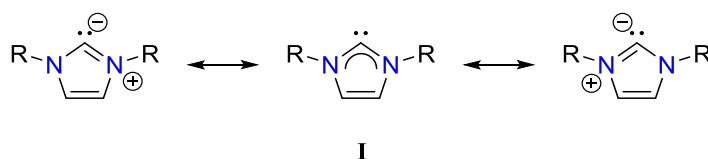


Figure 2. Resonance configurations of a general *N*-heterocyclic carbene (NHC).

The carbenic carbon of NHCs exist in the singlet state, distinguished by the presence of both s and p characters in the highest occupied molecular orbital (HOMO) and the lowest unoccupied molecular orbital (LUMO). The substituents surrounding the divalent carbon centre can play a crucial role in stabilising the carbene species by influencing the σ - π energy gap (also referred to as the HOMO-LUMO energy gap). Through both electronic and steric effects, these substituents can exert control over the ground-state multiplicity of the carbene.⁴⁶ Electronic effects can alter the energy levels of the molecular orbitals, affecting the electron distribution and reactivity of the carbene. On the other hand, steric effects can influence the spatial arrangement of the substituents around the carbon centre, impacting the stability and geometry of the carbene. For example, electron-withdrawing substituents increase the σ - π energy gap, favouring a singlet ground state. Bulky substituents induce a bent geometry, also promoting a singlet state, to compensate for the steric bulk. This control over the energy gap allows precise tuning of reactivity and stability in carbene-based systems. Additionally, the carbon atom in the N-C-N backbone of the NHC possesses an unoccupied p_z orbital, which allows for donation of electrons into another p_z orbital of other molecules (Figure 3). This vacant orbital plays a crucial role in the reactivity and coordination chemistry of NHCs, allowing them to form stable complexes.^{47, 48} These combined effects can significantly impact the reactivity and properties of the carbene, making it a versatile and tuneable platform for a variety of chemical applications.⁴⁹

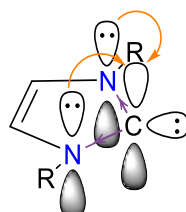


Figure 3. Ground-state electronic structure of imidazol-2-ylidenes. The σ -withdrawing (purple) and π -donating (orange) effects of the nitrogen heteroatoms help to stabilise the singlet carbene structure.

NHCs exhibit partial aromaticity, which contributes to their enhanced stability. This stability arises from the combination of s and p characters in the orbitals of NHCs, granting them their unique electronic properties. However, several stable carbenes do not benefit from aromaticity. In these cases, the significance of π -Delocalisation is relatively minor, especially when compared to the presence of C=C unsaturated carbenes, for example compound **I** (Figure 2).⁵⁰ The chemical difference between **I** and its saturated counterparts cannot be explained in terms of the specific electronic state at the carbene centre. They were instead explained in terms of kinetic barriers associated with electrostatic repulsion between the localised π -electrons of the C=C bond and a potential nucleophilic reaction partner.

The presence of heteroatoms adjacent to the carbene carbon further enhances the electronic stability of the NHCs through inductive and mesomeric effects.⁵¹ These effects exerted by adjacent heteroatoms in NHCs collectively contribute to an increase in the HOMO–LUMO gap, thereby stabilising the singlet ground state. The cyclic nature of NHC compounds also plays a significant role in stabilisation, as the cyclic structure forces the carbonic carbon to adopt a bent geometry, typical of the s and p character. This bent geometry helps maintain the singlet ground state and enhances the stability of NHCs.⁵² Another important factor that contributes to the stabilisation of NHCs is the kinetic effect provided by alkyl or aryl substituents on the nitrogen atoms. These substituents enhance the kinetic stability of the carbene centre by preventing it from undergoing the Wanzlick equilibrium, which leads to the formation of an olefin dimer.⁴⁴ Notably, NHCs are not limited to nitrogen as the two neighbouring atoms to stabilise the carbene centre. NHCs with alternative heteroatoms such as sulphur or oxygen, as well as stable carbenes with only one nitrogen substituent, are available.⁵³

The uses of NHCs can be divided into three main categories: NHCs as organocatalysts, NHCs coordinated to transition metals and NHCs coordinated to *p*-block elements. The evolution of NHCs has progressed beyond solely laboratory interests to become compounds of immense practical importance. NHCs are good ligands for transition metals, which have resulted in diverse functions in some of the most considerable catalytic transformations in the chemical industry.³⁷ The reactivity of the NHCs upon coordination with main group elements and as organocatalysts have also opened new fields of research.^{54, 55}

Neutral low-valent *N*-heterocyclic group 13 complexes serve as important precursors and models for understanding the reactivity and properties of anionic low-valent *N*-heterocyclic group 13 complexes. Furthermore, investigating the reactivity of anionic low-valent *N*-heterocyclic group 13 complexes provide further insights into group 13's chemical behaviour and potential applications (Figure 4).

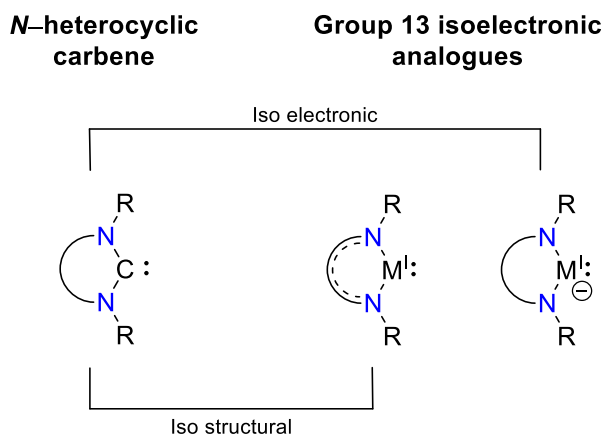


Figure 4. Group 13 isoelectronic analogues relative to an *N*-heterocyclic carbene.

The conventional structure of a *N*-heterocyclic carbene has been expanded through the replacement of the carbenic carbon with a group 13 element. Leading to the formation of isoelectronic analogues that closely resemble *N*-heterocyclic carbene structures. This thesis primarily centres around the examination of the ‘true’ valence isoelectronic analogues of carbenes, depicted on the right side of Figure 4.

1.4 Anionic *N*-Heterocyclic Group 13 Analogues

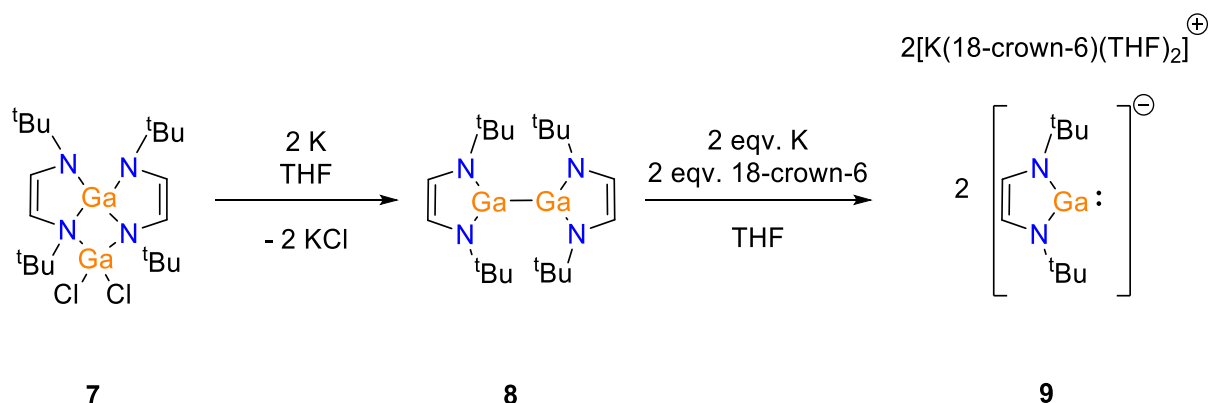
An anionic *N*-heterocyclic complex has a negative charge associated with the complex, that can be stable when the anionic compound can be stabilised by a cationic species.⁵⁶ This cationic species is typically a group 1 metal, (K, Na or Li metal) which has a formal positive charge, in its ionic form. This charge counterbalances the anionic compound to obtain an overall neutral species. Descending group 13 the anionic group 13 (I) complexes are known as the boryl, gallyl, aluminyl and indyl, respectively.

1.4.1 The Gallyl Anion

The enhanced stability demonstrated by *N*-heterocyclic carbene-based systems has prompted the investigation of similar architectures for the synthesis of low-valent group 13 complexes. The gallyl anion, which involves the stabilisation of Ga(I) by an *N*-heterocyclic ligand, was among the first group 13 anions reported.⁵⁷ In 1999 Schmidt, Jockisch and Schmidbaur conducted research on imidazole heterocycles containing group 13, 14 and 15 elements. This work was based on earlier computational studies by Sundermann and Schoeller, who predicted the stability of the carbene Arduengo-type structures, where a divalent centre such as gallium, constitutes the isovalent species.⁵⁸ These species exhibit C_2 symmetrical structures and possess singlet ground states. Schmidt, Jockisch and Schmidbaur provided further insights into the

architecture and synthesis of group 13 anions, particularly the gallyl anion. This work laid the foundation for exploring the properties and reactivity of group 13 anions and their potential applications in several fields of chemistry, such as catalysis, small-molecule activation and UV-photoelectron spectroscopic studies.⁵⁹⁻⁶¹

In their ground breaking research, Schmidt, Jockisch and Schmidbaur successfully synthesised a carbene analogue with a Ga(I) centre (Scheme 2). The synthesis involved the reaction of (chloro)galla-imidazole, $[\text{Ga}(\text{tBuN}=\text{CHCH}=\text{N}^{\text{tBu}})_2\text{GaCl}_2]$ (**7**), with potassium metal in THF (THF = tetrahydrofuran), leading to the formation of a Ga–Ga bond, $[(\text{tBuN}=\text{CHCH}=\text{N}^{\text{tBu}})\text{Ga}-\text{Ga}(\text{tBuN}=\text{CHCH}=\text{N}^{\text{tBu}})]$, **8**. Subsequently, the obtained dinuclear Ga(II) complex, **8**, underwent further reduction using two equivalents of potassium metal and two equivalents of 18-crown-6 in THF. This second reduction method resulted in the formation of a separated ion pair (SIP), where the potassium cations are encapsulated in the 18-crown-6, and the gallyl anion, $[(\text{tBuN}=\text{CHCH}=\text{N}^{\text{tBu}})\text{Ga}]^-$ (**9**), is a 'naked' anion.



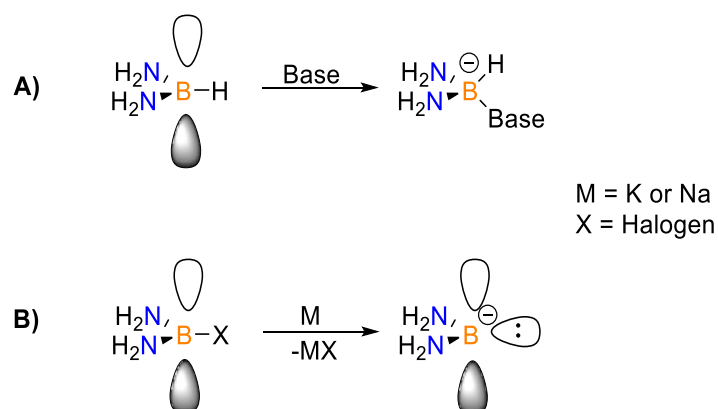
Scheme 2. Synthesis of the first group 13 metal anion, $[(\text{tBuN}=\text{CHCH}=\text{N}^{\text{tBu}})\text{Ga}]^-$ (**9**).

The presence of the first gallyl anion (**9**) was initially confirmed through MALDI TOF (*Matrix-Assisted Laser Desorption/Ionization–Time of Flight*) mass spectrometry. The mass spectrum revealed a peak at 237 m/z which corresponds to molecular anion, with the correct isotope pattern for ^{69}Ga . Additionally, the anion $[(\text{tBuN}=\text{CHCH}=\text{N}^{\text{tBu}})\text{Ga}]^-$ was also detected, as were peaks at $M^+ + 16$ and $M^+ + 32$, indicating the presence of the oxidation product. Furthermore, crystallographic data was obtained, providing insights into its molecular structure in the solid state. The 'naked' gallyl anion exhibits a nearly planar geometry and adheres closely to non-crystallographic C_{2v} symmetry, with the Ga–N bond lengths measured as 1.985(6) Å. The relatively small bite angle of N–Ga–N, measured to be 81.8(3)°, indicates an increased HOMO–LUMO gap. The observed energetic trend is similar to that observed in carbene chemistry, where the incorporation of heteroatoms into the structure often results in

significant σ – π energy gaps, as discussed in Section 1.3. The combination of mass spectrometry and single crystal X-ray crystallography provided valuable evidence for the formation of **9**, confirming the presence of the first gallyl anion. The successful synthesis of the gallyl anion represented a significant achievement in the field of low-valent group 13 complexes.

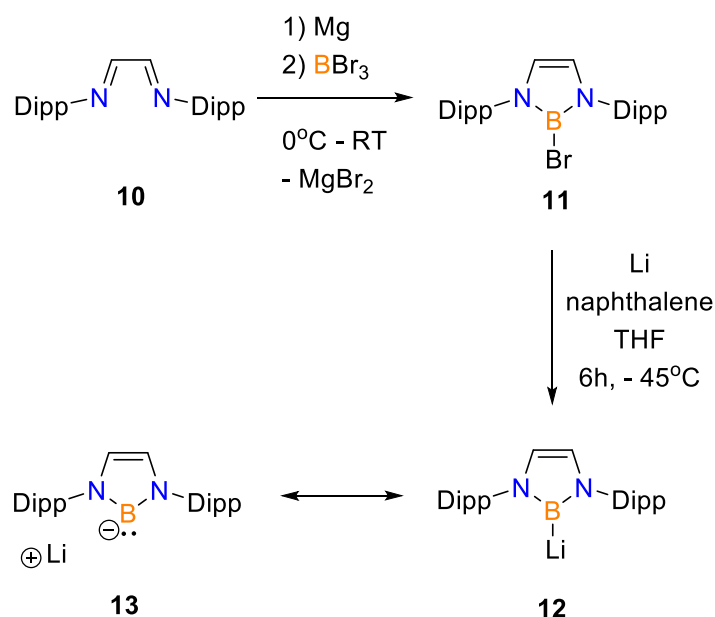
1.4.2 The Boryl Anion

Many subsequent studies on the other group 13 elements have drawn inspiration from the gallyl anion which exhibit similarities and differences in their structural features and reactivity patterns, including the boryl anion. The first boryllithium complex was reported in 2006 by Yamashita, in *Science*.⁶² The boron atom of boryllithium formally has six valence electrons. Yamashita believed that to satisfy the octet rule, extraction of a proton from a B–H bond should result in the production of a Lewis acid–base adduct rather than deprotonation to generate a boryl anion (Scheme 3).



Scheme 3. Two pathways to synthesise the boryl anion. A) Lewis acid–base adduct to borate anion. B) Reduction pathway to boryl anion.

The first *N*-heterocyclic boryl anion was synthesised from a Dipp diamine, **10** ($\text{DippN}=\text{CHCH}=\text{N}^{\text{Dipp}}$) with magnesium metal followed by the addition of BBr_3 to afford a borylbromine complex, **11**, $((\text{DippN}=\text{CHCH}=\text{N}^{\text{Dipp}})\text{BBr})$ (Scheme 4). This was then treated with a mixture of lithium metal and naphthalene in a THF solution which gave the boryllithium product, **12/13**, $(\text{DippN}=\text{CHCH}=\text{N}^{\text{Dipp}})\text{BLi}/((\text{DippN}=\text{CHCH}=\text{N}^{\text{Dipp}})\text{B}^-)\text{Li}^+$. Dipp groups are bonded to the nitrogen atoms to provide steric protection to prevent the boryl radical intermediates from dimerising to diborane. Boryllithium can be drawn as two resonance forms, where there is either a covalent bond (**12**) or a ionic bond (**13**) between the B and Li atoms.



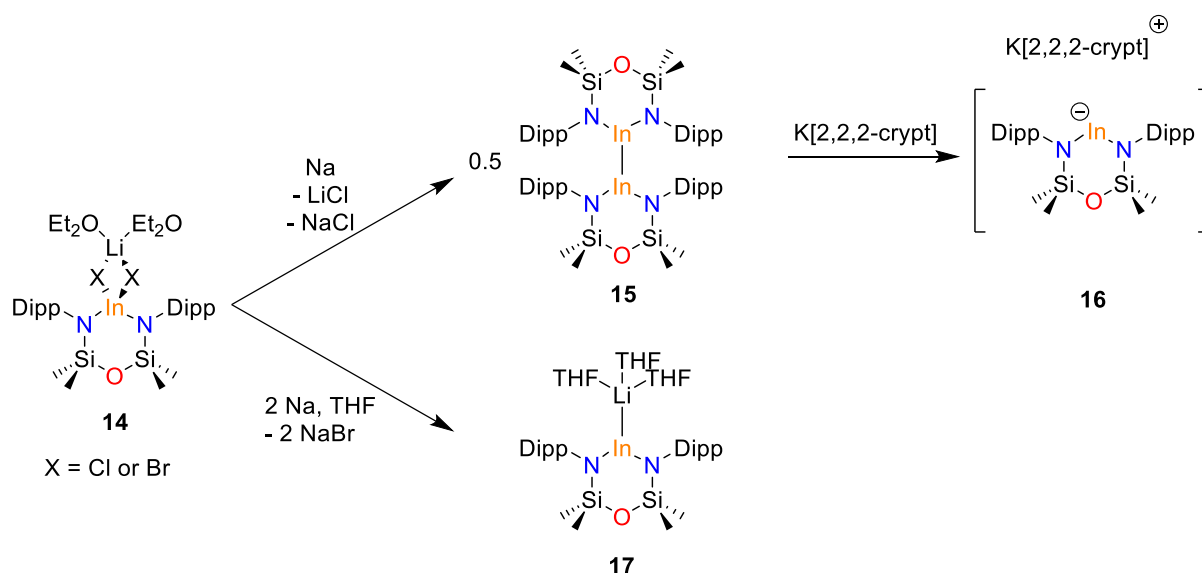
Scheme 4. Synthesis of Boryl anion.

Single crystal X-ray crystallographic data of compound **12/13** was obtained, to analyse whether the B–Li bond was ionic or covalent. The bond length of B–Li was determined to be 2.291 \pm 0.006 Å, which is larger than the sum of the covalent radii for boron and lithium, suggesting that there is an ionic interaction between boron and lithium like in compound **13**. Despite this the boryl anion is depicted as in **12**, in literature. The observed structural similarities between borylithium (**12/13**) and the DFT calculated free boryl anion, strongly suggest that boron is anionic.⁶³ The similar B–N bond lengths of 1.467 and 1.465 Å in **12/13**, compared to 1.475 Å for the free boryl anion, indicate similar bonding environments. Additionally, the bite angle of N–B–N in compound **12/13** is 99.2° which closely resembles that of the free boryl anion (97.2°). Several reactivity studies have been conducted on **12/13**, such as its ability to perform in addition reactions, and metal–metal bond formation.^{64, 65}

1.4.3 The Indyl Anion

Subsequently, after a span of 12 years, research in low-valent group 13 anions experience a resurgence. In 2018, Cole and colleagues reported the first low-valent anionic indium analogue of an *N*-heterocyclic carbene stabilised by a NON (NON = [O(SiMe₂N)₂]²⁻) ligand system (Scheme 5).⁶⁶ This anion has been synthesised *via* two different synthetic routes. To proceed with either synthetic route, their first step involves the synthesis of compound **14**, (In(NON^{Dipp})(μ-X)₂Li(Et₂O)₂) (Et₂O = diethyl ether, X = Cl or Br), obtained by reacting the lithiated ligand ((NON^{Dipp})Li₂) with the corresponding indium trihalide (InX₃). The first pathway involves the reduction of an indate compound, **14**, in the presence of sodium metal,

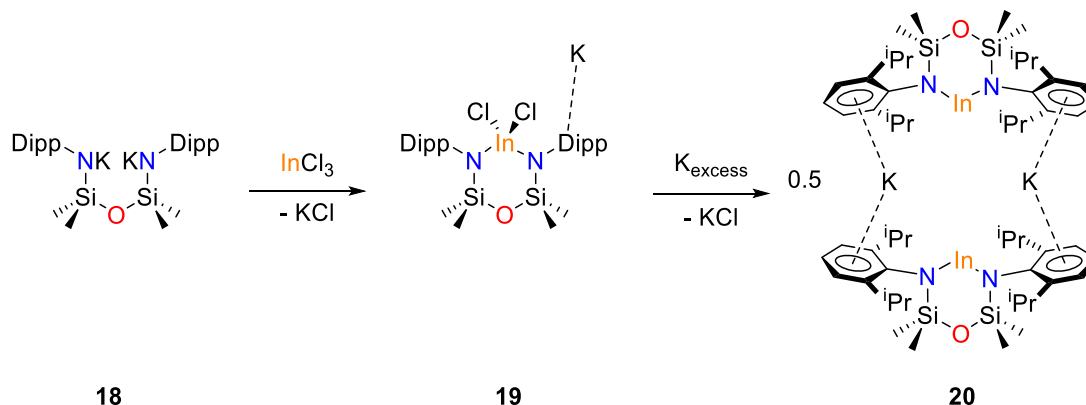
resulting in compound **15**, $[(\text{NON}^{\text{Dipp}})\text{In}-\text{In}(\text{NON}^{\text{Dipp}})]$. Subsequently, the addition of $\text{K}[2,2,2\text{-crypt}]$ ($2,2,2\text{-crypt} = \text{N}[(\text{CH}_2\text{CH}_2\text{O})_2\text{CH}_2\text{CH}_2]_3\text{N}$) to compound **15**, led to the formation of separated ions, namely **16**, $\text{In}(\text{NON}^{\text{Dipp}})$ and potassium encapsulated in $2,2,2\text{-crypt}$. During this reaction, when $\text{K}[2,2,2\text{-crypt}]$ is added to **15**, a noticeable colour change was observed, transitioning from a blue to a yellow solution. The formation of compound **16** was confirmed through a single crystal X-ray crystallographic experiment, which provided structural evidence for validating that the first low-valent indyl anion had been synthesised. The crystal structure of **16** revealed a bond angle of $\text{N}-\text{In}-\text{N}$ to be $95.53(10)^\circ$. In comparison, the bond angle of $\text{N}-\text{Al}-\text{N}$ in the aluminyl analogue was measured to be $103.89(8)^\circ$ and $105.05(8)^\circ$ for each monomer (see below). This indicates that the indyl anion, **16**, has a much smaller bite angle and can be attributed to the larger ionic radii of indium compared to aluminium, which necessitates the indium ion to sit further out of the NON ligand heterocycle.



Scheme 5. Synthesis of the first low-valent indyl anion, $[\text{In}(\text{NON}^{\text{Dipp}})][\text{K}(2,2,2\text{-crypt})]$ (**16**) and $(\text{NON}^{\text{Dipp}})\text{InLi}(\text{THF})_3$, (**17**).

The second method included the addition of compound **15** to two equivalents of sodium metal, resulting in the indyl anion, **17**, $(\text{NON}^{\text{Dipp}})\text{InLi}(\text{THF})_3$, where a reduction of the indium centre from $\text{In}(\text{III})$ to $\text{In}(\text{I})$ was observed through a single crystal X-ray crystallography experiment. In the solid state, the indyl is three-coordinate, bonded to lithium as well as the two nitrogen atoms from the ligand. Therefore, compound **17** can be described as a monomeric ion pair (MIP). Interestingly, the $\text{In}-\text{N}$ bond distances in **17**, as well as the $\text{N}-\text{In}-\text{N}$ bond angle, have slightly changed compared to compound **16**. The $\text{In}-\text{N}$ bond distances of **17** are now $2.198(4)$, $2.188(5)$ Å and the $\text{N}-\text{In}-\text{N}$ bond angle of **17** is $96.78(16)^\circ$. These values indicate slightly shorter $\text{In}-\text{N}$ bonds compared to **16**, and the $\text{N}-\text{In}-\text{N}$ bond angle is slightly wider in

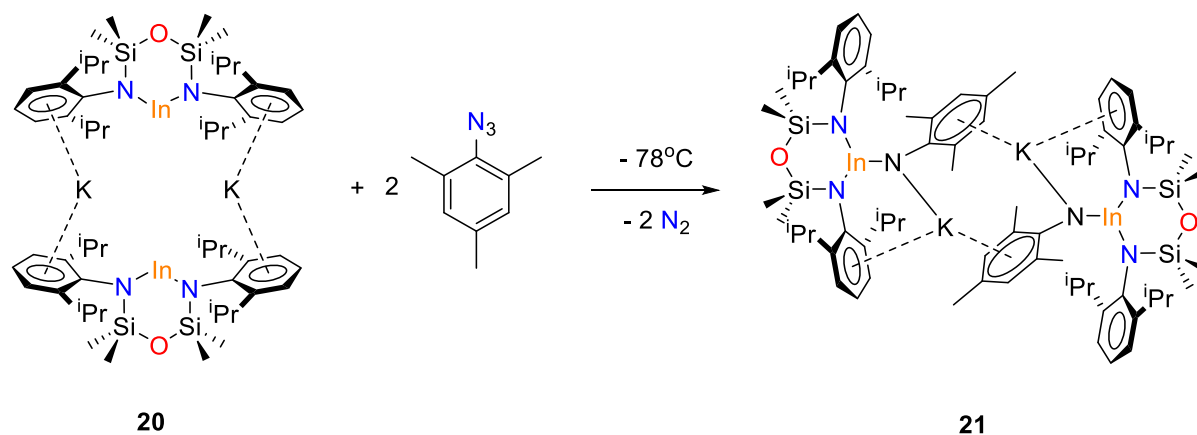
17. This suggests that when indium is bonded to another compound other than the NON ligand, it tends to retract into the NON ligand system. Whereas in **16**, where the complex is an SIP, the indium centre prefers to extend away from the NON ligand, which is shown in the X-ray crystallographic data. In compound **17**, it is notable that the addition of sodium metal to **14** formed the lithiated indyl instead of a sodiated indyl. This can be attributed to the differences in solubility of the respective NaBr vs LiBr salts in solution. Coles *et al* found through experimental procedure that **17** and **16** displayed inherent instability. Therefore, Coles *et al* decided that an alternative route to synthesise the indyl anion was necessary to accomplish stability of the indyl anion. The alternative route avoids the use of lithium reagents and eliminates the need for expensive 2,2,2-crypt reagents to stabilise the salt. In this route, the potassiated ligand, (NON^{Dipp})K₂ (**18**) is reacted with InCl₃ to form (NON^{Dipp})InCl₂, **19** (Scheme 6).⁶⁷ Subsequently, **19** is reduced using excess potassium metal, resulting in the formation of a contacted dimeric pair (CDP) indyl anion, [(NON^{Dipp})InK]₂, **20**, with two bridging potassium ions coordinating to the flanking Dipp substituents. This not only simplifies the synthetic procedure but also allows for stability of this indyl anion, permitting reactivity studies to be conducted.



Scheme 6. Improved synthesis of the first indyl anion, [(NON^{Dipp})InK]₂ **20**.

The reactivity of compound **20** has been explored through reactions with organic azides as well as zinc complexes. These investigations aim to uncover potential applications as intermediates in the formation of electronically significant InN materials. Additionally, there is an interest in forming bimetallic complexes that exhibit distinct differences compared to monometallic systems. Coles *et al* attempted to synthesise a In=N bond by using 2,6-bis(diphenylmethyl)-4-^tBu-phenyl azide in the reaction with **20** but, this resulted in the activation of the ligand. In contrast, when using mesityl azide instead, the desired imide bond was formed. The combination of **20** with mesityl azide at -78°C followed by 1 hour of stirring at room temperature resulted in deep orange crystals of [K{In(NON^{Dipp})(NMe₃)}]₂, **21** after

work up procedures (Scheme 7), which were identified by a single crystal X-ray crystallographic experiment.⁶⁷ It was found that **21**, crystallises as a non-symmetric dimer, wherein the potassium counter ions are engaged in π -aryl interactions with the Dipp and Mes substituents. The formation of **21** suggested that the indyl anion exhibits nucleophilic behaviour and can react with electrophilic species such as azides.

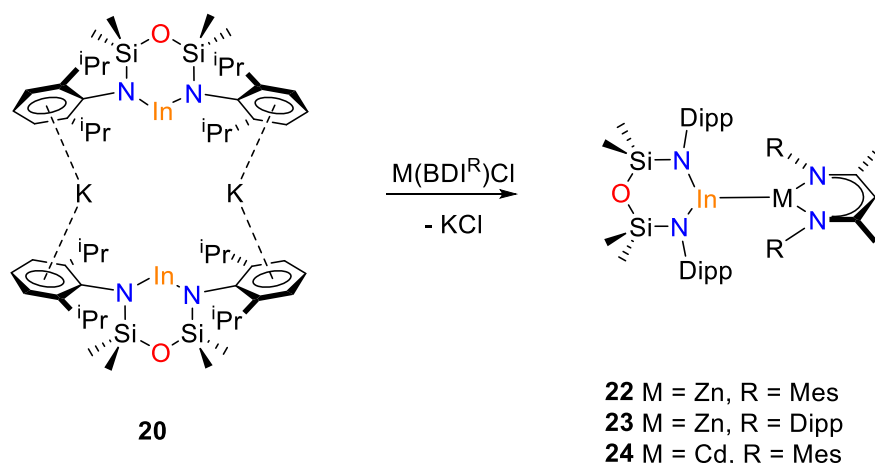


Scheme 7. Synthesis of first indyl imide, $[K\{In(NON^{Dipp})(NMes)\}]_2$, **21**.

The single crystal X-ray crystallography analysis of **21** revealed a short In–N_{imide} bond of 1.986(2) and 1.999(2) Å in each unit. This bond length is comparable to multiple bond character as shown computationally, suggesting a strong interaction between the indium ion and the imide nitrogen. The X-ray crystallography analysis also revealed short interactions of 2.661(3) and 2.646(3) Å between the imide nitrogen and the potassium cations. These interactions were initially considered to potentially affect the length of In–N_{imide} bond. To further investigate the influence of these interactions, Coles *et al* conducted an experiment to separate the potassium cation from the imide complex by adding 2,2,2-crypt, however, the resulting SIP structure exhibited the same bond length for the In–N_{imide} bond as observed in **21**. This finding suggests that the interactions between the azide nitrogen and the potassium cation have minimal impact on the structural component of the In–N_{imide} bond. To further explore the reactivity of **21**, it was subjected to additional reactions with different azides. Both mesityl and SiMe₃ azides were used in separate experiments, and both resulted in the formation of a tetrazole complex through a [2 + 3] cycloaddition reaction. These additional experiments provide further confirmation that the presence of potassium ions in **21** does not adversely impact the reactivity of the In–N_{imide} bond.

New metal–metal bond have been successfully synthesised by Coles and colleagues using the indyl anion, **20**, and a BDI^R–MX complex (R = Mes or Dipp, metal = Zn or Cd, X =

Cl) (Scheme 8).⁶⁸ The addition of the BDI^R–MX complex to the yellow solution of **20** in deuterated benzene resulted in an immediate colour change from yellow to colourless and the formation of a white precipitate for all cases.



Scheme 8. Synthesis of indium metal bonds.

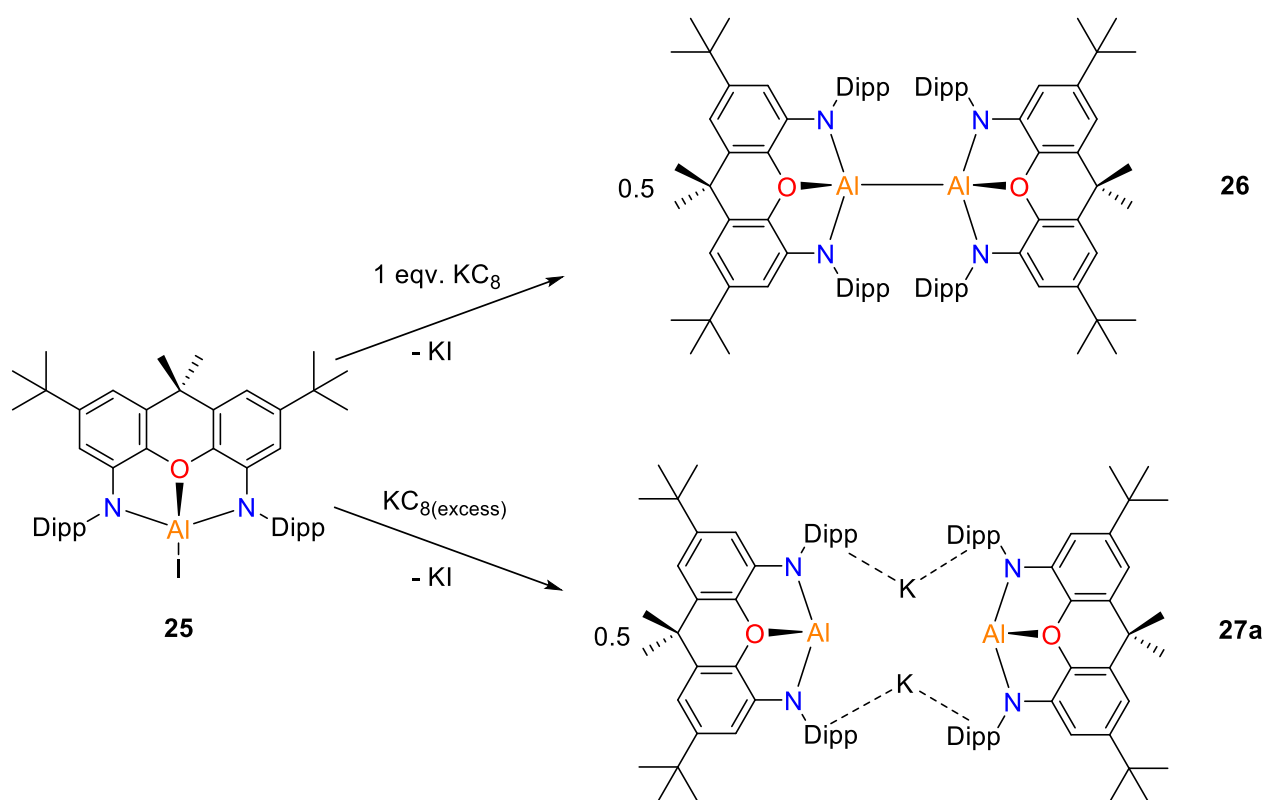
Single crystal X-ray crystallography was conducted on the new metal–metal complexes, revealing that half, one and two molecules crystallise in the asymmetric unit for **22** [(NON^{Dipp})In–Zn(BDI^{Mes})], **23** [(NON^{Dipp})In–Zn(BDI^{Dipp})], and **24** [(NON^{Dipp})In–Cd(BDI^{Mes})], respectively. In the case of **22** and **23**, the In–Zn bond distances were determined to be 2.5486(4) and 2.5622(5) Å, respectively. For **24**, where the two molecules are present in the asymmetric unit, the In–Cd bond lengths are measured as 2.6461(4) and 2.6427(4) Å for each monomer. In compounds **22**, **23** and **24** the In–M bond lengths are all shorter than the sum of the respective covalent radii, indicating the formation of new metal–metal bonds have been formed.⁶⁹

This indyl anion (**20**) has demonstrated its versatility in several reactions, showcasing its ability to form distinct types of bonds depending on the reaction conditions and metal counterparts. In reactions with azides, the indyl anion can participate in [2 + 3] cycloaddition reactions, leading to the formation of an indium nitrogen double bond. Furthermore, when combined with different metal complex such as zinc or cadmium complexes, the indyl anion can form metal–metal bonds. This reactivity of the indyl anion underscores its potential in numerous synthetic transformations and provides opportunities for further exploration.

1.4.4 The Aluminyl Anion

Building inspiration from the isolation of the gallyl, boryl and indyl anions, subsequent research has delved into investigating *N*-heterocyclic ligands with emphasise on the aluminyl anion. Aluminium is most commonly found in the +3 oxidation state, in trialkylaluminiums or aluminium trihalides.⁷⁰ Compounds in lower-than-usual oxidation or valence states display distinctly different structural characteristics, bonding modes, and reactivity than compounds containing the element in a more regular oxidation states.²⁴ Aluminium is considered to be in a low oxidation state when in the +2, +1, and 0 oxidation states, which have been less extensively investigated.⁷¹ When aluminium is in the +1 oxidation state, it exhibits strong reducing properties. In this state, aluminium can donate electrons and participate in reduction reactions. The reactivity of aluminyl anions demonstrates the reducing power of aluminium in its low-valent state. Aluminium compounds in the +1 oxidation state are archetypal Lewis acids, therefore, they are electron pair acceptors.⁷² The distinctive features of aluminium compounds lie in their electron deficiency and electrophilicity. These qualities enable these compounds to readily react with typically inert small-molecule substrates, such as CO and CO₂.⁷³ This is supported by the fact that the aluminium metal centre has a nucleophilic reactivity profile, as opposed to the electrophilic character of most aluminium compounds. The nucleophilicity is drawn from the pair of electrons located on the aluminium atom, that can be shared to bond to other molecules.

Aldridge and co-workers reported and characterised the first low-valent *N*-heterocyclic anionic Al(I) system in 2018, known as the aluminyl anion.⁷² Due to its anionic nature, the aluminyl anion can act as a nucleophile in contrast to the previous neutral Al(I) compounds, this provides access to new and unexplored reactivity. The synthesis of this dimethylxanthene-stabilised potassium aluminyl [KAl(*x*NON^{Dipp})], (*x*NON = 4,5-bis(2,6-diisopropylanilido)-2,7-di-*tert*-butyl-9,9-dimethylxanthene) initially begins with deprotonation of the (*x*NON^{Dipp})H₂ ligand with K-HMDS, followed by the addition of AlI₃ to obtain [(*x*NON^{Dipp})AlI] (**25**), the Al(III) iodide (Scheme 9). When differing amounts of KC₈ were added to **25**, two distinct products were synthesised, compound [(*x*NON^{Dipp})Al–Al(*x*NON^{Dipp})] (**26**), and [KAl(*x*NON^{Dipp})]₂ (**27a**) (Scheme 9). An Al–Al bond can form from one equivalent of KC₈ with **25**, which is predicted to occur through radical coupling of two (*x*NON^{Dipp})Al· units and/or by nucleophilic attack of [(*x*NON^{Dipp})Al]K on **25**, forming compound **26**. However, **27a** is prepared from a two-electron reduction of the neutral aluminium iodide complex, **25**, with excess KC₈.

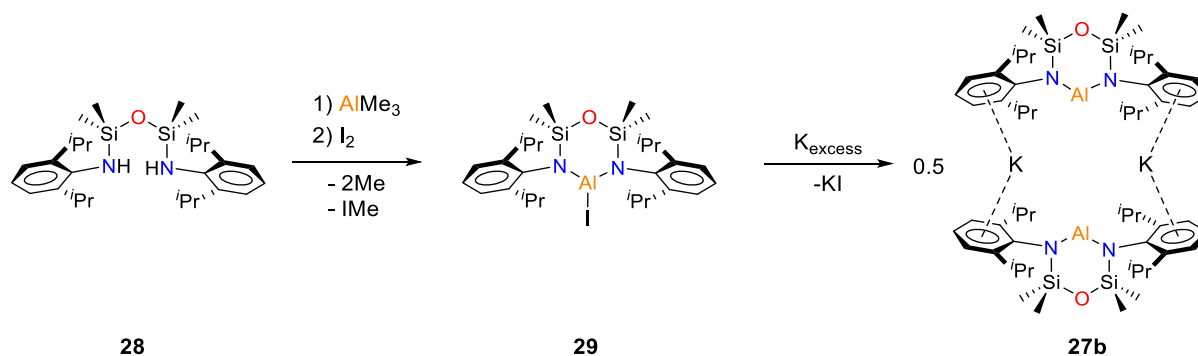


Scheme 9. Synthesis of the first aluminium anion, $[\text{KAl}(\text{xNON}^{\text{Dipp}})]_2$ (**27a**).

Single crystal X-ray crystallographic data validates structure **27a** and confirms the first reported low-valent *N*-heterocyclic aluminyl anion had been synthesised. The data presented reports a bond distance for Al–O is 2.279(2) Å, while the Al–N bond distances are 1.956(2) or 1.963(2) Å. Therefore, presenting a three-coordinate ligand system, where the Al–O interaction is relatively weak. Given aluminium’s tendency to be in the +3 oxidation state and the difficulties in accurately determining the positions of hydrogen atoms in single crystal X-ray crystallography, it was important for Aldridge *et al* to verify the absence of any hydrogen atoms bound to the aluminium within the dimeric molecular unit of **27a**. To determine whether there were any hydrogens present in **27a**, $[\text{K}\{\text{H}_2\text{Al}(\text{xNON}^{\text{Dipp}})\}]_2$ was synthesised by reacting **25** with $\text{K}[\text{AlH}_4]$.⁷² $[\text{K}\{\text{H}_2\text{Al}(\text{xNON}^{\text{Dipp}})\}]_2$ was then characterised using spectroscopic, analytical and crystallographic techniques. The obtained measurements of $[\text{K}\{\text{H}_2\text{Al}(\text{xNON}^{\text{Dipp}})\}]_2$ showed significant differences compared to **27a**, which included shifted ¹H NMR resonances of the ligand backbone and the presence of an additional hydride peak at 3.88 ppm. Furthermore, $[\text{K}\{\text{H}_2\text{Al}(\text{xNON}^{\text{Dipp}})\}]_2$ exhibited shorter Al–O and Al–N distances, compared to **27a**. The data obtained from the single crystal X-ray crystallography of $[\text{K}\{\text{H}_2\text{Al}(\text{xNON}^{\text{Dipp}})\}]_2$ helped confirm that compound **27a** is the first aluminyl anion with an aluminium centre having a formally negative charge. Compound **27a** exists as a dimer, with bridging potassium cations between the flanking aryl Dipp substituents. The positive charge

on the potassium counterbalances the charge of the aluminium centre to obtain an overall neutral charge on **27a**. Within the dimer the two aluminium centres are greater than 6.6 Å apart, which is greater than the sum of the covalent radii of aluminium (sum of covalent radii for Al–Al = 2.42 Å), therefore not producing a significant interaction, and there is not an Al–Al bond present.⁷⁴

In the same year, Coles *et al* reported the second aluminyll anion.⁷⁵ This also is a potassium aluminyll complex featuring a bidentate diamido ligand, which also exists as a dimer. This synthesis involved the metalation of the pre-ligand **28** ((NON^{Dipp})H₂) (NON^{Dipp} = [O(SiMe₂N^{Dipp})₂]²⁻, Dipp = *i*Pr₂C₆H₃), with AlMe₃, followed by the addition of iodine *in situ*, forming compound (NON^{Dipp})AlI, **29** (Scheme 10). Coles *et al* found it to be more convenient to carry out this reaction in a one-pot procedure, although the aluminium methyl complex can be isolated separately. The colourless solution of **29** was stirred over potassium metal for a duration of three days. Upon the addition of potassium, the Al–I bond in **29** is cleaved, through a salt metathesis reaction, resulting in the formation of a yellow solution of the aluminyll anion, [KAl(NON^{Dipp})]₂, **27b** and KI. This anion carries a negative charge and is stabilised by the coordination of a potassium cation, which interacts with the flanking aryl Dipp substituents. This charge balance is required for the stability of the aluminyll anion. It is noteworthy, that in this study no evidence of an Al–Al complex similar to **26** formed by this reduction. Coles *et al* conducted a single crystal X-ray crystallographic experiment on compound **27b**, and determined that the Al–Al distance of 5.673(1) Å falls outside the range typically associated with a bonding interaction.⁷⁶ This suggests that there is no direct covalent bond between the aluminium atoms in the dimeric complex. Instead, the observed distance implies the presence of weaker interactions, such as van der Waals forces or non-covalent interactions.⁷⁷



Scheme 10. Synthesis of [KAl(NON^{Dipp})]₂ aluminyll, **27b**.

Since the first report on the aluminyll anion, it was thought that an oxygen atom in the ligand system acted as a donor atom to help stabilise the three-coordinate aluminyll anion

complex. However, Coles *et al* demonstrated through crystallography that their aluminyl anion does not have an oxygen–aluminium interaction and only a κ_2-N, N' -bonding mode, as the Al–O distances are 3.418(2) and 3.356(2) Å for each monomer. These distances surpass the combined ionic radii for aluminium and oxygen, precluding the existence of an Al–O bond within compound **27b**. This confirms that oxygen is not essential for stabilising an aluminyl anion and that it can be stable as a two-coordinate system.

Aldridge and Coles have independently demonstrated, using single crystal X-ray crystallography, that their aluminyl anions, **27a** and **27b** respectively exist as contact dimeric pairs (CDPs) (Figure 5).^{72, 75} In this arrangement, two aluminyl anions are coordinated by flanking potassium interactions, creating a dimeric arrangement. This occurs for the *N*-heterocyclic aluminyl anions that don't require a coordinating solvent during their synthesis. This dimeric structure provides stability and influences the properties and reactivity of all these aluminyls fitting the CDP structural classification.

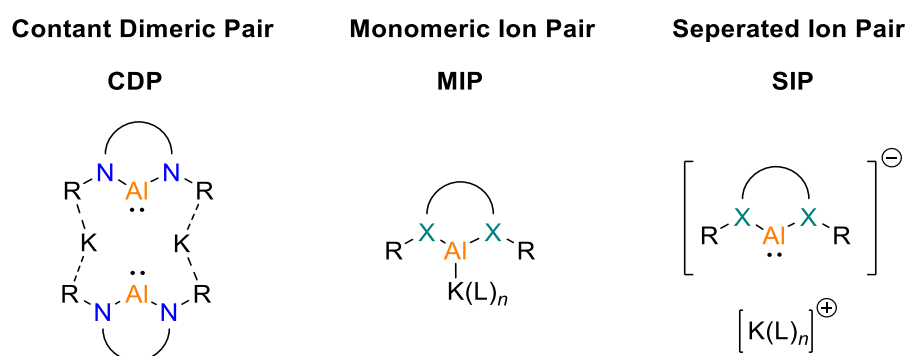


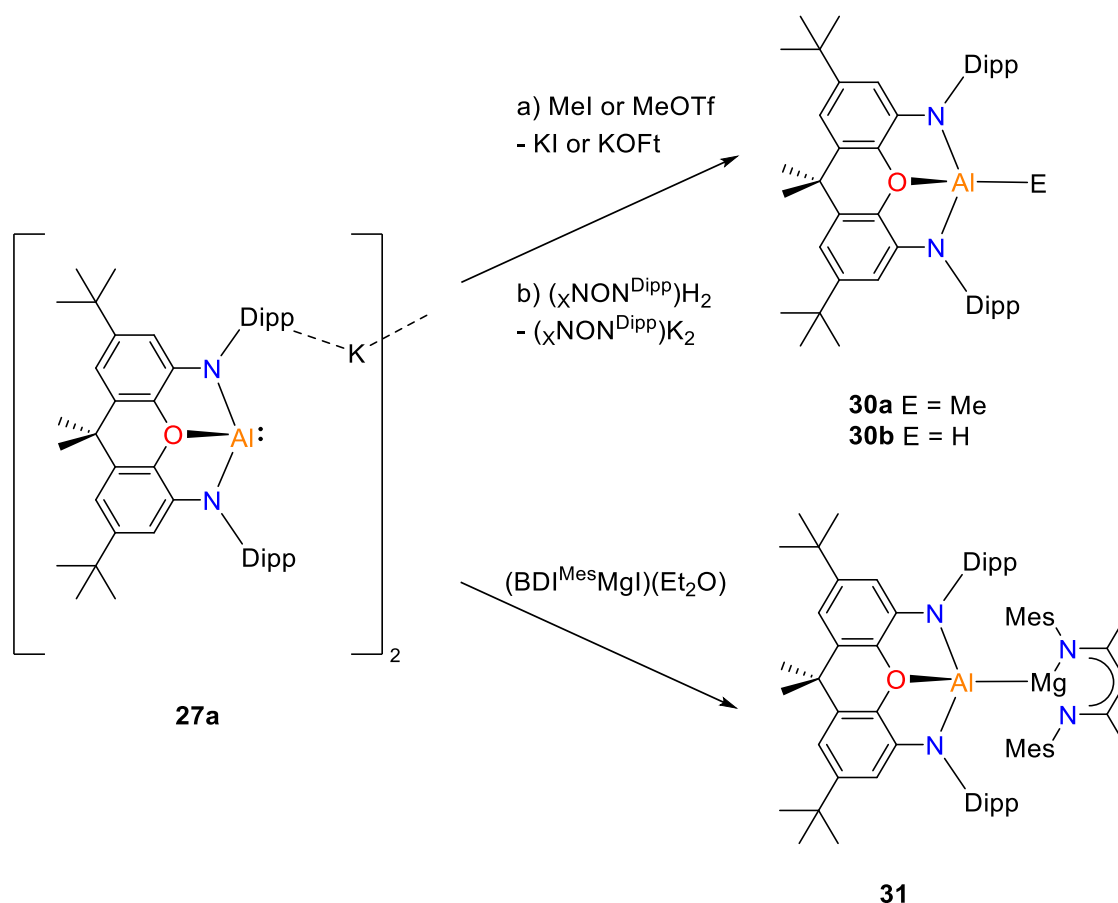
Figure 5. Structural classification of aluminyl compounds (R = Dipp, Depep or Mes, X = C or N, L = monodentate or polydentate ligand).

In addition to the CDPs structure, aluminyl anions can exist in two other arrangements known as monomeric ion pairs (MIPs) and separated ion pairs (SIPs). In the MIP structure, there are no stabilising K interactions present, so the aluminyl anion and the associated cationic component are connected by unsupported and highly polar Al–K bonds. A MIP structure can also form when no arene substituents are present so an aromatic solvent (for example toluene), coordinates to the potassium cation.⁷⁸ As well as, the addition of a suitable σ -donor like 18-crown-6 can result in the formation of MIPs.⁷⁹ The SIP structure is formed when encapsulating molecules, such as 12-crown-4, 18-crown-6 or 2,2,2-crypt are added during the workup process. In an SIP, the potassium cation is isolated from the aluminyl anion, creating a separated arrangement, which is also referred to as a ‘naked aluminyl’.⁷⁹⁻⁸¹

It is worth mentioning that other group 1 metals can also form CDPs, MIPs and SIPs, although these have not been discussed here. Additionally, these structural classifications have been observed for several of the other group 13 anionic complexes. However, they have not been mentioned primarily due to the extensive research conducted on aluminyll anions and the substantial body of work in the field of aluminium chemistry.

1.4.5 Reactivity of Aluminyll Anions

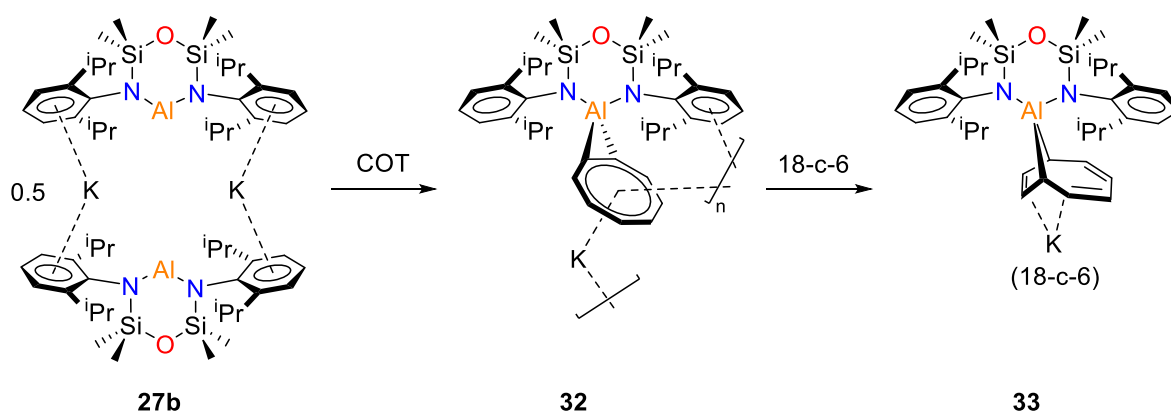
Extensive reactivity studies have been conducted on **27a** since its initial synthesis in 2018, revealing its versatile nature, therefore, more in depth examples with **27a** will be discussed. An initial reactivity study was conducted, demonstrating the nucleophilic behaviour for **27a**, where the addition of methyl triflate (MeOTf) or methyl iodide to **27a** resulted in the formation of $\text{MeAl}(\chi\text{NON}^{\text{Dipp}})$, **30a**,⁷² as well as the protonation of the aluminium centre in **27a** with a Bronsted acid leads to the formation of a monomeric aluminium hydride compound, $\text{HAl}(\chi\text{NON}^{\text{Dipp}})$, **30b** (Scheme 11). In this reaction, the interaction between the potassium and the aluminyll anion is disrupted, and the potassium is removed as a halide salt.



Scheme 11. Aluminium-centred nucleophilic reactivity of $[\text{K}\{\text{Al}(\chi\text{NON}^{\text{Dipp}})\}]_2$, **27a**, forming $\text{MeAl}(\chi\text{NON}^{\text{Dipp}})$ (**30a**), $\text{HAl}(\chi\text{NON}^{\text{Dipp}})$ (**30b**), and $(\chi\text{NON}^{\text{Dipp}})\text{Al-Ga}(\text{BDI}^{\text{Dipp}})$ (**31**).

Another notable reactivity study involving **27a** is the reaction with $\text{BDI}^{\text{Mes}}\text{MgI}$ (Mes = 2,4,6-trimethylphenyl) resulting in the formation of a covalent metal–metal bond, $(\text{xNON}^{\text{Dipp}})\text{Al-Mg}(\text{BDI}^{\text{Dipp}})$, **31**. The most notable feature in **31** is the presence of an unsupported Al–Mg bond, which was measured to be 2.696(1) Å. This distance is comparable to the sum of the covalent radii of both metals, being 2.62 Å, suggesting a strong interaction between the magnesium and aluminium ions.^{74, 82}

Alternatively, reactivity studies conducted by Coles *et al* on their aluminyll anion, **27b**, demonstrated the first cycloaddition reaction conducted with any of the aluminyll anions.⁷⁵ They reacted 1,3,5,7-cyclooctatetraene (COT) with **27b**, resulting in a two-electron reduction to the $[\text{COT}]^{2-}$ ion (Scheme 12). This reduction was observed as a gradual decrease in the intensity of the bright yellow solution, eventually forming a white solid identified to be $\text{KAl}(\text{NON}^{\text{Dipp}})(\text{COT})$, **32**. The characterisation of **32** using ^1H NMR spectroscopy showed a chemical shift of 5.86 ppm, which corresponds to the CH protons of the $[\text{COT}]^{2-}$ group. From the single crystal X-ray crystallographic data, revealed the structure of **32** exists as an asymmetric unit, that consists of an unsolvated compound. The asymmetric unit of **32** can be described as an inverse sandwich complex, where the $[\text{COT}]^{2-}$ is coordinated to the $(\text{NON}^{\text{Dipp}})\text{Al}$ fragment, and the potassium atom is now involved in a $\mu_2\text{-}\eta^2\text{:}\eta^8$ coordination interaction with the $[\text{COT}]^{2-}$ ring. The $[\text{COT}]^{2-}$ ring in **32** is observed to be essentially planar, with a small deviation from the mean square plane. It is noted that the distribution of C–C bond lengths in **32** does not indicate complete delocalisation, suggesting a lack of complete aromatic character in the $[\text{COT}]^{2-}$ ligand.



Scheme 12. Synthesis of $\text{K}[(\text{NON}^{\text{Dipp}})\text{Al}(\text{COT})]$ (**32**) and $[\text{K}(\text{18-c-6})][(\text{NON}^{\text{Dipp}})\text{Al}(\text{COT})]$ (**33**).

Compound **32** was further reacted with 18-crown-6 to yield compound **33**, $[(\text{NON}^{\text{Dipp}})\text{Al}(\text{COT})] [\text{K}(\text{18-crown-6})]$. Notably, the single crystal X-ray crystallography analysis of **33** reveals a change in the coordination of the $[\text{COT}]^{2-}$ ligand when compared to **32**.

In the structure of **33**, it is observed that the C–C bond distances within the COT ligand exhibit significant differences, with values associated with single bonds and those characterised as double bonds. This is consistent with the predicted triene unit. However, the potassium ion encapsulated in 18-crown-6 is still associated with the $[(\text{NON}^{\text{Dipp}})\text{Al}(\text{COT})]^-$ anion through K–C interactions.

Since the initial isolation of the first alumanyl anion, **27a**, reported by Aldridge *et al*, there has been a significant increase in the synthesis of alumanyl anions, extending the scope of anionic alumanyl synthesis to include a wide range of ligands, which has led to the discovery and characterisation of seven novel alumanyl anions (Figure 6). These modifications allow for comparisons in the stability and reactivity of the different analogues. Significant advancements have been made in understanding the reactivity of these alumanyl anions. These anions have demonstrated remarkable versatility in several reaction types, showcasing their potential as reactive materials. Some of these reactions include nucleophilic substitution, oxidative addition, cycloaddition and oxidation.^{72, 78, 83} Nucleophilic substitution reactions are commonly observed with alumanyl anions, where they can act as powerful nucleophiles and participate in metal–metal bond formation. Which can be seen for **27a**, **27c**, and **27g** alumanyl anions.^{72, 78, 84-86} Oxidative addition reactions are another prominent reactivity feature of alumanyl anions. Where very strong σ –bonds are cleaved to form the new products. Such reactions are reported with alumanyl anions **27a**, **27f**, and **27g**.^{72, 78, 80, 81} Cycloaddition reactions involving alumanyl anions have also been reported. These reactions involve the addition of compounds containing alkene, alkyne or polyaromatic functionalities. These cycloaddition reactions are apparent among alumanyl anions **27a**, **27b**, and **27f**.^{75, 81, 87} In addition, alumanyl anions have demonstrated reactivity in oxidation reactions. They can react with a range of oxidising agents, for example, CO_2 , PhNCO , N_2O , chalcogens, organic azides, CO and H_2 . Alumanyl anions **27a** and **27b**, have been reported to react with several of these reagents.^{83, 88-92}

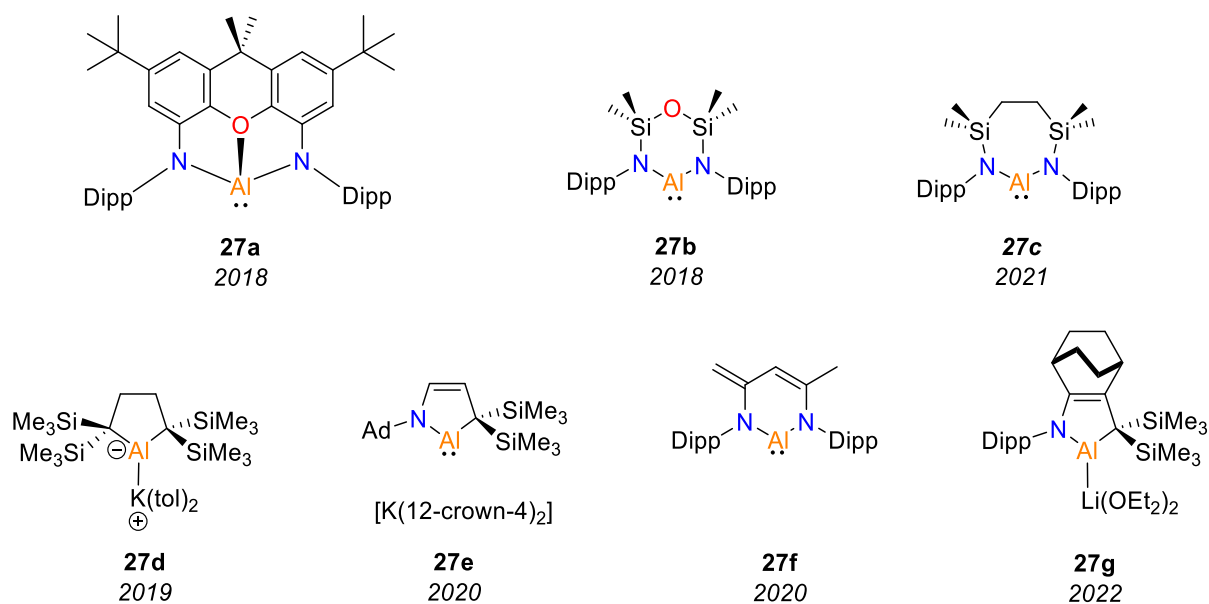


Figure 6. The seven reported aluminyl anions. Reported year present under compound number.

As each of these complexes exhibits distinctive structural attributes, their reactivity to similar molecules varies correspondingly. These advancements expand the repertoire of anionic aluminyl(I) chemistry providing further insights into the coordination behaviour and reactivity of these intriguing complexes. However, it is important to note that the synthesis and reactivity of these later synthesised aluminyls are beyond the scope of this thesis.

1.5 Overview of Literature Review

Both anionic and neutral group 13 systems, namely gallium, aluminium, and indium, have been demonstrated to be stabilised by *N*-heterocyclic systems. The initial synthesis of these metal complexes typically involves the utilisation of either monoanionic or dianionic ligand systems, specifically BDI, χ NON or NON ligands. Similar synthetic pathways are employed for both neutral and anionic low-valent group 13 complexes. These pathways include either a reduction of LMX_2 ($\text{L} = \text{BDI}, \chi\text{NON}$ or NON , $\text{M} = \text{B}, \text{Ga}, \text{Al}$ or In , $\text{X} = \text{halogen}$) with a group 1 metal or the addition of a metal-halide to the *N*-heterocyclic system. The resulting complexes exhibit high reactivity and can participate in diverse reaction pathways. While the research in the field on low-valent group 13 complexes, such as the boryl, gallyl, and aluminyl anions are now well established, this thesis aims to address the limited studies conducted on the indyl anion.

1.6 Project Outline and Research Aims

The main aim of this thesis research is to synthesise and explore the reactivity of a novel indyl anion. To accomplish this, the following three goals have been identified:

- 1) To synthesise a new $[\text{xNON}^{\text{TCHP}}]^{2-}$ (xNON = 4,5-bis(2,6-diisopropylanilido)-2,7-di-*tert*-butyl-9,9-dimethyl-xanthene, TCHP = 2,4,6-tricyclohexylphenyl) ligand system. The $[\text{xNON}^{\text{TCHP}}]^{2-}$ ligand system is an *N*-heterocyclic ligand that uses the nitrogens to donate π -electrons into the vacant p_z orbital of indium, thereby stabilising the target indyl anion complex. The use of this ligand system has not been previously employed for synthesising indyl complexes. However, it is anticipated that it will provide enhanced stability to our indium systems, drawing inspiration from the enhanced stability demonstrated by the xNON aluminyll anion. The xanthene backbone exhibits increased stability in comparison to the NON ligand used for the indyl anion, owing to its rigid nature. We anticipate that this different ligand system will avoid ligand rearrangement and enhance overall stability to our indyl anion.
- 2) Building upon the newly developed $[\text{xNON}^{\text{TCHP}}]^{2-}$ ligand system, our next goal is to utilise this ligand system to synthesise a new indyl anion. To achieve this, we will draw upon existing literature methods and procedures that have been successful for the synthesis of indyl and aluminyll anions. By adapting and optimising these synthetic routes, we aim to obtain the desired indyl anion.
- 3) Investigate the reactivity of our new indyl anion. We will then explore the reactivity of the new indyl anion towards a range of small-molecule substrates, such as isocyanides/isocyanates and azide complexes.

Chapter 2. Ligand Development

2.1 Introduction

Previous work in the Anker research group has demonstrated that the x NON ligand system is capable of supporting indyl anions. The rationale behind using this ligand system was based on the success of the x NON ligand in aluminyll chemistry and that the increased rigidity of the xanthene backbone could reduce unwanted side reactions that have been previously observed during the synthesis of the (NON^{Dipp})InK indyl complex. Two ligand systems have previously been developed, the first based on Dipp N -substituent ((x NON^{Dipp})InK) enabling a more direct comparison to the related aluminyll system (**27a**). The second is based on the Ar* N -substituent (Ar* = ((4-methyl-2,6-phenylene)bis(methanetriyl))tetrabenzene), (x NON^{Ar*}InK) where the increased bulk of the N -Ar* moiety could provide increased stability of the indium centre.

At the outset of this project, we planned to explore the reactivity of (x NON^{Dipp})InK towards a range of organic and inorganic substrates. With the goal of initially recreating the successful reactivity of the (NON^{Dipp})InK (**20**) indyl towards organic azides we sought to investigate the reactivity of (x NON^{Dipp})InK towards Dipp azide. However, due to the poor thermal stability and extreme light sensitivity of x NON^{Dipp}InK our initial trial reactions resulted in complex mixtures of breakdown products (Figure 7).

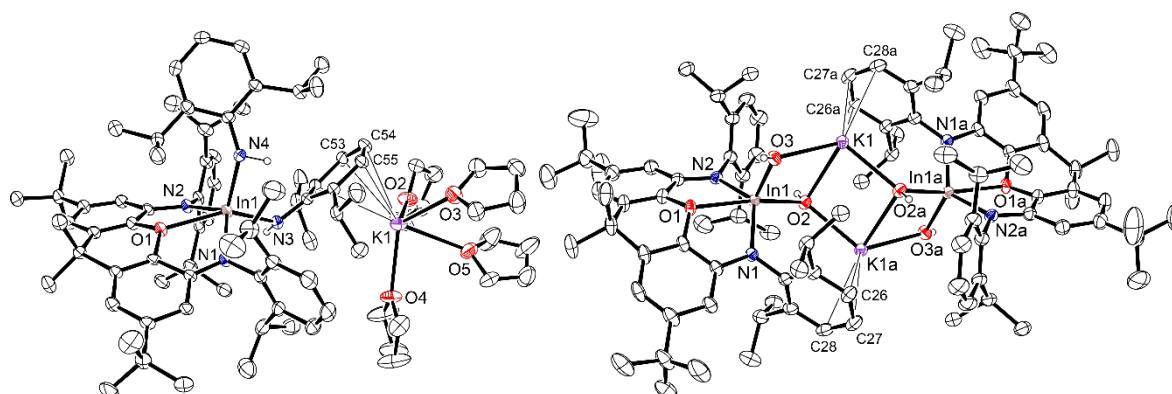


Figure 7. The non-reproducible products obtained from (x NON^{Dipp})InK with N₃-Dipp.

Due to the inherent instability observed in (x NON^{Dipp})InK we rationalised that increasing the bulk of the N -substituents could provide a more stable indyl anion, which would be valuable for investigating its reactivity. Previously the 2,4,6-tricyclohexyl phenyl (TCHP) group has been used to stabilise highly reactive main group complexes.⁹³ Therefore, we aimed to synthesise the new indyl anion (x NON^{TCHP})InK with TCHP N -substituents and then explore its stability and reactivity.

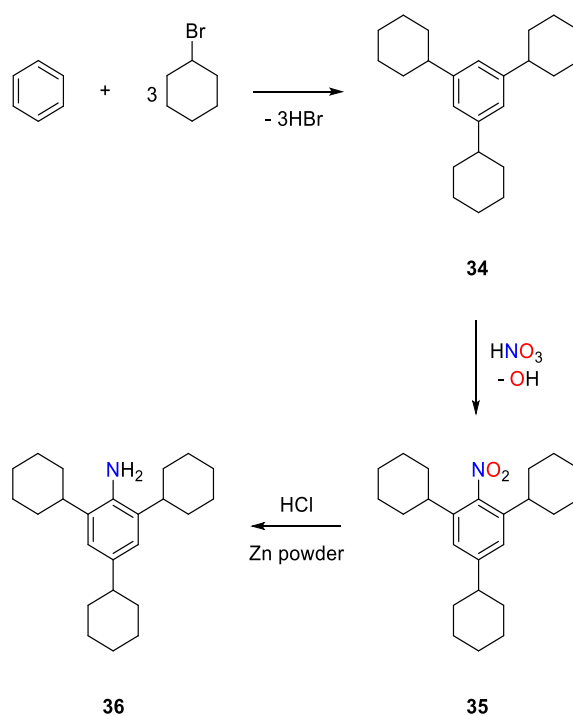
2.2 Ligand Selection

The selected ligand system for this project is $[(x\text{NON}^{\text{TCHP}})]^{2-}$ ($x\text{NON}$ = 4,5-bis(2,6-diisopropylanilido)-2,7-di-*tert*-butyl-9,9-dimethylxanthine). By altering the commonly used $x\text{NON}^{\text{Dipp}}$ (Dipp = 2,6-diisopropylphenyl) ligand with TCHP substituents, there are opportunities to alter the steric and electronic environments of the ligand system. This variability provides an opportunity to explore and observe diverse characteristics that differ from those exhibited by the commonly used $x\text{NON}^{\text{Dipp}}$ ligand system.⁹⁴

2.3 Synthesis of TCHP Amine

To synthesise the TCHP ligand system, the TCHP amine is initially prepared following a three-step procedure, resembling methods described in the literature.⁹³ The initial step encompasses an electrophilic aromatic substitution reaction, catalysed by AlMe_3 (Me = methyl) where bromocyclohexane reacts with benzene at the 2, 4 and 6 positions on the benzene ring (Scheme 13). Notably, the resultant product, 2,4,6-tricyclohexyl phenyl (**34**) is a brown oil, deviating from the colourless oil documented in the literature. However, this variance is not concerning as the transformation remains clean and free from the generation of additional side products, which is confirmed from the comparative ^1H NMR spectrums obtained.

The subsequent step entails the nitration of **34** to form 1-nitro-2,4,6-tricyclohexyl phenyl (**35**). This transformation is accomplished by introducing HNO_3 to **34** in an approximately 9:4:5 solvent ratio of DCM, Ac_2O and AcOH , respectively. The progress of this reaction is monitored by a distinct alteration in colour transitioning from red to a dark brown/purple hue. Following the completion of the reaction, a light brown powder is isolated. Efforts to recrystallise our obtained powder from hot ethanol, in accordance with Savka and Plenio procedure, proved unsuccessful. Instead, washing our isolated product with ethanol, allowed for a clean **35** product. Despite no recrystallisation, our approach obtained higher yields (94.6%), compared to the reported figures in the literature for this particular step (58%).



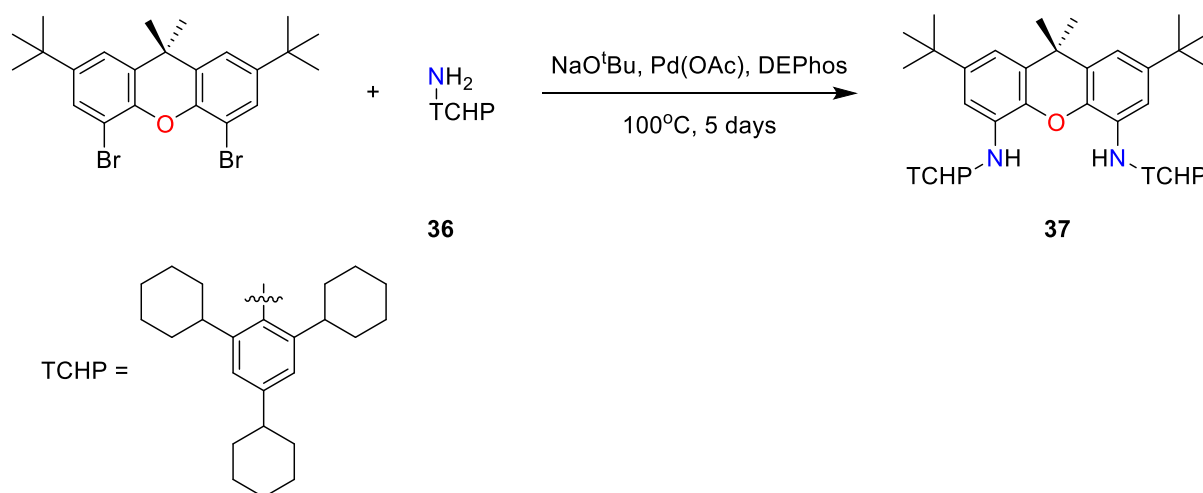
Scheme 13. Synthesis of THCP amine, 2,4,6-tri cyclohexyl phenyl aniline (**36**).

Finally, **35** undergoes reduction with HCl to yield the corresponding amine, 2,4,6-tri cyclohexyl phenyl aniline (**36**). This reduction process was executed in alignment with established literature methods. While the literature stated a pH adjustment to 9 – 10, we observed that following this protocol yielded minimal product and complicated the subsequent work-up protocols. Consequently, we made a modification to this step, adjusting the pH to approximately 6 – 7, which proved advantageous in achieving slightly improved yields compared to our efforts to follow the exact literature procedure. Despite these refinements, our yield for obtained for compound **36** was reduced (64%), compared to the 85% yield attained in the literature. This reduction in yield can be attributed to the need to isolate crystals to obtain the pure amine product. Consequently, the isolation of crystals was a multi-stage endeavour, distinguishing this step from the preceding two steps. With the TCHP amine synthesised, the synthesis of the $\text{xNON}^{\text{TCHP}}$ ligand can be initiated.

2.4 $\text{xNON}^{\text{TCHP}}$ Ligand Synthesis

Previously we have successfully followed the literature procedure for the synthesis of the $\text{xNON}^{\text{Dipp}}$ ligand system.⁹⁴ However, when changing the amine substituent to the TCHP amine (**36**) we observed that 16 hours was not long enough for this reaction to be successful. After subsequent trials conducted, the optimum reaction time was complete after 5 days at 100°C. This synthesis is conveniently performed in a ‘one pot’ manner to yield **37** (Scheme 14). The

starting materials, including 4,5-bis(2,4,6-tricyclohexylanilido)-2,7-di-tertbutyl-9,9-dimethyl-xanthene, palladium acetate (Pd(OAc)), TCHP amine (**36**), and (Oxydi-2,1-phenylene)bis(diphenylphosphine) (DEPhos) (Pd(OAc) and DEPhos are used in catalytic amounts), are combined in an oven-dried ampoule charged with a magnetic stir bar under an N₂-atmosphere. Afterwards, the ampoule is transferred into the glove box for the addition of sodium tert-butoxide (NaO^tBu) and toluene. The described procedure ensures the complete exclusion of air from the ligand itself, thereby maintaining an oxygen and moisture-free ligand for subsequent reactions. By eliminating air, the integrity and reactivity of the ligand and overall reaction can be preserved, ensuring reliable and reproducible results. While this precaution is not essential, we have observed an improved yield from 27.8% to 84.7% when following these conditions.



Scheme 14. Synthesis of TCHP ligand, [(xNON^{TCHP}) H₂]²⁻ (**37**) (catalytic amounts of Pd(OAc) and DEPhos are used in this reaction).

Upon completion of the reaction and work up preparations the organic layers are combined then dried over MgSO₄ and subsequently concentrated to approximately 10 mL, which obtained a concentrated brown solid, crude [(xNON^{TCHP})H₂]²⁻, **37**. To purify the crude **37**, a recrystallisation process is performed using a minimal amount of hot toluene to obtain off-white crystals, **37**.

The ¹H NMR spectrum of **37** suggests the synthesis of (xNON^{TCHP})H₂ was successful. Notably, a distinct singlet peak at 5.87 ppm with an integration for 2 protons is observed, indicating the presence of an N–H peak (Figure 8, indicated in the blue box). Furthermore, the ¹H NMR spectrum of **37** also exhibited corresponding aromatic peaks at 6.91 and 6.59 ppm, attributed to XA–CH (indicated in the orange box). These peaks, similarly, demonstrate an integration for two protons each. A comparison can be drawn between these peaks and those

of (xNON^{Dipp})H₂, specifically the N–H doublet peak observed at 5.93 ppm and the XA–CH peaks at 6.99 and 6.51 ppm. In addition to these ¹H NMR peaks of **37**, other distinctive peaks at 1.64 and 1.17 ppm exhibit integrations for 6 and 18 protons, indicating the presence of the methyl and ^tBu groups, respectively, located on the xanthene backbone. The inclusion of all these observed peaks and comparable values obtained to (xNON^{Dipp})H₂ provides evidence to suggest that (xNON^{TCHP})H₂ has been successfully synthesised.

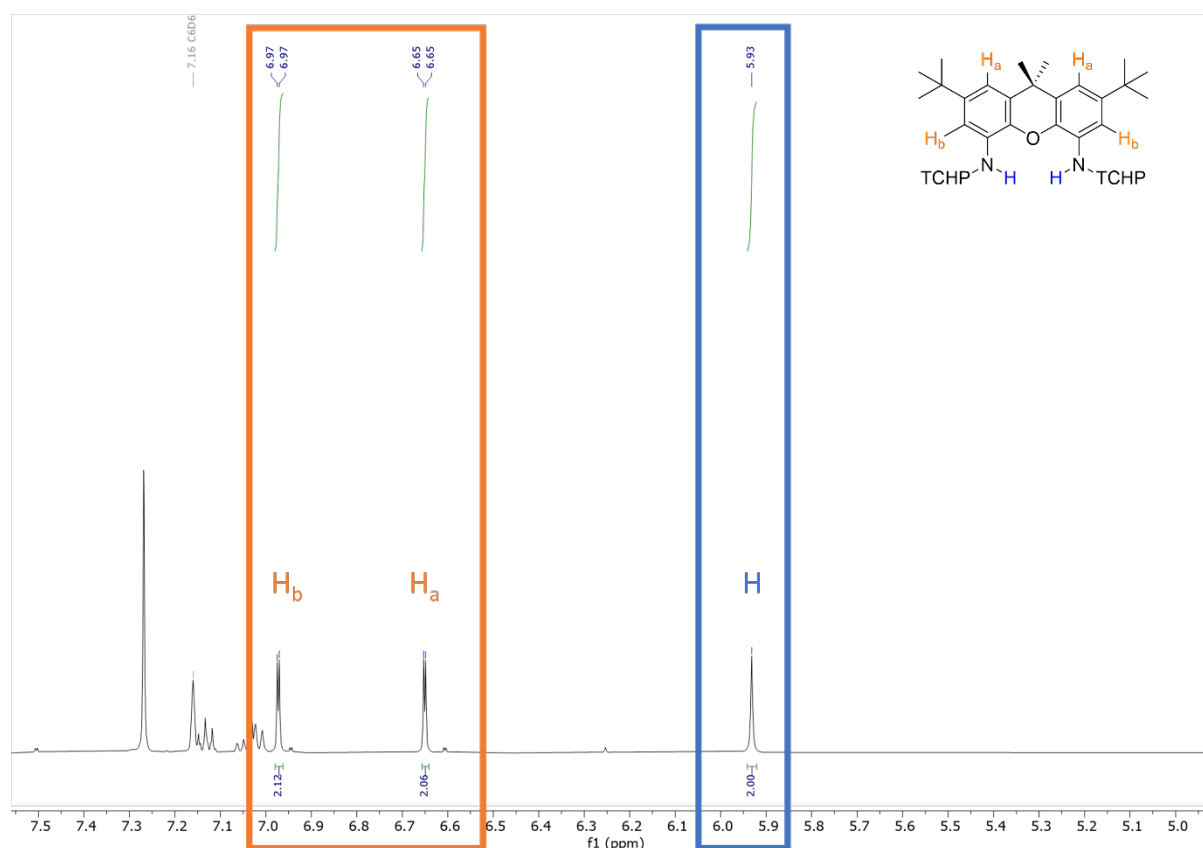


Figure 8. ¹H NMR spectrum (126 MHz, C₆D₆) of 4,5-bis(2,4,6-tricyclohexylanilido)-2,7-di-tertbutyl-9,9-dimethyl-xanthene, **37**. Orange box = XA–CH, blue box = NH. The spectrum has been enlarged between 5–7.5 ppm, peaks ranging from 1–3.5 ppm are removed for clarity.

Colourless blocks of **37** were suitable for a single crystal X-ray crystallographic experiment, showing that when **37** is in the solid-state it possesses a planar semi-symmetric structure centred around the oxygen atom in the ligand system (Figure 9). Within the xanthene backbone almost no bending is observed and C₂ symmetry is followed, giving **37** a planar xanthene backbone. The asymmetry in the ligand arises from the TCHP *N*-substituents, which are slightly twisted around the nitrogen atoms to account for their bulkiness. No comparable conclusions can be made between **37** and (xNON^{Dipp})H₂, due to lack of reported crystallographic characterisation conducted for the (xNON^{Dipp})H₂ ligand system (to note the Anker research group has crystallographic data for (xNON^{Dipp})H₂, however, this data has not

undergone a thorough work-up procedures and, consequently cannot be employed for direct comparison purposes).

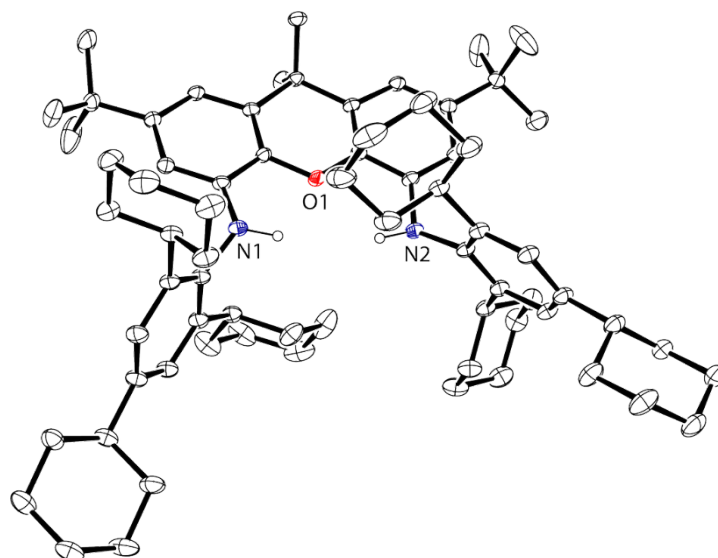


Figure 9. Ortep representation (ellipsoid 30% probability) of 4,5-bis(2,4,6-tricyclohexylanilido)-2,7-di- tertbutyl – 9,9-dimethyl-xanthene [(xNON^{TCHP})H₂]. Selected hydrogen atoms have been omitted for clarity.

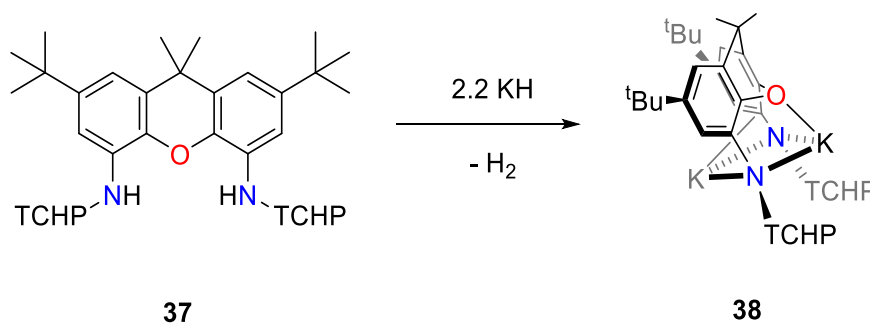
Following the successful synthesis of the (xNON^{TCHP})H₂ ligand system, our central focus revolves around the utilisation of this ligand to stabilise an indyl anion, surpassing the stabilisation achieved by the (xNON^{Dipp})H₂ ligand. The use of (xNON^{TCHP})H₂ as a ligand offers several potential advantages due to the bulky nature of the TCHP *N*-substituent, which should provide steric protection for the indium centre, and help to stabilise the reactive species as well as prevent unwanted side reactions. Additionally, the xanthene backbone should offer structural rigidity, and prevent ligand rearrangement which has been reported with the NON^{Dipp} ligand system.⁹⁴

Chapter 3. Synthesis of $x\text{NON}^{\text{TCHP}}$ Indyl Anions

With our newly acquired ligand in hand (**37**), we sort to synthesis a novel indyl anion. The initial strategy involved drawing inspiration from a reported literature example conducted by Coles *et al*, wherein the synthesis of $[(\text{NON}^{\text{Dipp}})\text{InK}]_2$, (**20**) was successfully accomplished (Scheme 6).⁶⁷ Firstly, Coles *et al* potassiated their $(\text{NON}^{\text{Dipp}})\text{H}_2$ ligand, obtaining $(\text{NON}^{\text{Dipp}})\text{K}_2$. Repeating this procedure on **37** allowed us to obtain a new potassiated ligand, described below.

3.1 Synthesis of $(x\text{NON}^{\text{TCHP}})\text{K}_2$ (**38**)

Compound $(x\text{NON}^{\text{TCHP}})\text{K}_2$ (**38**) is obtained by the addition of 2.2 equivalents of potassium hydride to **37** in toluene (Scheme 15). This reaction is heated for 48 hours at 80°C under a nitrogen atmosphere. After allowing the reaction to cool to room temperature, the compound in solution is filtered away from any remaining KH to obtain a light green solution, which is dried *in vacuo* to obtain **38**.



Scheme 15. Synthesis of $(x\text{NON}^{\text{TCHP}})\text{K}_2$, **38**. Each potassium atom is bound to one toluene molecule, which has been emitted for clarity.

In the resulting ^1H NMR spectra of **38**, we see a disappearance of the peak at 5.87 ppm consistent with the loss of the N–H groups found in **37**. Additionally, the aromatic backbone peaks have had an up-field shift, which now appears at 6.62 and 6.25 ppm. To further characterise **38**, a single crystal X-ray crystallography experiment was employed, to confirm the formation of our product (Figure 10).

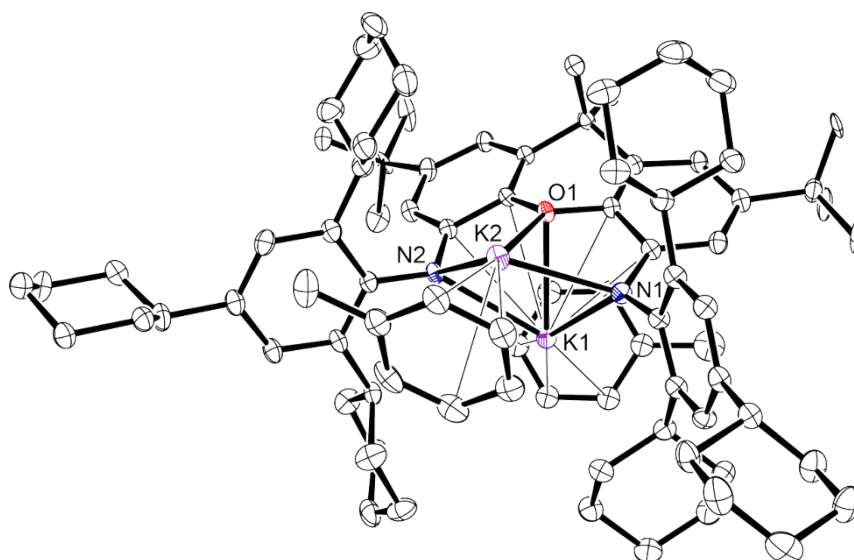


Figure 10. Ortep representation of (ellipsoid 30% probability) $(x\text{NON}^{\text{TCHP}})\text{K}_2$ (**38**). Hydrogen atoms have been omitted for clarity. Selected bond lengths (Å) and angles (deg). **38**: K1–N1 2.7231, K1–N2 2.7821, K1–O1 2.7373, K2–N1 2.7434, K2–N2 2.7566, K2–O1 2.6492.

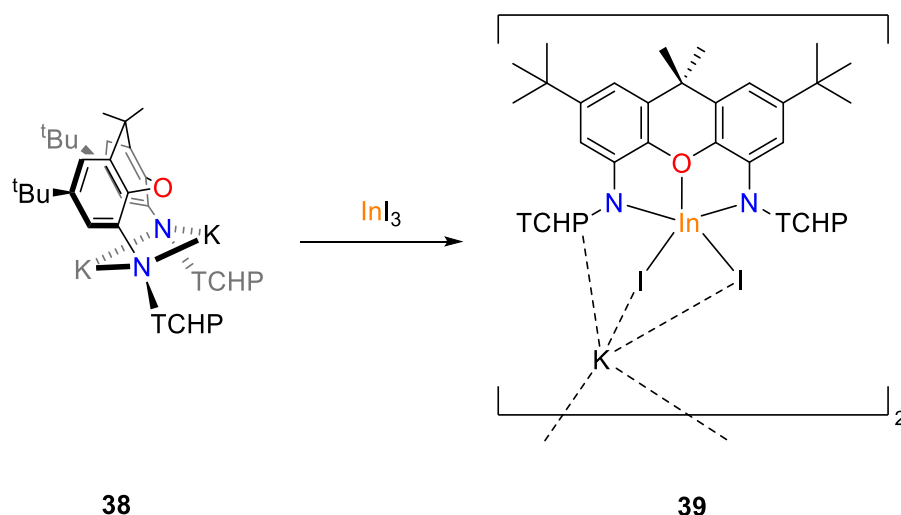
The solid-state data of compound **38**, exhibits a slightly bent xanthene backbone, with the two potassium ions coordinated to the inner regions of the xanthene backbone. Additionally, each potassium ion is also coordinated with one toluene molecule. The TCHP *N*-substituents are now symmetric around the ligand and follow C_2 symmetry. The crystallographic data further confirms the absence of the N–H bonds and the presence of two potassium cations. These two potassium ions exhibit similar bond length to nitrogen measuring 2.7231 Å and 2.7821 Å for K1, and for K2 measuring 2.7434 Å, and 2.7566 Å. As well as the K–O bond lengths for K1 and K2 are 2.7373 Å and 2.6492 Å correspondingly.

3.2 Synthesis of $(x\text{NON}^{\text{TCHP}})$ Indyl Anions

3.2.1 Synthesis of $(x\text{NON}^{\text{TCHP}})\text{InK}(\text{Et}_2\text{O})(\text{THF})_2$ (**40**)

Adhering to the methodology outlined by Coles *et al* for the next step towards the isolation of an indyl anion, they reacted InCl_3 with $(\text{NON}^{\text{Dipp}})\text{K}_2$ resulting in the formation of $(\text{NON}^{\text{Dipp}})\text{InCl}_2$ (**19**). However, considering the subsequent reaction involves a reduction with potassium metal to generate their indyl anion, **20**, with the formation of KCl as the reaction by-product (Scheme 6). Notably, potassium ions establish a more stable bond with iodide ions. Thus, an alteration was pursued wherein InCl_3 was substituted with InI_3 , aiming to determine if this modification yields the iodide derivative akin to Coles' original indium-chloride-containing complex, **19**. Our investigation led to the reaction of InI_3 with **38** in a 3:1 solvent ratio of Et_2O hexane resulting in the formation of $[(x\text{NON}^{\text{TCHP}})\text{InI}_2\text{K}]_2$ (**39**) (Scheme 16). The characterisation of **39** was obtained by 2D NMR spectra and a single crystal X-ray

crystallographic experiment. Shifted XA–CH aromatic peaks were observed in the ^1H NMR spectrum, which are now present at 6.75 and 6.46 ppm. Despite the considerable shifts in the majority of the ^1H NMR spectrum, there were still underlying peaks that did not correspond to **39**. Therefore, achieving complete isolation of **39** posed a challenge due to a consistent presence of approximately 15% of **37** remaining, as shown in the ^1H NMR spectrum. To address this issue, a hexane wash is implemented into the procedure, given that **37** is soluble in hexane while **39** is not.



Scheme 16. Synthesis of $[(x\text{NON}^{\text{TCHP}})\text{InI}_2\text{K}]_2$, **39**.

The recrystallisation process yielded light-green crystals of sufficient quality to conduct a single crystal X-ray crystallographic experiment, which provided structural features of **39** (Figure 11). In the solid state, **39** exists as a dimer, with the potassium atoms coordinated to a flanking aryl TCHP substituent and both iodide ions. The dimeric structure of **39** indicates the presence of intermolecular interactions between the potassium atoms and the indium iodide units. These interactions contribute to the stability of the dimeric form of **39** and play a crucial role in its reactivity. The bond distances within the dimer of **39** reveal that the indium centres are three-coordinate to the ligand, with the bond distance of 2.1330(18) Å, 2.1574(19) Å for In–N bonds and 2.2942(16) Å for In–O coordination. When compared to $(x\text{NON}^{\text{Dipp}})\text{AlI}$ (**25**), several similarities and differences are observed.⁷² The aluminium complex is also a three-coordinate ligand system, but the Al–N and Al–O bond distances (1.846(2) and 1.846(2) Å for Al–N and 1.967(2) Å for Al–O) are smaller compared to **39**. This could be attributed to the difference in ionic radii of indium and aluminium and/or the different *N*-substituent used for these complexes. It is noteworthy that the aluminium iodide complex does not form an iodide ate complex but rather a single Al–I bond (Al–I = 2.497(1) Å) is observed. Crystallographic data also shows that the indium centre in **39** is also bonded to two iodides, making it a five-

coordinated indium complex, with bond distances of 2.7660(2) Å and 2.7717(2) Å. A notable feature in **39** is the relatively large angle between N–In–N, which measures 132.31(7)°.

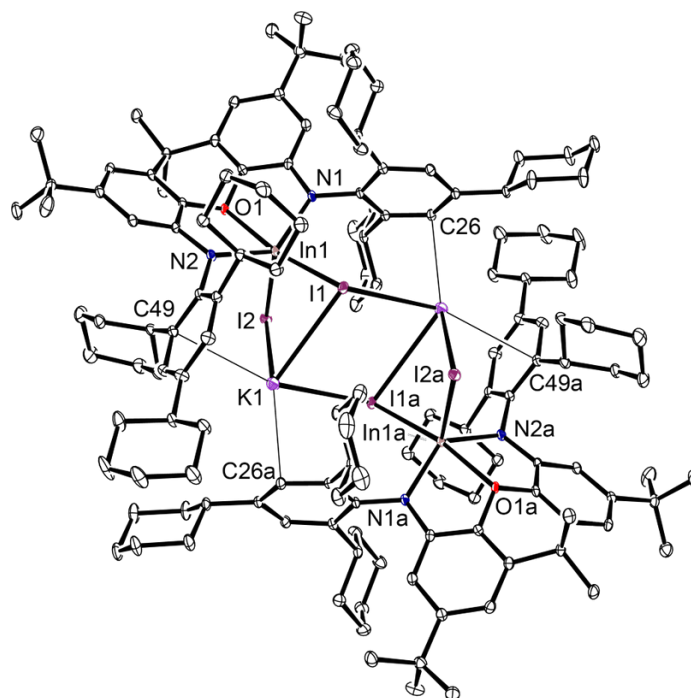


Figure 11. Ortep representation of (ellipsoid 30% probability) $[(x\text{NON}^{\text{TCHP}})\text{InI}_2\text{K}]_2$, (**39**). Hydrogen atoms have been omitted for clarity. Selected bond lengths (Å) and angles (deg). **39**: In1–O4 2.2942, In1–N1 2.1339, In1–N2 2.1573, In1–I1 2.7717, In1–I2 2.7670, I1...K1 3.5018, I2...K1 3.5080, N1–In1–N2 132.31.

The addition of an indium trihalide, namely InI_3 , to **38** results in a similar structure obtained by Cole *et al*, from their reaction of InCl_3 , to **18**. Both structures of these complexes exhibit two halides on the indium centre. However, the difference between these compounds is that **39** has a dimer ate structure, whereas **19** grows in a polymeric chain formation. As well as differences observed for the bond angles and lengths, due to the alteration in ligand systems used.

Continuing in the same manner of Coles *et al* approach, wherein they conducted a reduction on their original indium–chloride–containing complex, **19** using potassium metal, we replicated a similar procedure with **39**. However, the reduction of **39** was not a simple explanation, corresponding to Coles *et al* procedure. Therefore, we had to screen a range of reaction conditions, to find what worked for our $x\text{NON}$ system (Table 3). These attempts encompassed diverse strategies to acquire the new indyl anion and to obtain an improved yield. Differing solvents, including mixtures of hexane, diethyl ether, THF and toluene, were tested in different ratios during the experimentation process. As well as varying equivalents of potassium were utilised to evaluate their impact on the formation of the indyl anion. Additionally, alternative reducing agents were explored to investigate their effectiveness. The

type of potassium used for reducing the compound can have an impact on the reaction time due to variations in surface area. Different forms of potassium, such as K_{metal} , and KC_8 (KC_8 = potassium graphite), will have differing surface areas that can react with the other materials, therefore affecting their reactivity. A higher surface area for KC_8 allows for increased contact with reactants, potentially leading to faster reaction rates. The selection of the appropriate potassium form is crucial in optimising the reaction conditions and achieving the desired reaction kinetics. It is important to acknowledge that reaction times differed across experiments. In each case, the reaction was halted upon the observation of the desired distinct yellow colour. However, these times were inconsistent and not reproducible and therefore the most consistent procedure for identifying the completeness of reaction was monitoring colour.

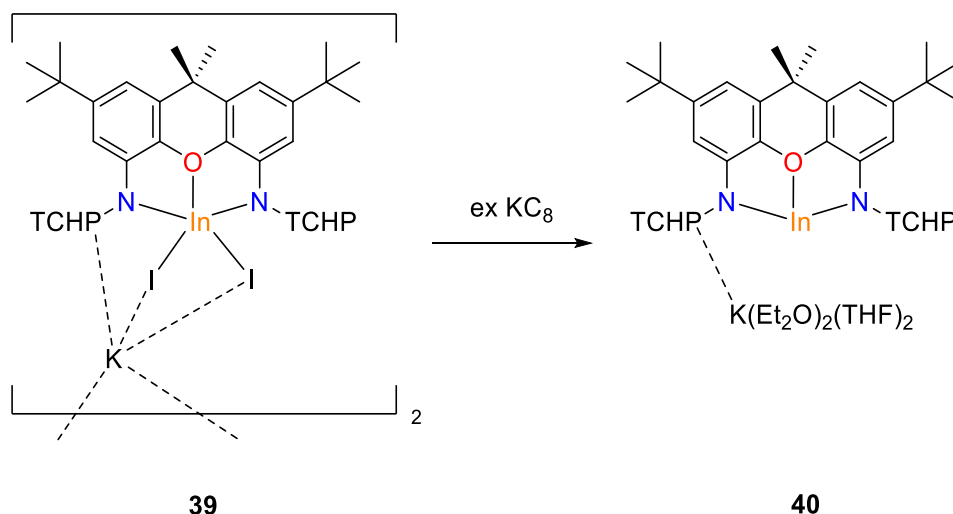
Table 3. Attempts to find the best reaction condition to the new indyl anion through the reduction route.

Starting materials	K equivalents	Reaction solvent	Success	Yield	Crystal structure
$(x\text{NON}^{\text{TCHP}})\text{InI}_2\text{K}$	3 K_m	1:3 Hexane: Diethyl ether	x	—	x
$(x\text{NON}^{\text{TCHP}})\text{InI}_2\text{K}$	2eq K_m	Hexane	x	—	x
$(x\text{NON}^{\text{TCHP}})\text{InI}_2\text{K}$	2eq KC_8	Hexane	✓	<10%	x
$(x\text{NON}^{\text{TCHP}})\text{InI}_2\text{K}$	2eq KC_8	Diethyl ether	x	—	x
$(x\text{NON}^{\text{TCHP}})\text{InI}_2\text{K}$	2eq KC_8	3:2 Hexane: Diethyl ether	✓	<10%	x
$(x\text{NON}^{\text{TCHP}})\text{InI}_2\text{K}$	2eq KC_8	Toluene	✓	<10%	x
$(x\text{NON}^{\text{TCHP}})\text{InI}_2\text{K}$	3eq KC_8	Toluene	✓	<10%	x
$(x\text{NON}^{\text{TCHP}})\text{InI}_2\text{K}$	2eq KC_8	2:1 Hexane: Diethyl ether	✓	53.5%	✓

During these reactions, we encountered challenges in achieving satisfactory yields of the indyl anion despite employing an assortment of techniques. These difficulties may be attributed to several factors, such as reaction conditions, solubility of materials and choice of reagents. However, from the research conducted, we found that the addition of $(x\text{NON}^{\text{TCHP}})\text{InI}_2$ (**39**) to two equivalents of KC_8 in a 2:1 solvent ratio of hexane and Et_2O obtained the greatest yield of 53.5% forming $(x\text{NON}^{\text{TCHP}})\text{InK}(\text{Et}_2\text{O})(\text{THF})_2$, **40** (Scheme 17). The chosen solvent ratio provides the necessary reaction conditions allowing for optimal solubility and increased yields.

A slight disparity is evident in the ^1H NMR spectra of compounds **40** and **39**, particularly in their respective $\text{XA}-\text{CH}$ peaks at 6.76 and 6.51 ppm versus 6.75 and 6.46 ppm for **40** and **39** respectively. This small distinction presents challenges in distinguishing the

formation of the indyl anion. However, the visual differentiation in the colours of the crystals for **40** (bright yellow crystals) and **39** (light green/yellow crystals) offered a notable contrast.



Scheme 17. Synthesis of $[(x\text{NON}^{\text{TCHP}})\text{InK}(\text{Et}_2\text{O})_2(\text{THF})_2]$, **40**.

To confirm the existence of an indyl anion, a single crystal X-ray crystallographic experiment was conducted on the bright yellow crystals of compound **40** (Figure 12). In the crystal structure of **40**, the potassium cation is coordinated to one of the phenyl rings on the TCHP *N*-substituent. Additionally, two Et_2O molecules and two THF molecules are coordinated to the potassium cation. The crystallographic analysis of **40** also provided bond distances for the three-coordinated indium centre. The bond lengths for the In–N bonds were determined to be 2.268(2) and 2.345(2) Å, while the In–O bond length was found to be 2.5171(18) Å. Furthermore, the X-ray crystallography analysis revealed that the bond angle between N–In–N atoms in **40** was determined to be 119.40(8)°. Notably, this bite angle is significantly larger than the N–In–N bite angle of Coles *et al* indyl anion, **20**, which is 98.24(9)°. This disparity arises from the distinct dimensions of the ligand attachments for NON and $x\text{NON}$.

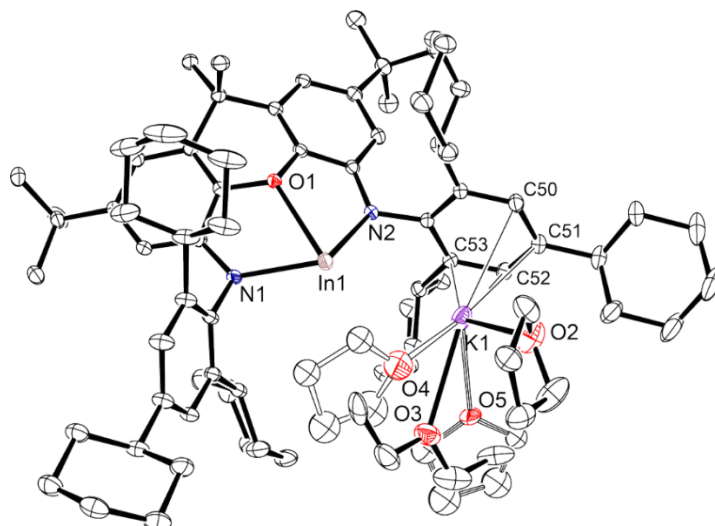
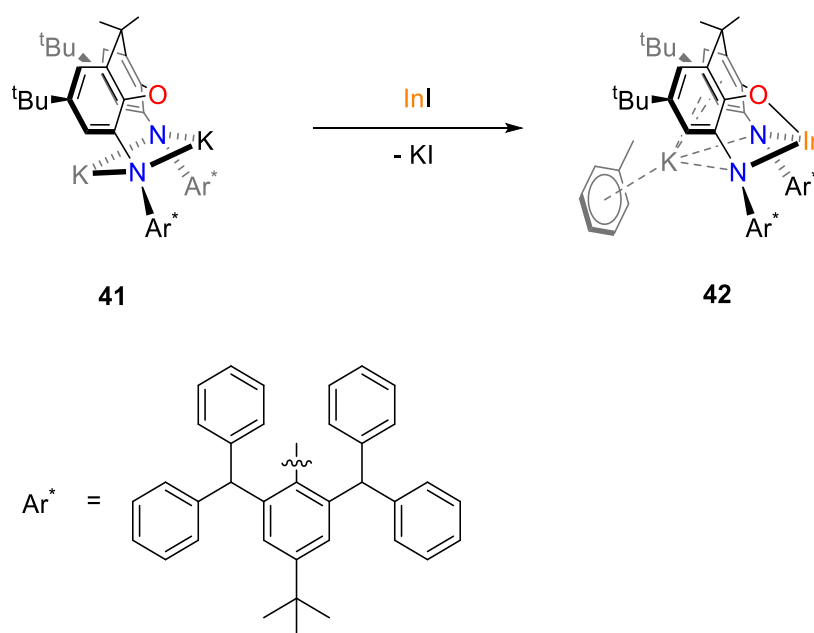


Figure 12. Ortep representation of (ellipsoid 30% probability) $(x\text{NON}^{\text{TCHP}})\text{InK}(\text{Et}_2\text{O})_2(\text{THF})_2$, (**40**). Hydrogen atoms have been omitted for clarity. Selected bond lengths (Å) and angles (deg). **40**: In1–O4 2.5171, In1–N1 2.2680, In1–N2 2.3448, In1...K1 3.6074, N1–In1–N2 119.40.

The use of **39** as a precursor to obtaining a new indyl anion has its limitations, as it often results in a mixture of **37**, unreacted **39**, and **40** which are all present in the ^1H NMR spectrum. Despite efforts to wash and isolate the desired product **40**, solubility issues and difficulties in separating the unwanted materials, lead to a poor yield and an impure product (yield = 53.5%, mixture of **37**, **39**, and **40**). To overcome these challenges and obtain a cleaner indyl anion, alternative synthetic routes were explored. The decision to exclude the use of **39** in the next two synthetic routes for the indyl anion synthesis is a strategic approach to address the issues encountered with unwanted starting materials and breakdown products present in the ^1H NMR spectrum. These approaches also simplify the synthetic pathway by eliminating the synthesis of **39**. This allows for a more direct route to the desired indyl anion. Furthermore, different starting materials were examined to assess their suitability for the synthesis of the indyl anion. Through these modifications, we aimed to optimise the synthetic route and improve the efficiency of the new low-valent indyl anion formation.

3.2.2 Synthesis of $(x\text{NON}^{\text{TCHP}})\text{InK}(\text{Cp}^{4*})\text{K}$ (**46**)

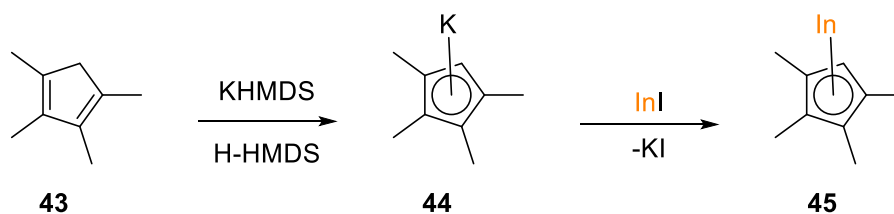
In the Anker research laboratory, we have synthesised the super bulky indyl anion using Ar^* as the *N*-substituent. In this route the addition of $(x\text{NON}^{\text{Ar}^*})\text{K}_2$ (**41**) to InI resulted in a high yielding (94.0%) reaction to give $(x\text{NON}^{\text{Ar}^*})\text{InK}$, **42** (Scheme 18).



Scheme 18. Synthesis of $(x\text{NON}^{\text{Ar}^*})\text{InK}(\text{tol})$, **42**.

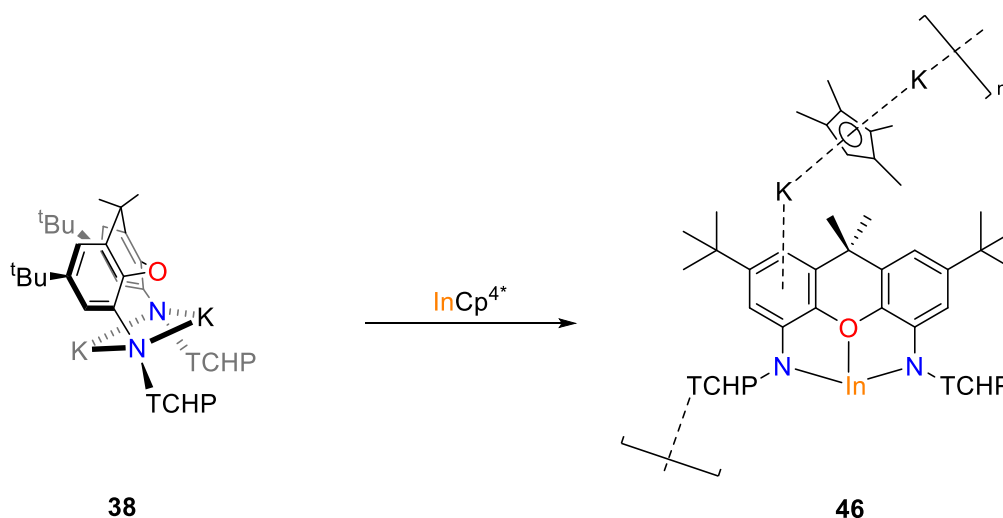
Given the substantial bulk of both Ar^* and TCHP N -substituents, we questioned the applicability of this approach to our ligand system, $(x\text{NON}^{\text{TCHP}})$. However, InI is poorly soluble in coordinating solvents, which pose a constraint for the reaction to occur. As an alternative, we explored a different source of In(I) that displayed enhanced solubility, namely Cp (Cp = cyclopentadienyl) and Cp^{4*} (Cp^{4*} = 1,2,3,4-tetramethyl cyclopentadiene). Given InCp and InCp^{4*} are both soluble we can observe the reaction *in situ* in a *J Youngs* NMR tube. Despite our attempts with the synthesis of InCp we encountered challenges and failed to achieve the desired results, attributed to the absence of chemical reaction occurring. Subsequently, we decided to switch to a slightly bulkier Cp^{4*} precursor to form the In(I) complex.

Before the reaction of **38** can be tested, it is necessary to synthesise InCp^{4*} . The synthesis of InCp^{4*} involves a two-step process. The first step is the potassiation of Cp^{4*} , which is achieved by reacting $\text{Cp}^{4*}\text{-H}$ with potassium hexamethyldisilazide (KHMDs) in toluene, to form $\text{K}(\text{Cp}^{4*})$, **44** (Scheme 19). It should be acknowledged that InCp^{4*} is a light sensitive compound, thereby introducing a slight complication in the reaction conditions. Nonetheless, conducting the reaction under subdued light, will eliminate additional issues in proceeding reactions.



Scheme 19. Synthesis of InCp^{4*} , **45**.

In the second step, **44** is reacted with InI in the dark in a solution of THF. This reaction leads to the formation of InCp^{4*} , **45**. This two-step process allows for the synthesis of the indyl anion to take place. Correspondingly, the synthesis involves the combination of $(\text{xNON}^{\text{TCHP}})\text{K}_2$ (**38**) with InCp^{4*} (**45**) in a C_6D_6 solvent, followed by heating at 60°C for the duration of 2 hours, resulted in the formation of $(\text{xNON}^{\text{TCHP}})\text{InK}(\text{Cp}^{4*})\text{K}$, **46** (Scheme 20). A gradual alteration in colour was noted during the application of heat, transitioning from light green to a yellow/orange solution. Following the completion of this reaction, ^1H NMR spectroscopy was employed to observe shifts in the spectrum. Indeed, noticeable shifts were observed, the aromatic $\text{XA}-\text{CH}$ peaks were recorded at 6.63 and 6.25 ppm, indicating the formation of a new product.



Scheme 20. Synthesis of $(\text{xNON}^{\text{TCHP}})\text{InK}(\text{Cp}^{4*})\text{K}$, **46**.

To confirm the nature of the synthesised compound, a single crystal X-ray crystallographic experiment was conducted on **46**, showcasing a unique structure (Figure 13). The crystal structure analysis revealed that the unit cell of **46** contains the indyl anion, two potassium counter ions and the Cp^{4*} ligand. One of the potassium ions is coordinated to both an aryl group on the xanthene backbone and the Cp^{4*} ligand. Additionally, the Cp^{4*} ligand itself is coordinated with another potassium cation. The arrangement of Cp^{4*} within the crystal structure allows the unit cell of **46** to grow into a polymer structure. Where K_2 is coordinated with another xanthene part of a different indyl anion unit. The crystal structure analysis of **46**

revealed an N–In–N bond angle of 119.72(12)°, indicating a similar spatial arrangement as observed in **39**. The bond distances between In–N were measured as 2.355(4) Å and 2.295(4) Å, while the In–O bond distance was found to be 2.519(3) Å. This confirms the presence of a three-coordinate indyl anion has been synthesised. Furthermore, the bond distance of In–K3 is recorded to be 3.6005(15) Å, indicating that there is the coordination of a potassium cation to compound **46**.

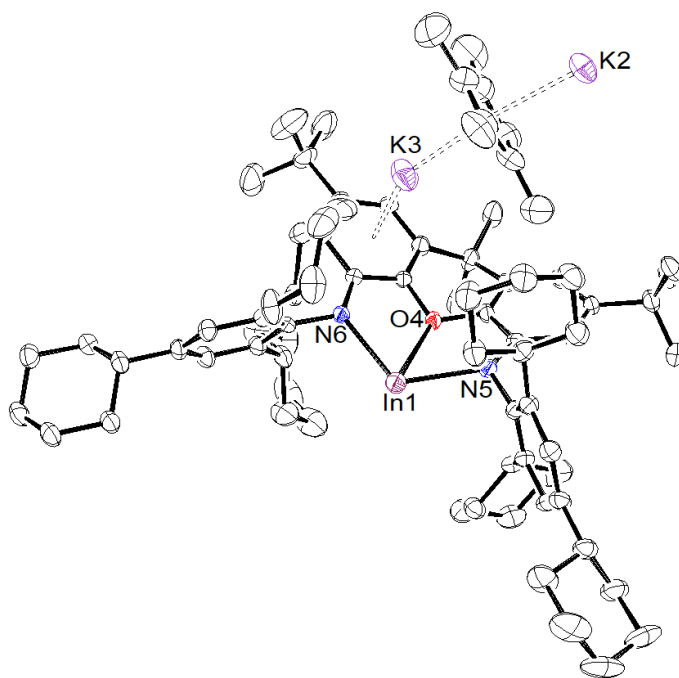


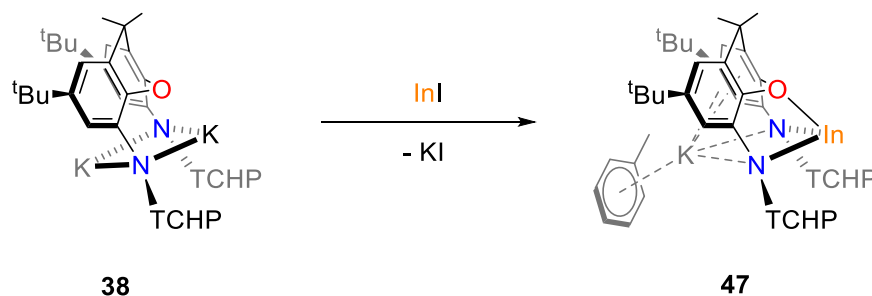
Figure 13. Ortep representation of (ellipsoid 30% probability) (x NON^{TCHP})InK(Cp^{4*}K) (**46**). Hydrogen atoms have been omitted for clarity. Selected bond lengths (Å) and angles (deg). **46**: In1–O4 2.5254, In1–N5 2.3484, In1–N6 2.2910, In1···K2 3.6061, N5–In1–N6 119.88.

Although this synthetic route resulted in the formation of a different indyl anion (**46**), a considerable decrease in yield was obtained, 24.1%. Furthermore, in the analysis of the synthesis of **46**, it involves the synthesis of Cp^{4*}In, which introduced additional steps into the procedure. To simplify the synthetic procedure and avoid the need to synthesise Cp^{4*}In, we explored the use of a different source of In(I) in combination with **38** to investigate the possibility of obtaining an indyl anion.

3.2.3 Synthesis of (x NON^{TCHP})InK(tol) (**47**)

In the next synthetic route, InI is employed as the source of In(I), eliminating the need for additional steps to obtain an In(I) material. Despite InI's relatively insoluble nature, the utilisation of THF and increased reaction time resulted in the desired product. The reaction

between **38** and InI resulted in the formation of $(\chi\text{NON}^{\text{TCHP}})\text{InK}(\text{tol})$, **47** (Scheme 21). This indyl anion exhibits a different arrangement of the potassium cation.



Scheme 21. Synthesis of $[(\chi\text{NON}^{\text{TCHP}})\text{InK}(\text{tol})]$, **47**.

Through a single crystal X-ray crystallography experiment, it was confirmed that the potassium is coordinated at the back of the xanthene backbone, while also being coordinated to a toluene molecule (Figure 14). This coordination induces a bending effect in the xanthene backbone, evidenced by an N–In–N angle of 105.15(10)°. Additionally, the bond distances of the three-coordinate indyl anion are measured at 2.434(3), 2.455(3) and 2.498(2) Å for In–N and In–O respectively. The bond distance of In–K at 3.6226(8) Å is noteworthy, as it is longer than the typical ionic radii of both indium and potassium combined.⁹⁵ Therefore, confirming that indium is not directly bound to the potassium cation in **47**. Instead, the potassium has multiple attachments to the xanthene backbone, as illustrated in Figure 14. The unique coordination pattern supports the distinct reactivity potential of **47** as an indyl anion, which has not been seen in aluminyll anion chemistry.

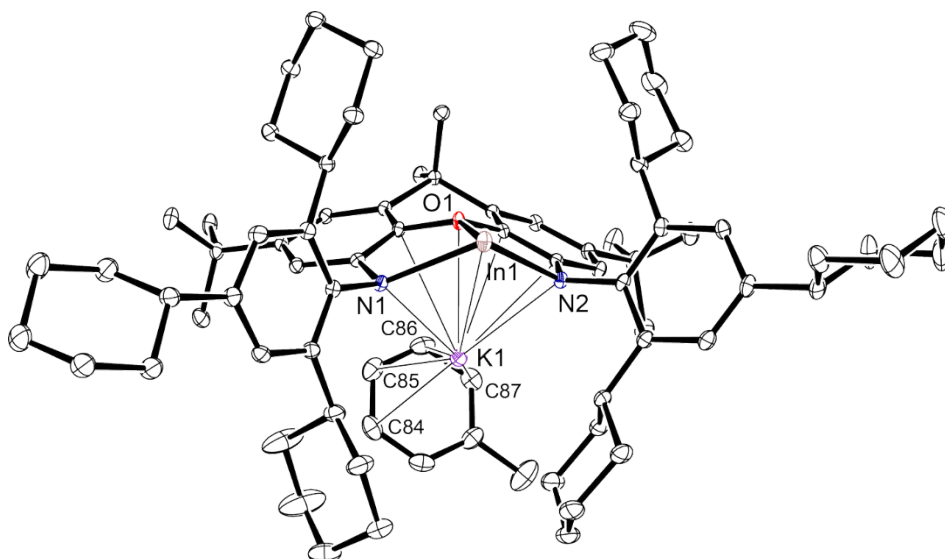


Figure 14. Ortep representation of (ellipsoid 30% probability) $(\chi\text{NON}^{\text{TCHP}})\text{InK}(\text{tol})$ (**47**). Hydrogen atoms have been omitted for clarity. Selected bond lengths (Å) and angles (deg). **47**: In1–O1 2.4979, In1–N1 2.4550, In1–N2 2.4338, In1···K1 3.5018, In1···K1 3.6226, N1–In1–N2 105.15.

During the reactions to synthesise a new indyl anion, we encountered challenges in achieving satisfactory yields despite employing an assortment of techniques. These difficulties may be attributed to several factors, such as reaction conditions, solubility of materials and choice of reagents. However, from the research conducted, we found that the addition of (xNON^{TCHP})K₂ to InI in THF obtained the greatest yield of 63%. By bypassing the need to synthesise an indium halide, or synthesise a In(I) precursor, this reaction method proved to be remarkably streamlined and required fewer steps.

3.2.4 Comparison of (xNON^{TCHP}) Indyl Anions

The initial distinction among these indyl anions (**40**, **46**, **47**) lies in the positioning of the potassium ion. In **40**, the potassium coordinates with one of the TCHP *N*-substituent as well as two Et₂O molecules and two THF molecules (Scheme 17). In **46**, the potassium is coordinated to one of the aryl rings on the xanthene backbone. This potassium is also coordinated to the Cp^{4*}, which in turn, is coordinated to another (xNON^{TCHP})InK unit, which grows to have a polymer arrangement (Scheme 20). In **47**, the potassium is coordinated to the inner parts of the xanthene backbone, causing a bending of the backbone around the potassium. Additionally, the potassium is also coordinated with a toluene molecule (Scheme 21).

When comparing these three recently developed indyl anion derivatives, it becomes evident that **40** and **46** display relatively comparable bond distances and angles (Table 4), despite the diversity in structures. On the other hand, **47** stands out with distinctively individual bond distances and angles, demonstrating the longest In–N bond lengths, measuring 2.434(3) and 2.455(3) Å, and the shortest In–O bond length of 2.498(2) Å. Additionally, **47** displays the smallest N–In–N bond angle of 105.15(10)°, setting it apart from the other indyl anions, **40** and **46**. The distinct bond distances and angles observed among these indyl anion compounds can be attributed to varying interactions between the indyl anion and its respective counter ions associated with the complex. Such disparities in the molecular geometry of these derivatives are likely to exert a significant influence on their chemical reactivity and physical properties. Therefore, it is essential to conduct in-depth investigations on all their reactivity patterns to obtain a comprehensive understanding of the underlying factors driving the observed structural differences.

Table 4. Comparing bond distances and bond angles for new MIP indyl anions, $(\chi\text{NON}^{\text{TCHP}})\text{InK}(\text{Et}_2\text{O})(\text{THF})_2$ (**40**), $(\chi\text{NON}^{\text{TCHP}})\text{InK}(\text{Cp}^{4*})\text{K}$ (**46**), and $(\chi\text{NON}^{\text{TCHP}})\text{InK}(\text{tol})$ (**47**).

Bond distance/angles	Indyl anion		
	$(\chi\text{NON}^{\text{TCHP}})\text{InK}(\text{Et}_2\text{O})_2(\text{THF})_2$ (40)	$(\chi\text{NON}^{\text{TCHP}})\text{InK}(\text{Cp}^{4*})\text{K}$ (46)	$(\chi\text{NON}^{\text{TCHP}})\text{InK}(\text{tol})$ (47)
In–N (Å)	2.268(2), 2.345(2)	2.295(4), 2.355(4)	2.434(3), 2.455(3)
In–O (Å)	2.5171(18)	2.519(3)	2.498(2)
In–K (Å)	3.6074(8)	3.6005(15)	3.6226(8)
N–In–N	119.40(8)°	119.72(12)°	105.15(10)°

The three synthesised indyl anions presented (**40**, **46** and **47**) all exhibit an MIP (monomeric ion pair) structural classification, where the potassium cation remains coordinated with the indyl anion complex. This structural classification also appears for several aluminyl anions⁹⁶⁻⁹⁸ as well as CDP^{97, 99-101} and SIP structures.^{76, 78, 79, 100} However, prior literature studies on the indyl anion by Coles *et al* confirmed through crystallography, that their indyl anion can be either in a CDP structure⁶⁷ or a SIP structure.⁶⁶ Considering these previous findings, efforts have been directed towards investigating the possibility of forming SIP complexes with our indyl anions, **40**, and **47**. By sequestering the potassium cation away from the indyl anion, it is anticipated that new reactivities and reaction pathways can be accessed.

Chapter 4. Reactivity of (xNON^{TCHP}) Indyl Anions

Drawing inspiration from the reactivity studies conducted on [(NON^{Dipp})InK]₂, (**20**), the research discussed below is directed towards subjecting our new indyl anions to comparable studies.

4.1 Stability of (xNON^{TCHP})InK(Et₂O)₂(THF)₂ (**40**)

The assessment of the new indyl anion's stability is necessary before other reactivity studies can be conducted. The stability was tested by subjecting **40** to variable temperatures ranging from 30 – 70°C. The sample was maintained at each temperature for 2 minutes before acquiring the ¹H NMR measurement, after which the temperature was increased for the next measurement. Due to the insoluble nature of **40** in C₆D₆ and toluene-d₈, cyclohexane-d₁₂ was the chosen solvent. Owing to the solvent choice of cyclohexane-d₁₂ higher temperatures could not be tested (boiling point of cyclohexane-d₁₂ = 80.7 °C). This method was monitored through the analysis of the ¹H NMR spectrum of **40**, which exhibits a consistent spectrum across a range of temperatures (Figure 15). Even when subjected to increasing temperatures from 30°C to 70°C, the structure of **40** remains unaffected. This indicates that **40** is a stable compound, allowing for its application in reactions that may require heating to solubilise in minimal amounts of solvent. The risk of **40** forming a breakdown product or becoming inert appears minimal, further supporting its potential utility.

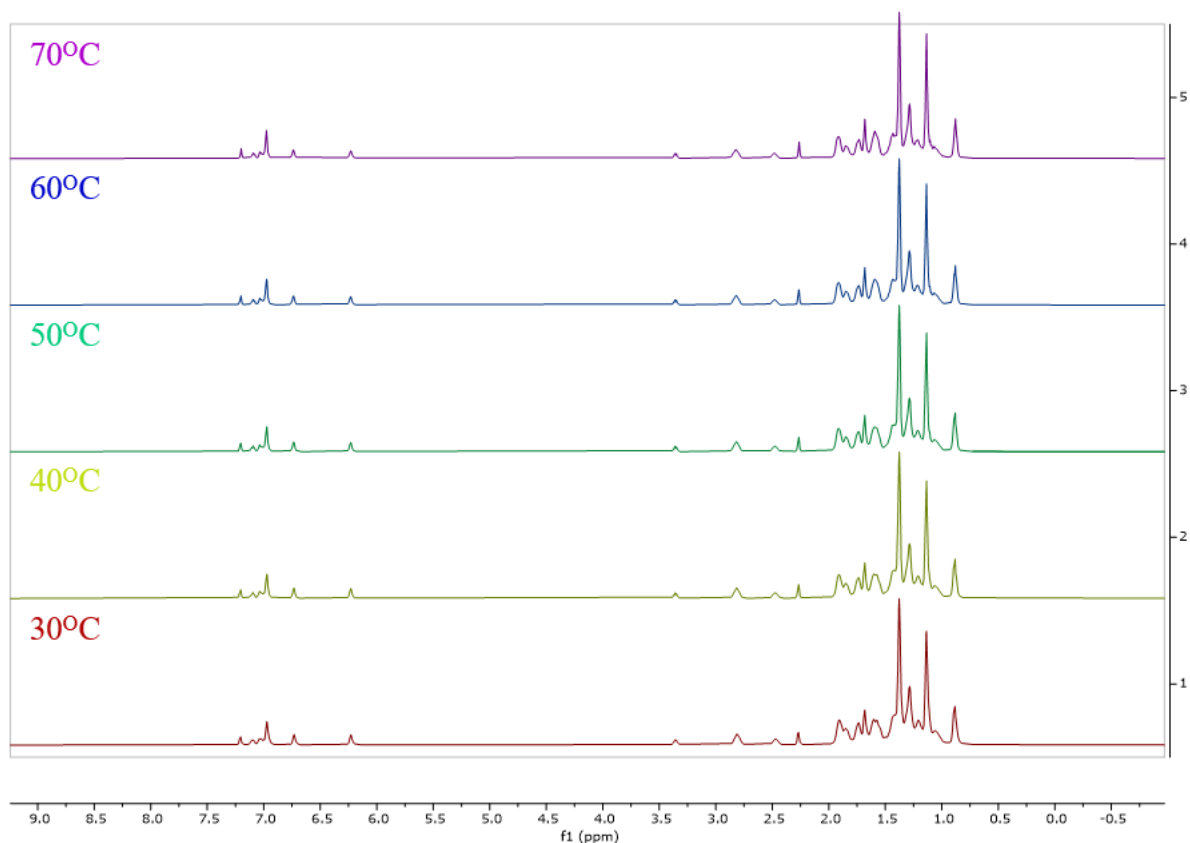


Figure 15. ^1H NMR spectrum of $(x\text{NON}^{\text{TCHP}})\text{InK}(\text{Et}_2\text{O})_2(\text{THF})_2$ (**40**) at varying temperatures.

Additionally, it is worth mentioning that the colour of **40** remains unchanged during the variable temperature analysis. This further confirms the stability of the compound is regular light conditions and provides additional evidence that there is no structural alteration occurring when **40** is subjected to higher temperatures.

4.2 Reactions With 18-crown-6

Cryptands and crown ethers are both complexes that can be utilised to encapsulate group 1 cations,¹⁰² which has previously been employed for aluminyl and indyl chemistry.^{66, 79-81, 103} These macrocyclic ligands differ in their dimensional states. Crown ethers are two-dimensional macrocyclic polyethers.¹⁰⁴ Whereas cryptands are bicyclic or oligocyclic macro heterocycles and are often described as three-dimensional analogues of crown ethers.¹⁰⁵ Both cryptands and crown ethers are well-known for their selective complexation with different ionic species, including alkali-metals and alkaline-earth-metal cations.^{106, 107} One of the characteristic properties of crown ethers is their ability to form complexes with high affinity towards specific cations. This selectivity is determined by the size of the cavity in the crown ether, which can accommodate specific cations most effectively. The stability of these

complexes is influenced by factors such as the size of the ion relative to the cavity size, the charge of the ion, the conformation of the crown ether ring, and the nature of the solvent.

Attempts to form the separated ion pair (SIP) with the new indyl anions and sequester the potassium cation away from the indyl anion, have been explored. Although both 18-crown-6 and 2,2,2-cryptand compounds can sequester potassium ion and form stable complexes, the decision to use 18-crown-6 instead of 2,2,2-cryptand was primarily driven by accessibility and cost considerations. In this case, 18-crown-6 (Figure 16) has been specifically chosen to encapsulate the potassium cation, to ideally form a indyl anion SIP structure with **40**, **46**, or **47**. The selection of 18-crown-6 is based on its cavity size, which is well-suited for accommodating the potassium cation. The cavity size of 18-crown-6 typically ranges from 1.34–1.55 Å, while the effective ionic radius of potassium is approximately 1.38 Å.¹⁰⁸ Therefore allowing for efficient encapsulation of the potassium cation by 18-crown-6.

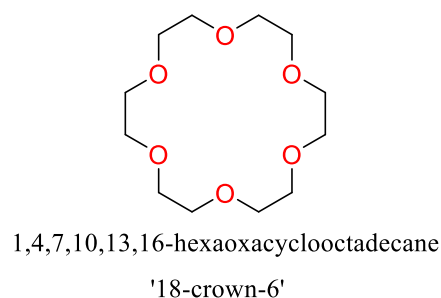
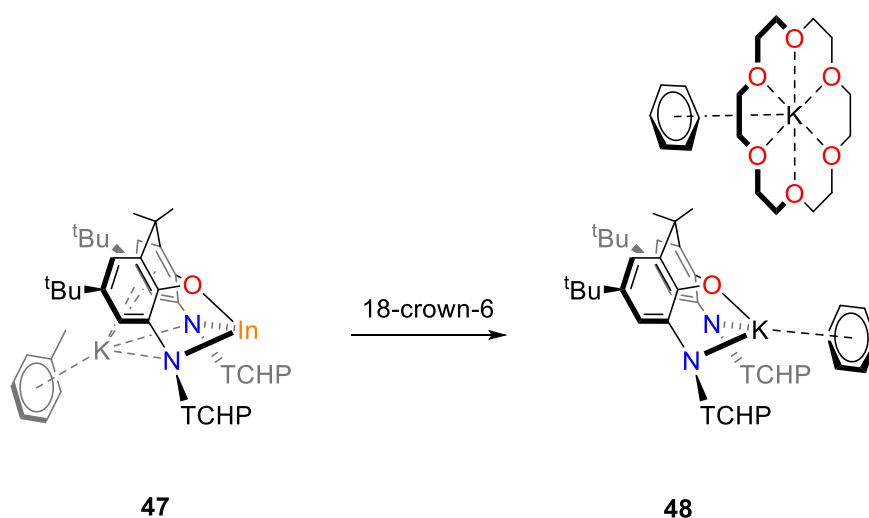


Figure 16. Structure of 18-crown-6.

The reaction of **47** with 18-crown-6 unexpectedly yielded a novel product, identified as $[(x\text{NON}^{\text{TCHP}})\text{K}][(\text{18-c-6})\text{K}]$, **48** (Scheme 22). This compound deviates from the expected product and represents a breakdown product. An alternative explanation for the formation of the breakdown product is that **47** is prone to decomposition. This decomposition to $x\text{NON}^{\text{TCHP}}\text{K}_2$ could occur before or during the reaction with 18-crown-6, resulting in the formation of **48**. One notable feature of **48** is that the xanthene backbone is only bonded to one potassium ion, resulting in a net charge of -1 for $(x\text{NON}^{\text{TCHP}})\text{K}$. This is due to the other potassium cation being sequestered within the 18-crown-6 ligand. Both potassium ions are also coordinated with a benzene molecule.



Scheme 22. Synthesis of $[(x)NON^{TCHP})K][(18-c-6)K]$, **48**.

Isolation of light-yellow crystals allowed for the structure of **48** to be successfully determined by a single crystal X-ray crystallographic experiment, revealing its arrangement as presented in Figure 17. Interestingly, the K2 cation is positioned in the centre of the xanthene backbone, occupying a slightly different position to where the indium atom is typically found in **40**, **46** and **47** (Table 4). Consequently, there is a slight expansion observed in the bond distance between the potassium cation (K2) and the N4, N5 and O5 atoms, with recorded values of 2.6172 Å, 2.6260 Å, and 2.7298 Å respectively in compound **48**. This observation is intriguing given the comparable ionic radii of potassium ion and indium(I) at 1.33 and 1.32 Å, respectively. As a result, the interplay of forces between K2 and the benzene must induce a displacement on potassium from the xanthene backbone, resulting in the increased distances. Additionally, the bond angle of N–K–N is measured at 117.308°, a value that aligns well with the expected range for the N–In–N bond angle of an indyl anions **40**, **46** and **47**, measuring at 119.40(8)°, 119.72(12)° and 105.13(10)° respectively.

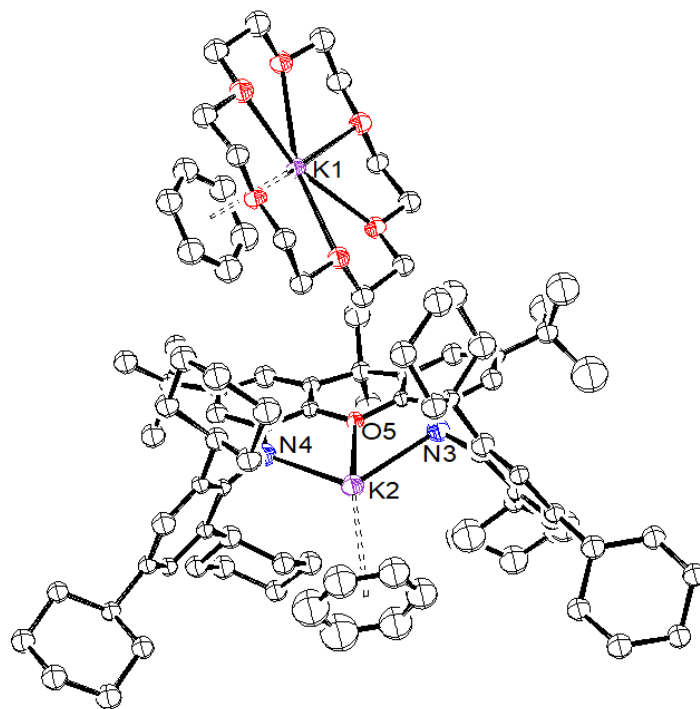
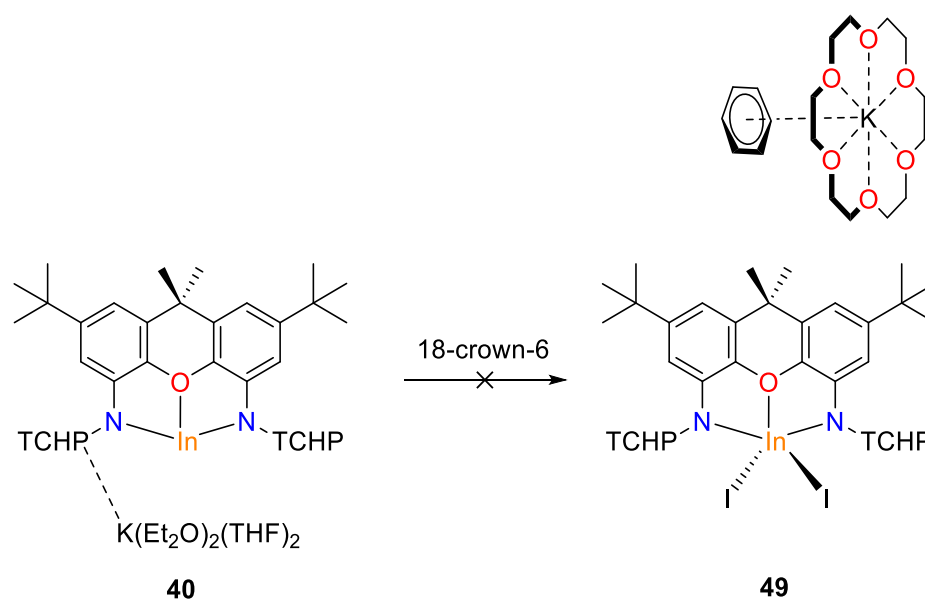


Figure 17. Ortep representation of (ellipsoid 30% probability) of $[(x\text{NON}^{\text{TCHP}})\text{K}][(\text{18-c-6})\text{K}]$, (**48**). Hydrogen atoms have been omitted for clarity. Selected bond lengths (Å) and angles (deg). **48**: K2–N3 2.6255, K2–N4 2.6150, K2–O5 2.7331, N1–In1–N2 117.26.

In the subsequent attempt using the similar reaction conditions, of **40** with 18-crown-6 (Scheme 23), light yellow crystals were obtained of the indium iodide complex in the presence of 18-crown-6 resulting in the encapsulation of the potassium cation in the cavity of the crown ether ($[(x\text{NON}^{\text{TCHP}})\text{InI}_2][(\text{18-c-6})\text{K}]$, **49**). This suggests that the isolation of the ‘indyl anion, **40**’ is not a pure isolation, but rather a mixture of **39** and **40**. Under this assumption, we can confirm that the iodide complex prefers to react with the crown ether and form a SIP complex, rather than reacting with the indyl anion.



Scheme 23. Synthesis of $x\text{NON}^{\text{TCHP}}\text{InI}_2 (18\text{-c-6})\text{K}$, **49**.

The structural analysis of compound **47** obtained from a single crystal X-ray crystallographic experiment (Figure 18) reveals that its bond parameters are similar to those observed in **39**. However, a slight difference is that the structure of **49**, displays the indium centre in a more symmetric and slightly ‘pushed’ arrangement from the xanthene backbone. This structural change is reflected in bond distances, with the In–N bond lengths measuring 2.1540 Å and 2.1568 Å and In–O bond length measuring 2.3622 Å in **49**.

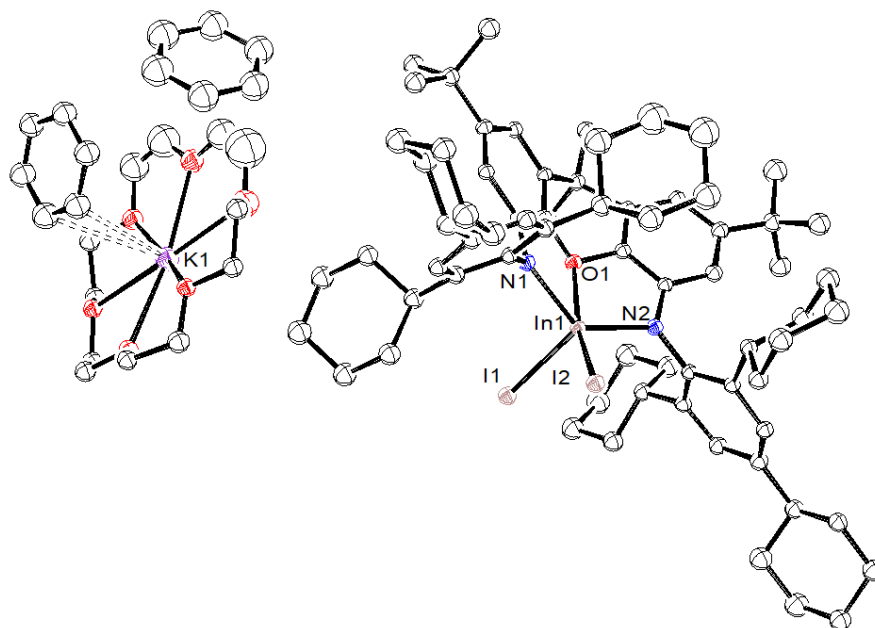
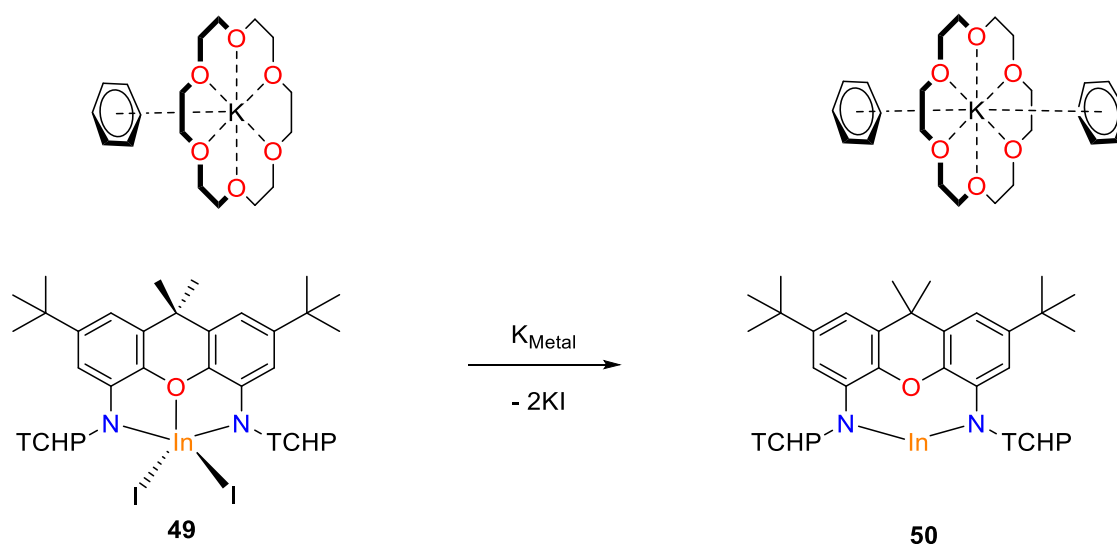


Figure 18. Ortep representation (ellipsoid 30% probability) of $(x\text{NON}^{\text{TCHP}})\text{InI}_2 (18\text{-crown-6})\text{K}$, **49**. Hydrogen atoms have been omitted for clarity. Selected bond lengths (Å) and angles (deg). **49**: In1–N1 2.1557, In1–N2 2.1547, In1–O1 2.3608, In1–I1 2.7536, In–I2 2.7716, N1–In1–N2 131.09.

Moreover, the ‘pushing’ out of the indium centre is further confirmed by the relatively large N–In–N bond angle, which is measured at 131.105°, this is comparable to the N–In–N bond angle for **39** being 132.31(7)°. The crystallographic analysis also provides the In–I bond distances, as 2.7533 and 2.7718 Å. The structural differences between **39** and **49** influence their reactivity. While **39** exists in a dimeric indium iodide ate form, it is hindered reactivity due to steric effects. Whereas **49** has SIP structure with the potassium encapsulated in the 18–crown–6, which may allow for more accessible reactivity.

In the final attempt to synthesise the SIP of the new indyl anion with 18–crown–6, a slightly modified synthetic route was employed. The addition of **49** with excess potassium resulted in the formation of the desired product, [(xNON^{TCHP})In][(18–c–6)K], **50**, with KI precipitating out (Scheme 24).



Scheme 24. Synthesis of [(xNON^{TCHP})In][(18–c–6)K], **50**.

Upon completion of the reaction and work–up procedures conducted, a light–yellow solution yielded bright yellow crystals of **50** upon crystallisation (Figure 19). This confirms that the formation of the SIP of **49** allows for improved reactivity compared to the original indium iodide ate complex, **39**. This enhanced reactivity enables the successful reduction of **49** to form the SIP of the indyl anion, **50**. This successful synthesis of this new (xNON^{TCHP}) indyl anion, adopts a SIP structure. In this configuration, the potassium is encapsulated by 18–crown–6, resulting in the indyl anion being uncoordinated to the potassium ion, in other words, a ‘naked’ indyl anion. The crystal structure of **50**, has been characterised by single crystal X–ray crystallographic experiment, showing the In–N bond distances were measured as 2.3506(18) Å and 2.3875(17) Å, while the In–O bond distance was found to be 2.5403(15) Å,

which are all comparable bond distances to the other indyl anions, **40**, **46**, and **47**. The crystallographic analysis also displayed that the angle between N–In–N was determined to be 122.36(6)° which is significantly larger than the angles observed in the other indyl anions synthesised above, due to potassium no longer being coordinated to the indyl anion. The analysis of the crystallographic data also displays the indyl anion is no longer three-coordinate, potentially giving rise to interesting reactivity properties.

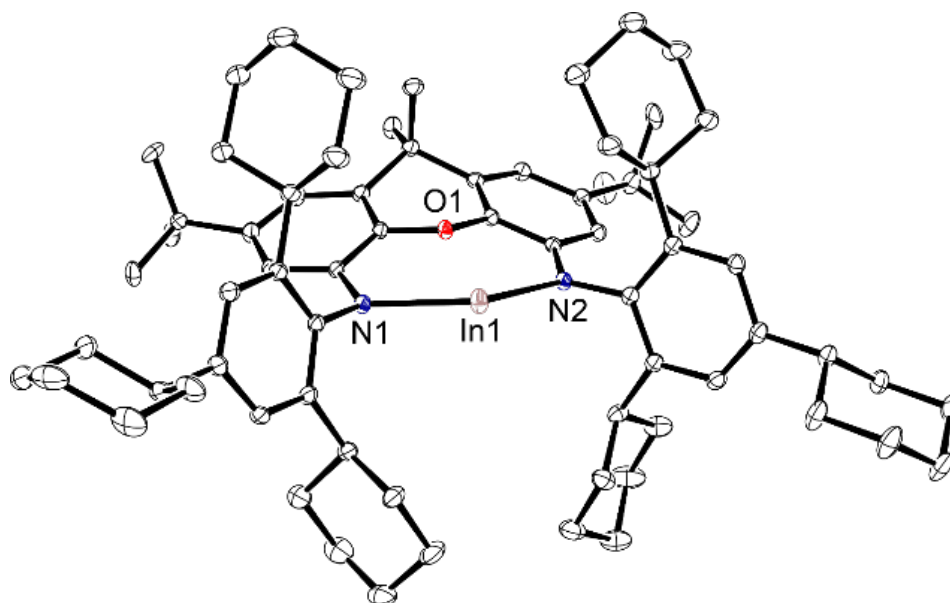


Figure 19. Ortep representation (ellipsoid 30% probability) of $[(x\text{NON}^{\text{TCHP}})\text{In}][(\text{18-crown-6})\text{K}]$, **50**. Hydrogen atoms and $[\text{K}(\text{18-c-6})]^+$ have been omitted for clarity. Selected bond lengths (Å) and angles (deg). **50**: In1...O1 2.5403, In1–N1 2.3506, In1–N2 2.3875, N1–In1–N2 122.36.

The data collected from the single crystal X-ray crystallographic experiments on **40**, **46**, **47**, and **50** present a comparative analysis of bond lengths and angles of specific atoms (Table 5). Notably, compound **47** exhibits the longest In–N bond lengths, while compound **40** has the shortest. In terms of In–O bond lengths, compound **47** showcases the shortest value, and compounds **40**, **46**, and **50** demonstrate relatively similar lengths. In contrast, compound **50** lacks an In–K coordination, due to the encapsulation of potassium by 18-crown-6. Whereas In–K bonds are present in compounds **40**, **46**, and **47**, displaying relatively similar lengths. Regarding the N–In–N bond angle, **47** features the smallest bite angle, correlating to the longest In–N bond lengths, and **50** displays the largest N–In–N bond angle. Overall, these compounds exhibit distinct variations in bond lengths and angles, with compound **47** standing out for its unique bond characteristics and angle measurements.

Table 5. Bond distance and angles of $(\chi\text{NON}^{\text{TCHP}})\text{InK}(\text{Et}_2\text{O})(\text{THF})_2$ (**40**), $(\chi\text{NON}^{\text{TCHP}})\text{InK}(\text{Cp}^4)\text{K}$ (**46**), $(\chi\text{NON}^{\text{TCHP}})\text{InK}(\text{tol})$ (**47**), and $[(\chi\text{NON}^{\text{TCHP}})\text{In}][(\text{18-crown-6})\text{K}]$ (**50**).

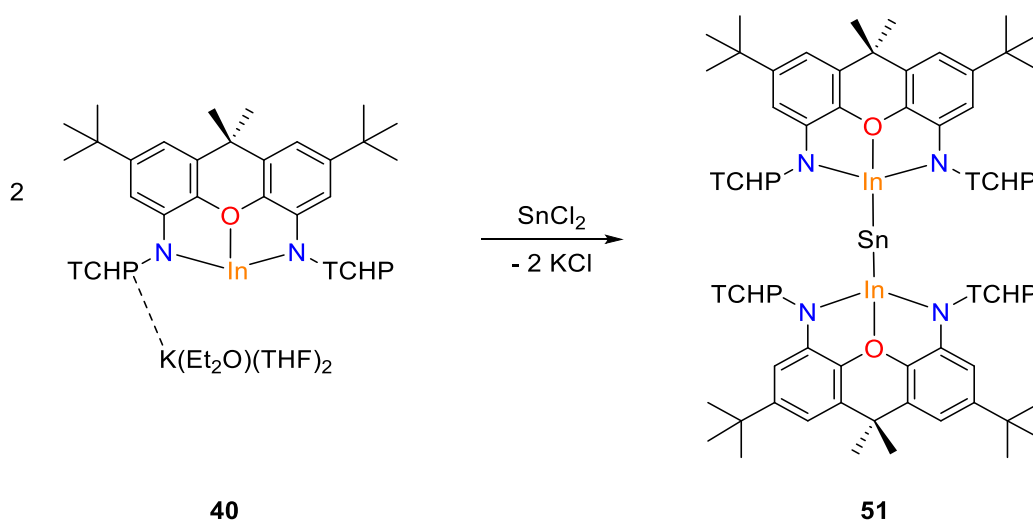
Bond distance/angles	Indyl anion			
	40	46	47	50
In–N (Å)	2.268(2), 2.345(2)	2.295(4), 2.355(4)	2.434(3), 2.455(3)	2.350(6), 2.387(5)
In–O (Å)	2.5171(18)	2.519(3)	2.498(2)	2.540(3)
In–K (Å)	3.6074(8)	3.6005(15)	3.6226(8)	–
N–In–N	119.40(8)°	119.72(12)°	105.15(10)°	122.35(9)°

4.3 Initial Reactivity Studies of the Indyl Anion

Certain reactivity studies conducted on the indyl anions have yielded unexpected products, particularly in the context of reactions involving SnCl_2 and 2,6–dimethyl phenyl isocyanide, which will be discussed below. These reactions have led to the formation of intriguing exchange products or have exhibited partial success.

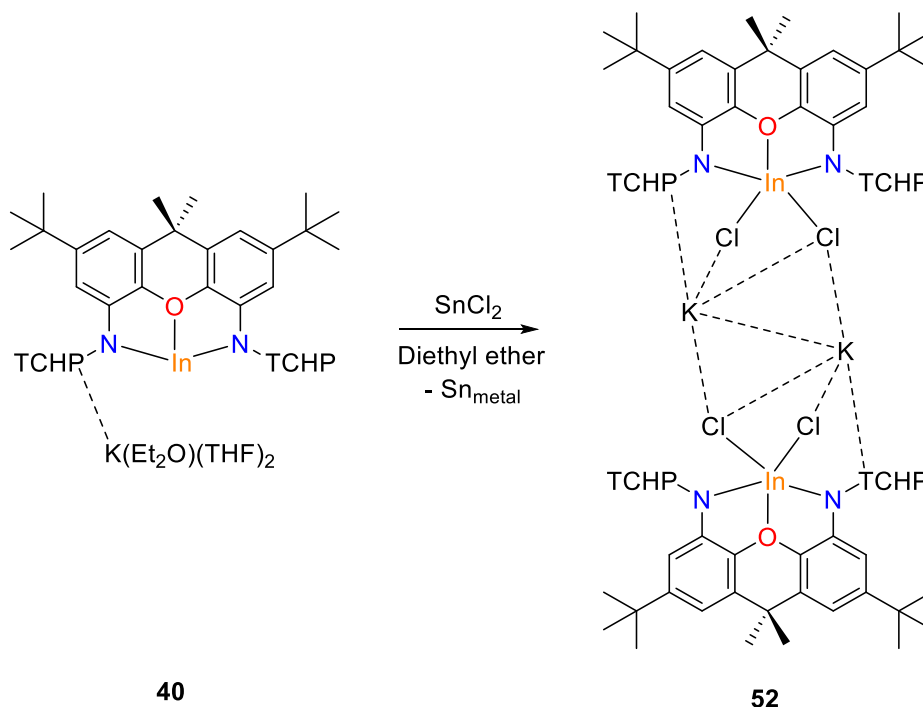
4.3.1 Reactivity With SnCl_2

Inspired by the interesting interactions of several aluminyll anions and the indyl anion with various metal complexes, we sought to embark on similar endeavours ourselves. The preliminary experiments conducted on **40** involved the reactions of ZnI amidinate, and Se. These reactions led to metal dropping out of the solution and, the absence of crystallisation. Returning to the exploration phase, we aimed to discover more straightforward methods for establishing an indium–metal bond. Our hypothesis led us to consider utilizing a metal halide as a viable option, thus prompting our experimentation with SnCl_2 . In the context of this reaction, we hypothesised the formation of $(\chi\text{NON}^{\text{TCHP}})\text{In–Sn–In}(\chi\text{NON}^{\text{TCHP}})$, (**51**) and the precipitation of KCl (Scheme 25).



Scheme 25. Predicted product of **40** with SnCl_2 , $(\chi\text{NON}^{\text{TCHP}})\text{In-Sn-In}(\chi\text{NON}^{\text{TCHP}})$, (**51**).

However, this was not the results we obtained. In the reaction involving **40** and SnCl_2 in Et_2O an interesting displacement reaction occurs, leading to the formation of $[(\chi\text{NON}^{\text{TCHP}})\text{InCl}_2\text{K}]_2$, **52** (Scheme 26). Compound **52** shares a similar structure as the previously mentioned **39** complex. Both these complexes exhibit an ate formation, where the iodine and choline atoms are held in a similar arrangement in their perspective complexes, **39** and **52** respectively.



Scheme 26. Synthesis of $[(\chi\text{NON}^{\text{TCHP}})\text{InCl}_2\text{K}]_2$ (**52**).

The initial product, **52**, characterised by a single crystal X-ray crystallographic experiment, obtained that there was an addition of two chloride ions to the indyl centre,

resulting in the formation of an indium chloride ate complex, **52** (Figure 20). However, during the crystallisation process of the bright orange solution, two distinct crystals co-crystallised, presenting a challenge in their NMR characterisation. As well as, obtaining reasonable crystallographic data for the second unit cell within this co-crystallisation proved to be unattainable.

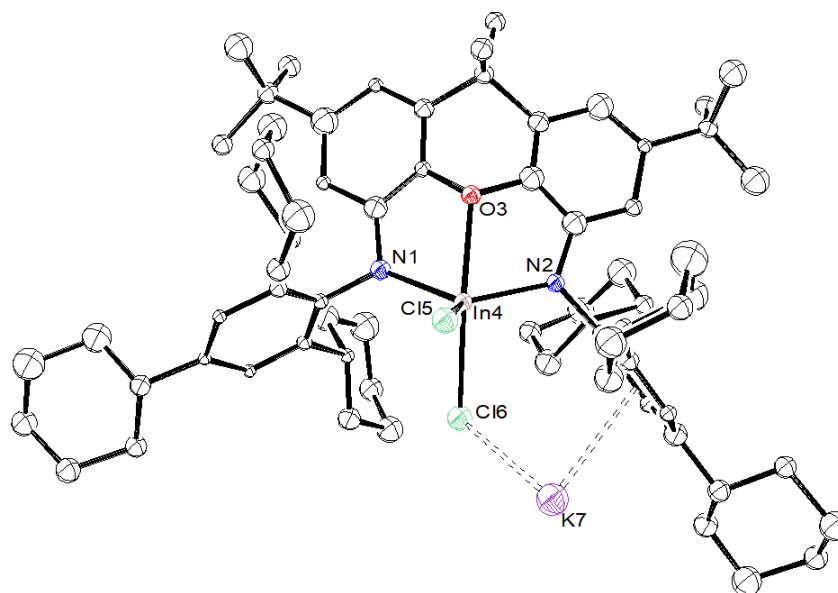
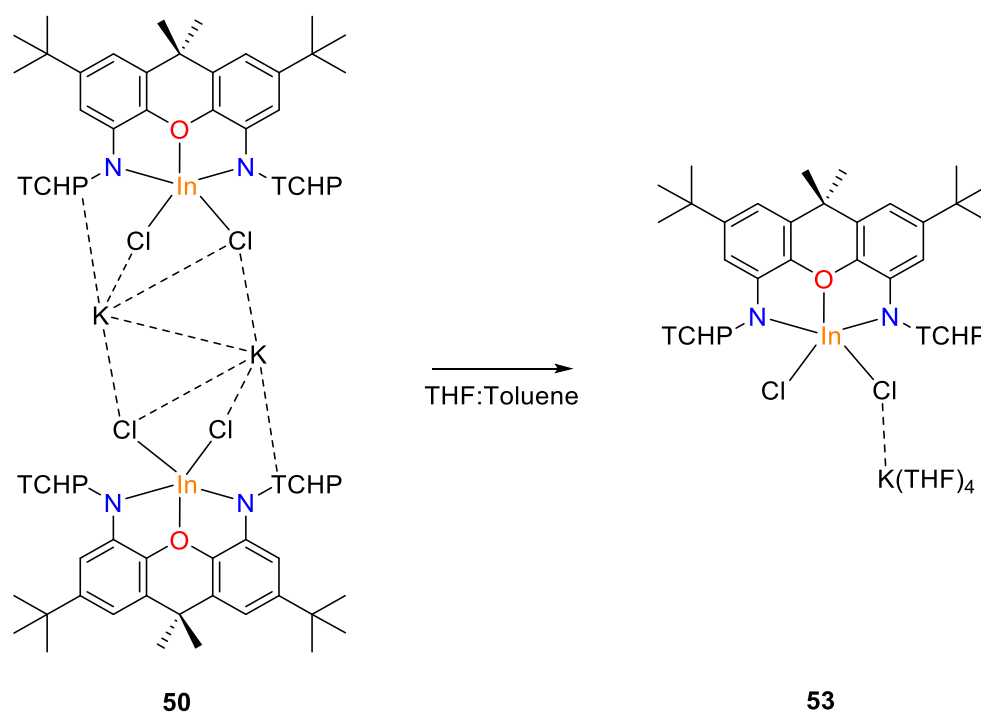


Figure 20. Ortep representation (ellipsoid 30% probability) of $[(x\text{NON}^{\text{TCHP}})\text{InCl}_2\text{K}]_2$, **52**. Hydrogen atoms have been omitted for clarity. Selected bond lengths (Å) and angles (deg). **52**: In4–N1 2.1325, In4–N2 2.0476, In4–O1 2.3291, In4–Cl5 2.6733, In4–Cl6 2.6240, Cl5···K7 3.3990, Cl6···K7 3.1233, N1–In1–N2 135.65.

Efforts to successfully isolate and separate the two different crystals proved challenging within the co-crystallisation vial. Therefore, recrystallisation was the next process to try to separate these two different crystals. Through the process of concentrating the orange solution and subsequent recrystallisation from THF: toluene, colourless crystals were obtained of $(\text{NON}^{\text{TCHP}})\text{InCl}_2\text{K}(\text{THF})_4$, **53** (Scheme 27). However, rather than obtaining the second original unit cell as intended, a new unit cell emerged. This unit cell bears a resemblance to **52**, however, it no longer represents a dimer ate complex.



Scheme 27. Synthesis of $(x\text{NON}^{\text{TCHP}})\text{InCl}_2\text{K}(\text{THF})_4$ (**53**).

Instead, the new unit cell of **53** features four THF molecules coordinated with the potassium cation (Figure 21). In this newly obtained crystallisation vial, the presence of two different coloured crystals or different unit cells is no longer observed. Upon the addition of THF into the vial, both the chloride ate complex, and the previously unidentified complex are no longer present. Alternatively, the complex **53** dominates the crystalline content of the vial.

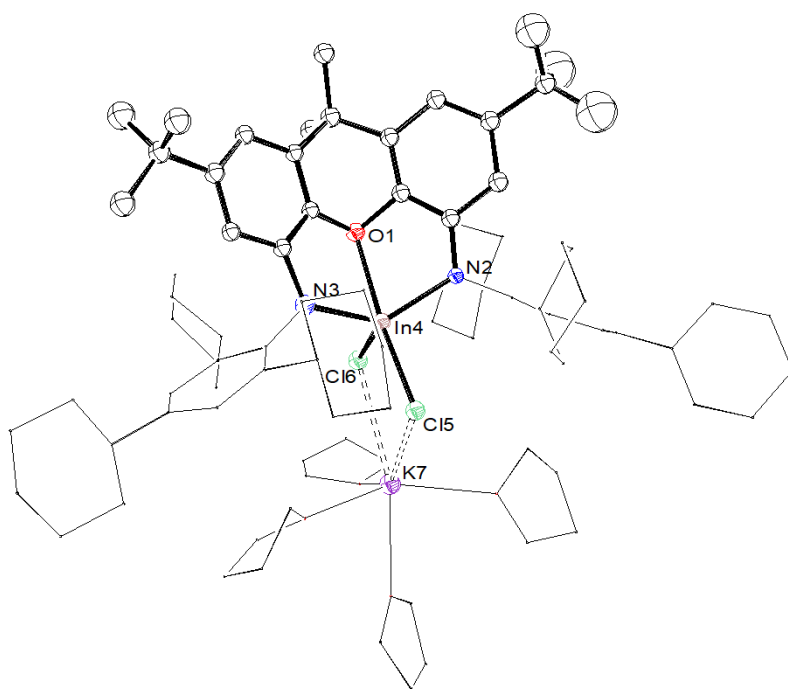


Figure 21. Ortep representation (ellipsoid 10% probability) of $(x\text{NON}^{\text{TCHP}})\text{InCl}_2\text{K}(\text{THF})_4$, **53**. Hydrogen atoms have been omitted and selected atoms are shown in wireframe format for clarity. Selected bond lengths (Å) and angles (deg). **53**: In4–N2 2.1083, In4–N3 2.112, In4–O1 2.3071, In4–Cl5 2.4478, In4–Cl6 2.4375, Cl5···K7 3.3220, Cl6···K7 3.1562, N1–In1–N2 131.24.

Both **52** and **53** have been characterised through a single crystal X-ray crystallography experiment, allowing for a comparison between the two complexes based on their crystal structures. Both these chloride complexes, **52** and **53** can also be compared to **39** (Table 6).

Table 6. Comparison of bond angles and bond distances of **39**, **52** and **53** (X = Cl or I).

Bond distance/angles	$[(x\text{NON}^{\text{TCHP}})\text{InI}_2\text{K}]_2$ (39)	$[(x\text{NON}^{\text{TCHP}})\text{InCl}_2\text{K}]_2$ (52)	$(x\text{NON}^{\text{TCHP}})\text{InCl}_2\text{K}(\text{THF})_4$ (53)
In–N (Å)	2.1568, 2.1540	2.0476, 2.1325	2.1083, 2.1112
In–O (Å)	2.3622	2.3291	2.3071
In–X (Å)	2.7533, 2.7718	2.6240, 2.6733	2.4375, 2.4475
N–In–N	131.105°	135.65°	131.24°

The comparison of **39** and **52**, both being ate complexes, reveals a significant difference in their In–N bond distances and N–In–N bond angles. The In–O bond distance for all complexes appears relatively similar, measuring 2.3622 Å, 2.3291 Å and 2.3071 Å for **39**, **52**, and **53** respectively. The observed In–X bond distances for **39** and **52**, of 2.7533 Å, 2.7718 Å and 2.6240 Å, 2.6733 Å respectively, align with expectations based on the ionic radii of iodide and chloride ions.¹⁰⁹ Iodide has a larger ionic radius than that of chloride, it is reasonable to anticipate longer In–I bond distances compared to In–Cl bond distances. However, it is

noteworthy that the In–Cl bond distances in **52** and **53** differ noticeably, suggesting that the coordination environment or the presence of solvent molecules may have an impact on the bonding interactions between indium and chloride. Overall, there is not a strong correlation between all the bond distances and angles of **39**, **52**, and **53**.

4.3.2 Reactivity With 2,6–dimethylphenyl Isocyanide

Several reported examples showcased the reactivity of alkyminyl(I) anions with different isocyanides, forming a range of C₂– and C₃– coupled isocyanide products.¹¹⁰⁻¹¹² To extend upon this research, our focus shifted towards examining the potential of our indyl anions with different isocyanides, thereby drawing comparative conclusions. Subsequently, the reactivity of a range of isocyanides was tested on our indyl(I) anions. Of these reactions, a noteworthy outcome was that with DMP–NC (DMP–NC = 2,6–dimethyl phenyl isocyanide) with (xNON^{TCHP})InIK(Et₂O)₂(THF)₂. Aligning with literature examples, the anticipated product is a dimerisation product, **54** (Figure 22).¹¹³

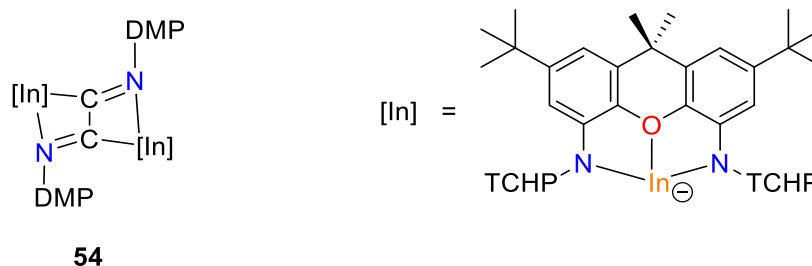
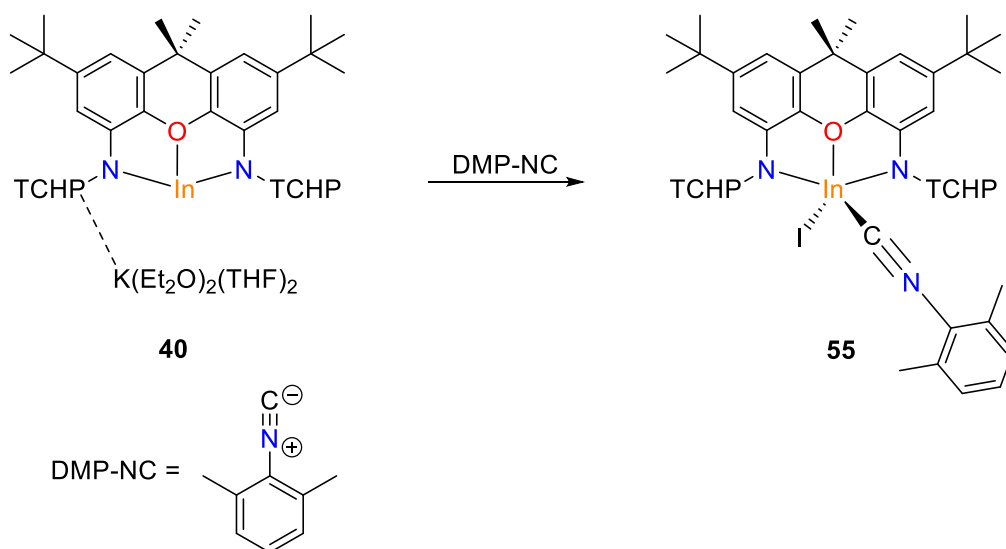


Figure 22. The expected product from the addition of DMP–NC to **40**.

However the reaction of **40** with DMP–NC leads to the formation of product (xNON^{TCHP})InI(DMP–NC), **55** (Scheme 28). Instead of a dimerization product, we observe the addition of DMP–NC to the indium centre, which also is now bonded to an iodide.



Scheme 28. Synthesis of $(\text{xNON}^{\text{TCHP}})\text{InI}(\text{DMP-NC})$, **55**.

The structure of this complex was characterised by a single crystal X-ray crystallography experiment and obtained that the indium centre is bonded to an iodide ion and one isocyanide, along with three bonds to the xanthene ligand system (Figure 23). A notable feature in **55** is the C6–N7 bond distance, which measures 1.1102 Å. This bond distance is consistent with a triple bond between carbon and nitrogen.¹¹⁴ The presence of a triple bond between C6–N7 in **55** indicates that no bonds were broken in the isocyanide molecule during the reaction with the indyl anion, **40**. In the resulting product (**55**) the DMP–NC unit is coordinated to the indium centre through a bond formation. As a result, the partial negative charge that was initially present on the C6 carbon of the isocyanide is now delocalised by its interaction with the indium atom. This charge redistribution leads to a stable coordination complex where the indium atom obtains a partial negative charge, associated with its coordination with the isocyanide ligand. The N7 nitrogen however, still carries the partial positive charge to make $(\text{xNON}^{\text{TCHP}})\text{InI}(\text{DMP-NC})$ an overall neutral complex. This charge distribution ensures that the entire complex is overall electronically neutral, maintaining charge balance in the coordination sphere of the indium atom.

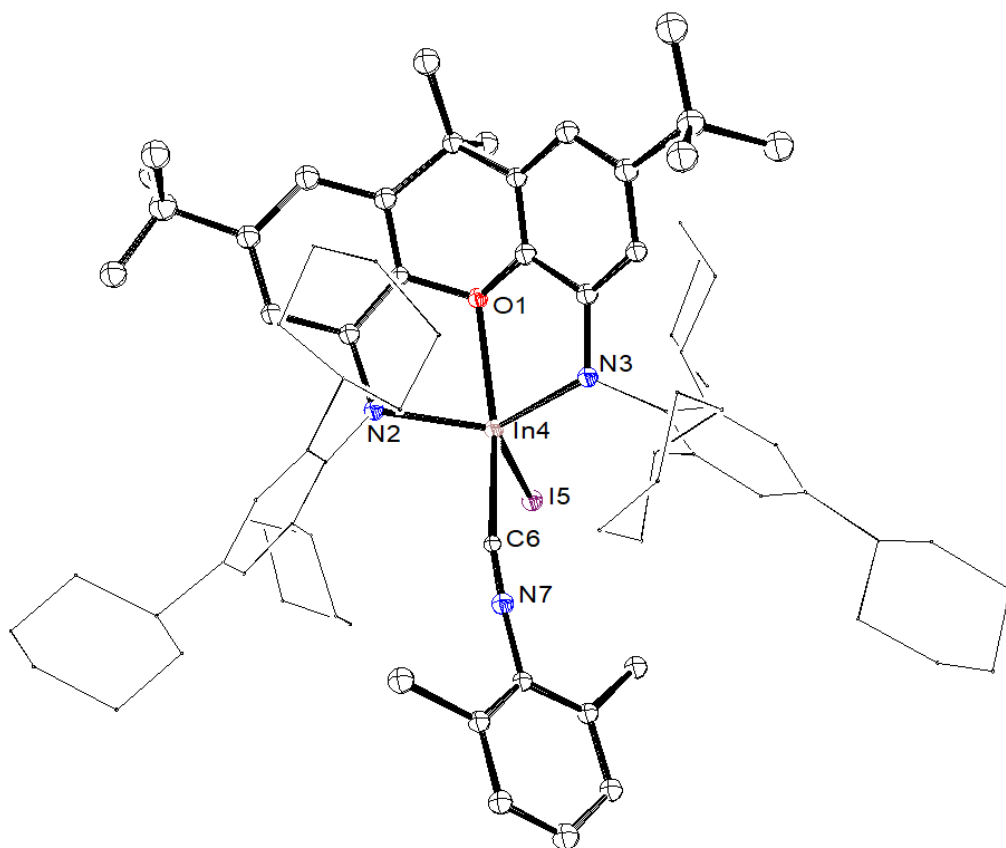


Figure 23. Ortep representation (ellipsoid 30% probability) of $(x\text{NON}^{\text{TCHP}})\text{InI}(\text{DMP-NC})$, (**55**). Hydrogen atoms have been omitted and selected carbon atoms are shown in wireframe format for clarity. Selected bond lengths (Å) and angles (deg). **55**: In4–N2 2.1328, In4–N3 2.0712, In4–O1 2.3636, In4–I5 2.7113, In4–C6 2.30305, N1–In1–N2 134.05.

Upon closer examination, we have come to consider the possibility that the starting material, **40**, is contaminated with a small but significant amount of $[(x\text{NON}^{\text{TCHP}})\text{InI}_2\text{K}]_2$ (**39**). As these reactivity studies were conducted with indyl anions synthesised *via* the reduction route (Scheme 17). This observation could explain the unexpected formation of certain products during the reactivity studies. To gain more clarity on the true composition of **55**, further studies are needed.

4.4 Unsuccessful Reactivity of $x\text{NON}^{\text{TCHP}}$ Indyl Anions

Numerous additional reactions were attempted using the synthesised low-valent indyl anions, **40** and **47** (Table 7). Regrettably, the outcomes of these reactions proved unproductive, despite some of these reactions displaying intriguing alterations in colouration and/or exhibited varied NMR spectra. However, the crystallised products ultimately proved to be either starting materials or yielded no discernible compounds at all.

Table 7. Failed reaction table.

Reaction	Final colour	Crystallised product
40 + N ₃ Dipp	Light green	(^x NON ^{TCHP})InI ₂
40 + CO ₂	Yellow	(^x NON ^{TCHP})H ₂ and (^x NON ^{TCHP})InI ₂
40 + N ₃ Mes	Light yellow	(^x NON ^{TCHP})H ₂
40 + CO ₂	Yellow	(^x NON ^{TCHP})H ₂
47 + cyclohexyl isocyanide	Yellow/orange	(^x NON ^{TCHP})H ₂
40 + cyclohexyl isocyanide	Yellow	(^x NON ^{TCHP})In(Et ₂ O) ₂ (THF) ₂
47 + CO ₂	Dark yellow/brown	(^x NON ^{TCHP})H ₂
47 + N ₃ Mes	Orange	(^x NON ^{TCHP})K ₂
47 + cyclohexyl isocyanate	Light yellow	(^x NON ^{TCHP})H ₂
40 + cyclohexyl isocyanate	Cloudy yellow/orange	(^x NON ^{TCHP})InI ₂
40 + N ₃ Dipp	Cloudy light yellow	(^x NON ^{TCHP})InI ₂
40 + CO ₂	Cloudy dark green	(^x NON ^{TCHP})InI ₂

The reactions involving azide derivatives, CO₂, and different sources of isocyanides/isocyanates were repeated several times to explore their reactivity with **40/47**. The CO₂ reaction was conducted on four separate occasions due to the observed variations in colour and differences in the ¹³C{¹H} NMR spectra (Figure 24), suggesting the possibility of a new product formation. The appearance of six additional peaks ranging from 161.5 to 168.1 ppm highlighted with the orange boxes in Figure 24 of the ¹³C{¹H} NMR spectra indicates the addition of several new carbon atoms into the indyl anion, implying the formation of a new product. As well as the peak at 124.8 ppm in the ¹³C{¹H} NMR spectra corresponding to the presence of CO₂, confirming that CO₂ was indeed added to the *J Youngs* NMR tube during the experiment, further supporting the formation of a new product. Despite these promising signs, all four attempts to carry out the reaction resulted in the crystallisation of starting materials instead of the expected products, leading to inconclusive results.

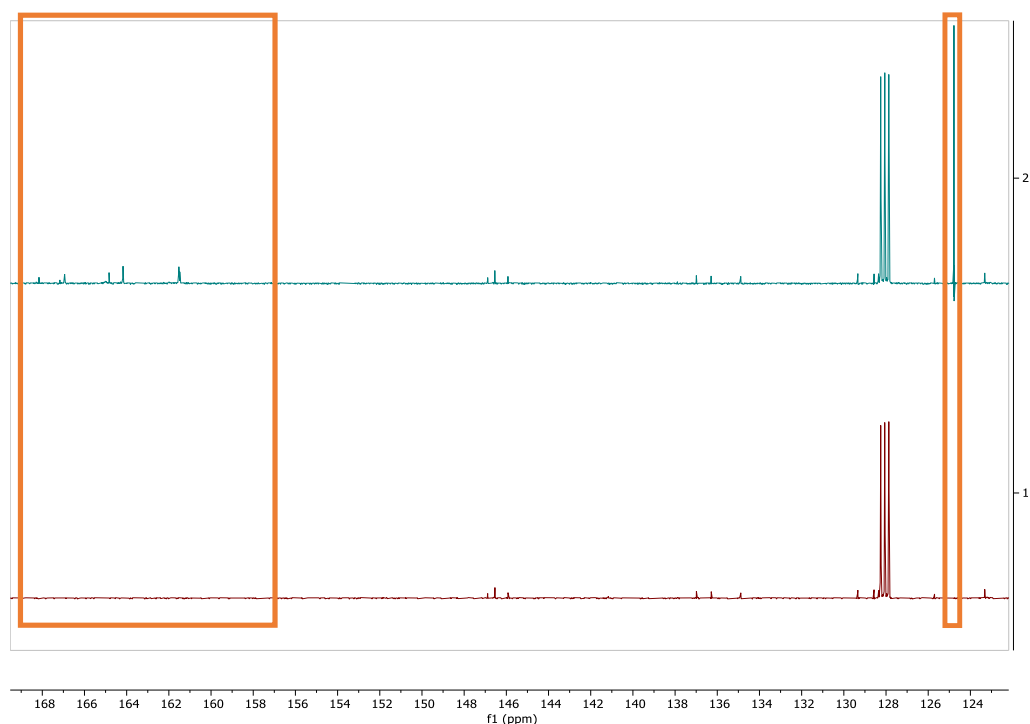


Figure 24. ^{13}C NMR spectra of **40** + CO_2 . Red spectrum (bottom) = before CO_2 has been added, and blue spectrum (top) = after CO_2 has been added.

The reactions with Mes and Dipp organic azide derivatives were added to indyl anions **40** and **47**. During these reactions, noticeable colour changes were observed, shifting from yellow to red/orange hues. However, when subjected to single crystal X-ray experiments, the results revealed no imide product formed as initially expected. Instead, only $(\text{xNON}^{\text{TCHP}})\text{H}_2$, (**37**) or $(\text{xNON}^{\text{TCHP}})\text{K}_2$ (**38**) were detected as end products. For the repetition of these reactions, numerous parameters were modified, including the reaction time, temperature, and equivalents of azides. These alterations were made to optimise the conditions and increase the chances of obtaining an imide product. Unfortunately, despite using different conditions the crystallisation of these products was not able to form. Therefore, the desired imide product was not obtained.

Several sources of isocyanides/isocyanates were also explored, including cyclohexyl, $t\text{Bu}$, 2,6-dimethylphenyl isocyanides and cyclohexyl, 4-nitrophenyl isocyanates. Although some reactions indicated promising colour changes and yielded different coloured crystals to starting materials, the obtained single crystal X-ray crystallographic experiments revealed the presence of either the $(\text{xNON}^{\text{TCHP}})\text{H}_2$ (**37**), $(\text{xNON}^{\text{TCHP}})\text{InI}_2\text{K}$ (**39**), or unreacted indyl (**40/47**). In cases where crystal growth was limited no crystallographic data could be obtained. Other reactions were attempted however, these reactions did not yield any significant crystals and no

meaningful changes in the NMR spectrum for these reactions was observed. As a result, these products were not able to be characterised.

4.5 Conclusion and Future Work

This research project encompassed the synthesis and characterisation of a novel ligand, $(\text{xNON}^{\text{TCHP}})\text{H}_2$, **37**, through the utilisation of the TCHP *N*-substituent. This ligand was synthesised akin to that established by Emslie *et al*, however, exchanging the *N*-substituent and altering the reaction conditions, yielded the desired bulky $(\text{xNON}^{\text{TCHP}})\text{H}_2$ ligand.

In a manner similar to the methodology outlined by Coles *et al* for the synthesis of their indyl anion, (**20**, $[(\text{NON}^{\text{Dipp}})\text{InK}]_2$) the potassiation of **37** occurs to obtain **38**, $(\text{xNON}^{\text{TCHP}})\text{K}_2$. Subsequent to this, the addition of InI_3 to **38** resulted in the formation of $[(\text{xNON}^{\text{TCHP}})\text{InI}_2\text{K}]_2$, **39**. The reduction of **39** with potassium metal yielded our first indyl anion encompassing the $(\text{xNON}^{\text{TCHP}})$ ligand system. However, issues concerning solubility as well as difficulties in separating the unwanted materials, lead to a poor yield and an impure product (yield = 53.5%, mixture of **37**, **39**, and **40**) of our first indyl anion. Consequently, a revision of our indyl anion synthesis was undertaken, involving the utilisation of an In(I) source. This strategic modification removed the necessity of forming **39**. The first attempt of utilising a source of In(I) involved the development of Cp^{4*}In , a soluble source of In(I). Although this methodology proved successful, it yielded an indyl anion with the inclusion of a KCp^{4*} . Thus, a further refinement of the procedure was executed, wherein InI was employed as the In(I) source. Despite the partially insoluble characteristics of InI, this modification yielded a new indyl anion. Notably, this latter method of the synthesis of the indyl anion exhibited a distinct placement of the potassium ion within the central region of the xanthene backbone. Following the successful isolation of the novel indyl anions, selected reactivity studies were conducted. While certain reagents yielded interesting results, others led to the reformation of the initial starting materials, signifying a lack of success. In instances where novel products were obtained a combination of NMR spectroscopy and single crystal X-ray crystallography were employed to characterise the resulting complexes.

The present research has yielded several notable findings. Firstly, to obtain reproducible products, the utilisation of clean starting materials is evident. Notably, the observed sensitivity of our indyl anions to $(\text{xNON}^{\text{TCHP}})\text{H}_2$ (**37**) and $(\text{xNON}^{\text{TCHP}})\text{K}_2$ (**38**) when

present in solution underscores the need for careful handling. Moreover, forthcoming reactions of the indyl anions need clean material to be successful and comparable to literature examples. Finally, the difficulty separating the indyl anion from unreacted starting materials possesses a problem that should be addressed.

The immense potential reactivity investigations involving these indyl anions stretch far beyond our current explorations, which leaves a vast area for possible investigations. A central objective would persist with the addition of small-molecules, azide derivatives, and isonitriles to the indyl anions (Figure 25).

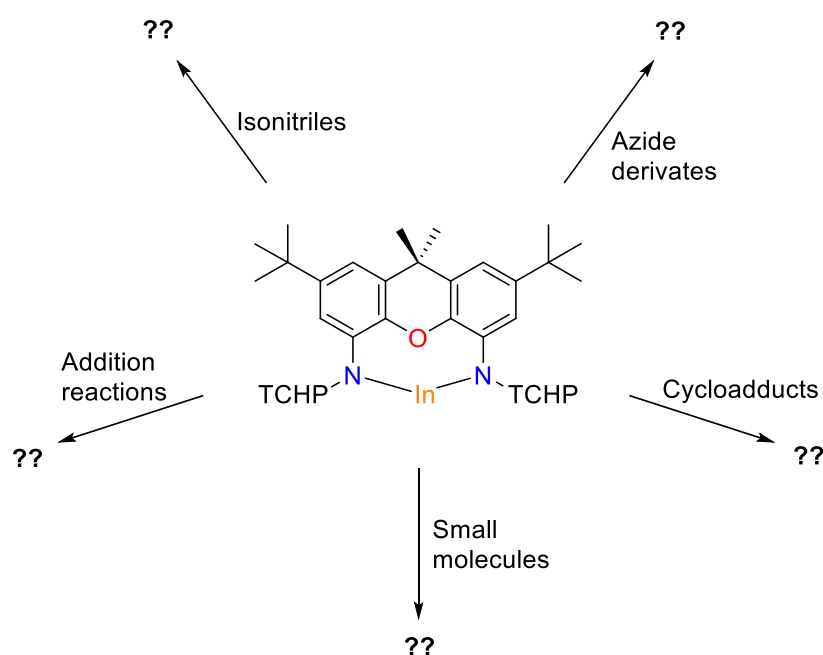


Figure 25. Possible future work to do on all $\chi\text{NON}^{\text{TCHP}}$ indyl anions. Depicted indyl **50** in figure.

Furthermore, a simultaneous endeavour would entail an all-encompassing exploration of interactions between indyl anions and alkali metal complexes, alongside their potential engagement in forming cycloadduct complexes. This multifaceted approach holds the potential to unlock valuable insights into the intricate chemical behaviours exhibited by these novel indyl anions. Performing these reactivity studies and obtaining new compounds would allow for opportunities to conduct comparable studies on Aldridge *et al*'s aluminyll anion, **27a**, and Coles *et al*'s indyl anion, **27b**.

Chapter 5. Experimental

5.1 General Experimental

The experimental procedures were conducted under a dry argon atmosphere using standard Schenk–line techniques or in a conventional nitrogen–filled glovebox. Diethyl ether (Et₂O), tetrahydrofuran (THF), toluene and hexane solvents were obtained from a PureSolv MD 5 system and were stored over activated 5 Å molecular sieves for 24 hours before use. The alkali metals used in the experiments were obtained as chunks and stored under mineral oil. Before their use, the metals were washed with hexane to remove the mineral oil, and any oxidised surfaces were mechanically removed under an inert atmosphere. Unless indicated otherwise, all other chemicals utilised in the experiments were purchased from Sigma–Aldrich and used without additional purification. The synthesised compounds were characterised using 2D NMR spectra which were acquired using a JOEL 500 MHz (11.747 Tesla) spectrometer equipped with a ROYAL digital auto–tune probe S. The spectrometer operated at frequencies of 500.1 MHz for proton (¹H) NMR and 125.8 MHz for carbon (¹³C) NMR. Spectra were recorded at a temperature of 294 K. Proton and carbon chemical shifts were referenced internally to residual solvent resonances. Coupling constants were reported in Hz. Data processing was performed using Mestrenova software suites. Crystals were prepared and mounted by Sophie G. Unsworth and modelled by Scott Cameron. Single crystal X–ray diffraction was collected using an Agilent diffractometer system located at the Victoria University of Wellington.

5.2 Characterisation Techniques

To determine the structure of newly synthesised products, the following characterising techniques were performed.

5.2.1 Nuclear Magnetic Resonance Spectroscopy (NMR)

Nuclear magnetic resonance spectroscopy (NMR) is a powerful technique for small–molecule characterisation as well as the structural and dynamical studies of biomolecules.¹¹⁵ This technique is widely used in organic chemistry due to its ability to provide detailed information about the connectivity and arrangement of atoms within a molecule. By employing these NMR techniques, comprehensive information about the structure, connectivity and chemical properties of the synthesised compounds can be obtained using a minimal amount of product to acquire a full data set.

NMR spectroscopy is based on the fundamental principles of spin and magnetic properties of nuclei. Nuclei with an odd number of protons or neutrons possess a property called spin, which causes a charged nucleus to spin on an axis and create its own magnetic dipole moment. When placed in an external field, these spinning nuclei can align either parallel or antiparallel to the field. The nuclei either align in the lower energy state (parallel to the field) or the higher energy state (anti-parallel to the field).¹¹⁶ The energy difference between these two states corresponds to the radio-frequency range, and by applying a radio-frequency pulse, the nuclei can absorb energy and undergo a transition from one state to another. After the radio-frequency pulse is applied, the nuclei return to their equilibrium state, releasing energy. This energy is detected by the NMR spectrometer, and the resulting signal is recorded as an NMR spectrum.¹¹⁷ The position and intensity of the peaks in the spectrum provide information about the chemical environment and connectivity of the compounds.

Specifically in the research conducted here, the utilisation of ^1H and $^{13}\text{C}\{^1\text{H}\}$ NMR spectroscopy were used as the primary techniques for characterising the novel compounds. Additionally, within ^1H and $^{13}\text{C}\{^1\text{H}\}$ NMR spectroscopy, several specialised experiments can provide more specific structural information, this includes heteronuclear single quantum coherence (HSQC), heteronuclear multiple bond correlation (HMBC), homonuclear correlation spectroscopy (COSY) and distortionless enhancement by polarisation transfer (DEPT). The combined information obtained from the ^1H and $^{13}\text{C}\{^1\text{H}\}$ NMR spectra along with insights provided by techniques like HSQC, HMBC, COSY and DEPT, we can gain a comprehensive understanding of the compounds created.

5.2.2 Single Crystal X-Ray Diffraction

The use of X-rays for crystal structure research has risen in the last two decades, due to the vast expansion of computer hardware and software for completing the necessary calculations, as well as the development of quick and automated data collection technologies. Because of its extensive application and accuracy, single crystal X-ray crystallography has become one of the most important methods in both organic and inorganic chemistry research.

Most laboratories have operable four-circle diffractometers, which are valued for their ability to measure refractive intensities automatically and precisely. The present market equipment has three computer-controlled "circles" whose rotation axes coincide to within

approximately 10 μm of one another.¹¹⁸ To obtain the crystal structure of a compound a single crystal must be used.¹¹⁹ In single crystal X-ray diffraction, a crystal of the compound of interest is mounted on a diffractometer. X-ray beams are directed onto the centre of the crystal, and the crystal causes the X-rays to diffract, resulting in a diffraction pattern observed on the connected monitor. By analysing the angles and intensities of the diffraction pattern a three-dimensional image of the electron density within the crystal can be computer generated. From this electron density map, the average positions of atoms in the crystal can be determined. Additionally, other properties such as bond strength, bond disorder, defects and chemical bonds between atoms can be determined from single crystal X-ray crystallography. Single crystal X-ray crystallography provides detailed structural information at the atomic level, allowing scientists to understand the arrangement of atoms within a crystal and gain insight into the chemical properties of the compounds.

5.3 Synthetic Procedures

5.3.1 Preparation of $(\text{xNON}^{\text{TCHP}})\text{H}_2$, **37**

Sodium tert-butoxide (311.4 mg, 3.24 mmol), palladium(II) acetate (5.4 mg, 0.02 mmol), Oxydi-2, 1-phenylenebis(diphenylphosphine (18.6 mg, 0.03 mmol), 4,5-dibromo-2,7-di-tert-butyl-9,9-dimethyl-9H-xanthene (526.2 mg, 1.17 mmol) and TCHP amine (794.2mg, 2.34 mmol) were added in a toluene solution and stirred for 5 days at 100°C. The resulting solution was quenched with water, extracted into toluene (3 x 50 mL), dried over MgSO_4 , and concentrated to approximately 10 mL. Recrystallisation was achieved from hot toluene to obtain off-white crystals. Yield 987.7 mg, 84.7 %.

^1H NMR (500 MHz, C_6D_6) δ 7.20 (s, 4H, ArH), 6.91 (d, $J = 2.2$ Hz, 2H, XA-*p*-CH), 6.59 (d, $J = 2.2$ Hz, 2H, XA-*o*-CH), 5.87 (s, 2H, NH), 3.19 (tt, $J = 8.1, 3.2$ Hz, 4H, *o*-CyH), 2.55 – 2.44 (m, 2H, *p*-CyH), 2.00 – 1.83 (m, 15H, CyH₂), 1.79 – 1.70 (m, 15H, CyH₂), 1.64 (s, 6H, C(CH₃)₂), 1.60 – 1.38 (m, 22H, CyH₂), 1.35 – 1.22 (m, 8H, CyH₂), 1.17 (s, 18H, C(CH₃)₃).

$^{13}\text{C}\{^1\text{H}\}$ NMR (126 MHz, C_6D_6) δ 146.9, 146.6, 145.9, 136.99, 136.3, 134.9, 129.3, 125.7, 123.3, 111.9, 108.6 (ArC), 45.3 (*p*-CyC), 39.9 (*o*-CyC), 35.8, 35.1, 34.8, 34.3 (C(CH₃)₂, C(CH₃)₃, CyCH₂), 32.9 C(CH₃)₂), 31.7 (C(CH₃)₃), 27.8, 27.4, 27.3, 26.7, 26.6 (C(CH₃)₂, C(CH₃)₃, CyCH₂).

5.3.2 Preparation of (xNON^{TCHP})K₂, 38

A solution of (xNON^{TCHP})H₂ (412.7 mg, 0.414 mmol) in toluene was added to an excess of potassium hydride (36.5 mg, 0.919 mmol) in toluene and stirred for 48 hours under nitrogen at 80°C. The mixture was filtered *via* a cannula to give a green solution. The solvent was removed *in vacuo* and the resulting green powder was heated under vacuum (10⁻² mbar) to remove the coordinated toluene yielding “(xNON^{TCHP})K₂”. Recrystallisation was achieved from a saturated toluene solution obtained light green crystals. Yield 425 mg, 97.0 %.

¹H NMR (500 MHz, C₆D₆) δ 7.15 (s, 4H, ArH), 6.62 (d, *J* = 2.1 Hz, 2H, XA-*p*-CH), 6.25 (d, *J* = 2.1 Hz, 2H, XA-*o*-CH), 2.65 (qt, *J* = 12.2, 3.2 Hz, 6H, CyH), 2.07 (d, *J* = 13.6 Hz, 6H, CyH₂), 1.89 (d, *J* = 15.0 Hz, 8H, CyH₂), 1.85 (s, 6H, C(CH₃)₂), 1.79 (t, *J* = 13.8 Hz, 6H, CyH₂), 1.69 (m, 12H, CyH₂), 1.58 (m, 4H, CyH₂), 1.43 (m, 10H, CyH₂), 1.33 (s, 18H, C(CH₃)₃), 1.30 (s, 6H, CyH₂), 1.07 (m, 8H, CyH₂).

¹³C {¹H} NMR (126 MHz, C₆D₆) δ 152.6, 149.8, 147.2, 140.4, 137.6, 133.5, 129.3, 128.6, (Ar), 125.7 (C(CH₃)₂), 122.8 (ArH), 111.8 (XA-*p*-CH), 100.5 (XA-*o*-CH), 45.3 (*p*-CyH), 40.1 (*o*-CyH), 36.1, 35.8, 35.3, 33.1 (CyH₂), 34.9 (C(CH₃)₂), 32.1 (C(CH₃)₃), 28.6 (CyH₂), 28.4 (CH₃), 28.3 (CyH₂), 27.7, 26.9, 26.9 21.4 (C(CH₃)₂, C(CH₃)₃, CyCH₂).

5.3.3 Preparation of (xNON^{TCHP})InI₂K, 39

A solution of xNON^{TCHP}K₂ (425 mg, 0.400 mmol) in a 1:5 hexane: diethyl ether solution was added to InI₃ (198.7 mg, 0.400 mmol) in a 1:5 hexane: diethyl ether solution and stirred for 18 hours under nitrogen at room temperature. The mixture was filtered *via* a cannula to give a yellow/green solution. The solvent was removed *in vacuo* and the resulting green powder was heated under vacuum (10⁻² mbar) to remove the coordinated diethyl ether and hexane yielding “(xNON^{TCHP})InI₂K”. Recrystallisation was achieved from a saturated toluene solution to give light green crystals. Yield 504.1 mg, 92.1 %.

¹H NMR (500 MHz, C₆D₆) δ 7.19 (s, 4H, TCHP-ArH), 6.75 (s, 2H, XA-*p*-CH), 6.46 (s, 2H, XA-*o*-CH), 3.45 (s, 4H, Phen-*p*-CH), 2.50 (d, *J* = 12.2 Hz, 5H, CyH₂), 2.45 (s, 2H, Phen-*m*-CH), 2.13 (d, *J* = 8.9 Hz, 5H, CyH₂), 1.90 (d, *J* = 12.6 Hz, 6H, CyH₂), 1.82 – 1.76 (m, 17H, CyH₂), 1.70 (s, 6H, C(CH₃)₂), 1.64 – 1.62 (m, 10H, CyH₂), 1.34 (dt, *J* = 12.6, 3.7 Hz, 17H, CyH₂), 1.28 (s, 18H, C(CH₃)₃).

¹³C {¹H} NMR (126 MHz, C₆D₆) δ 148.62, 146.47, 144.15, 139.43, 136.95, 133.23, 127.06, 124.18 (ArC), 123.09 (TCHP-ArC), 112.47 (XA-*o*-CH), 106.17 (XA-*p*-CH), 44.69 (TCHP-*p*-CyH), 39.88 (CyH₂), 39.29 (TCHP-*o*-CyH), 37.14, 35.13, 34.77 (CyCH₂), 31.63 C(CH₃)₃,

31.50, 29.06 ($C(CH_3)_3$, $CyCH_2$), 27.25 $C(CH_3)_2$, 27.17, 27.14, 26.73, 23.31 ($C(CH_3)_3$, $CyCH_2$, $C(CH_3)_2$).

5.3.4 Preparation of $(xNON^{TCHP})InK(Et_2O)_2(THF)_2$, 40

A solution of $(xNON^{TCHP})InI_2K$ (500 mg, 0.360 mmol) in a 1:1 hexane: diethyl ether solution was added to KC_8 (97.3 mg, 0.720 mmol) in a 1:1 hexane: diethyl ether solution and stirred for 18 hours under nitrogen at room temperature. The solution was filtered through celite, the solvent was removed *in vacuo* and the residue was washed three times in hexane. The resulting light-yellow powder and hexane solution were concentrated *in vacuo* and the powder was extracted with THF and left to crystallise at room temperature, giving bright yellow crystals suitable for an X-ray diffraction experiment. Yield 251.9 mg, 53.5 %.

1H NMR (500 MHz, C_6D_6) δ 7.21 (s, 4H, Ar-H), 6.76 (d, $J = 2.1$ Hz, 2H, XA-*p*-CH), 6.51 (d, $J = 2.2$ Hz, 2H, XA-*o*-CH), 3.48 (tt, $J = 8.9, 3.6$ Hz, 4H, *p*-CyH), 2.54 (d, $J = 11.4$ Hz, 4H), 2.46 – 2.38 (m, 2H, *o*-CyH), 2.19 (d, $J = 12.5$ Hz, 4H, CyH_2), 1.94 (d, $J = 12.7$ Hz, 5H, CyH_2), 1.76 (q, $J = 11.6$ Hz, 19H, CyH_2), 1.68 (s, 6H, CH_3), 1.65 – 1.62 (m, 2H, CyH_2), 1.44 – 1.30 (m, 22H, CyH_2), 1.28 (s, 18H, $CH(CH_3)_3$), 1.11 (ddt, $J = 9.5, 6.7, 2.3$ Hz, 4H, CyH_2).

$^{13}C\{^1H\}$ NMR (126 MHz, C_6D_6) δ 148.39, 146.01, 144.00, 143.26, 142.89, 139.25, 133.06, 129.03 (Ar), 122.93 (ArC), 112.15 (XA-*p*-CH), 105.95 (XA-*o*-CH), 65.60 (Cy), 44.44 (*p*-CyH), 39.03 (*o*-CyH), 37.10, 36.78, 34.93, 34.70, 34.57 ($C(CH_3)_2$, $C(CH_3)_3$, $CyCH_2$), 31.65 ($C(CH_3)_3$), 31.50, 27.46, 26.97 ($C(CH_3)_2$), 26.56, 22.74, 15.27, 14.04 ($C(CH_3)_2$, $C(CH_3)_3$, $CyCH_2$).

5.3.5 Preparation of $(xNON^{TCHP})InK(Cp^{4*})K$, 46

A deuterated benzene (C_6D_6) solution of $Cp^{4*}In$ (10 mg, 0.04 mmol) was added to a scintillation vial containing $(xNON^{TCHP})K_2$ (45 mg, 0.04 mmol) in C_6D_6 and transferred to an *J Youngs* NMR tube to be heated at 60°C for 2 hours under nitrogen. The solvent was removed *in vacuo* and the residue was extracted with toluene. The solution was filtered through celite, concentrated, and left to crystallise at room temperature, giving bright yellow crystals suitable for an X-ray diffraction experiment. Yield 13.4 mg, 24.1 %.

1H NMR (500 MHz, C_6D_6) δ 7.15 (s, 4H, ArH), 6.63 (d, $J = 2.2$ Hz, 2H, XA-*p*-CH), 6.25 (d, $J = 2.2$ Hz, 2H, XA-*o*-CH), 2.65 (m, 6H, CyH), 2.09 – 2.02 (m, 13H, CyH_2), 1.92 – 1.87 (m, 6H, CyH_2), 1.85 (s, 6H, $C(CH_3)_2$), 1.83 – 1.76 (m, 8H, CyH_2), 1.75 – 1.61 (m, 16H, CyH_2), 1.61 – 1.50 (m, 6H, CyH_2), 1.49 – 1.37 (m, 11H, CyH_2), 1.33 (s, 18H, $C(CH_3)_3$).

^{13}C $\{^1\text{H}\}$ NMR (126 MHz, C_6D_6) δ 152.3, 149.5, 146.9, 140.1, 137.3, 133.2, 129.0, 128.3, 128.3 (*Ar*), 122.4 (*ArH*), 111.5 (*XA-p-CH*), 100.2 (*XA-o-CH*), 45.0, 39.8 (*CyH*), 35.8, 35.5, 35.0, 34.8, 34.6 ($\text{C}(\text{CH}_3)_2$, $\text{C}(\text{CH}_3)_3$, CyCH_2), 31.8 $\text{C}(\text{CH}_3)_3$, 31.7, 28.3, 27.9, 27.4, 26.4, 14.0 ($\text{C}(\text{CH}_3)_2$, $\text{C}(\text{CH}_3)_3$, CyCH_2).

5.3.6 Preparation of $(\text{xNON}^{\text{TCHP}})\text{InK}(\text{Tol})$, 47

A solution of $(\text{xNON}^{\text{TCHP}})\text{K}_2$ (500 mg, 0.47 mmol) in THF was added to InI (114 mg, 0.47 mmol) in the dark and stirred for 48 hours under nitrogen at room temperature. The solution was filtered through celite, and the solvent was removed *in vacuo* and the residue was extracted with toluene. The solution was filtered again through celite, concentrated, and left to crystallise at room temperature, giving bright yellow crystals suitable for an X-ray diffraction experiment. Yield 375.6 mg, 63.0%.

^1H NMR (500 MHz, C_6D_6) δ 7.22 (s, 4H, *ArH*), 6.72 (d, $J = 2.1$ Hz, 2H, *XA-p-CH*), 6.30 (d, $J = 2.1$ Hz, 2H, *XA-o-CH*), 3.56 – 3.51 (m, 3H, *CyH*), 2.56 (tt, $J = 11.9$, 3.3 Hz, 3H, *CyH*), 2.00 (d, 9H, CyH_2), 1.93 – 1.86 (m, 6H, CyH_2), 1.85 (s, 6H, $\text{C}(\text{CH}_3)_2$), 1.78 (td, $J = 12.6$, 6.2 Hz, 11H, CyH_2), 1.71 – 1.62 (m, 13H, CyH_2), 1.61 – 1.50 (m, 11H, CyH_2), 1.30 (s, 18H, $\text{C}(\text{CH}_3)_3$), 1.26 – 1.21 (m, 10H, CyH_2).

$^{13}\text{C}\{^1\text{H}\}$ NMR (126 MHz, C_6D_6) δ 147.8, 147.0, 146.0, 143.9, 141.2, 137.9, 129.3, 128.3, 128.6, 125.7(*ArH*), 111.5 (*XA-p-CH*), 103.1 (*XA-o-CH*), 67.83(*p-CyH*), 45.05 (*o-CyH*), 40.74, 36.72, 35.48, 35.28, 35.00 (CyH_2), 32.04 ($\text{C}(\text{CH}_3)_3$), 31.96, 28.27, 28.00 (CyH_2), 27.55 ($\text{C}(\text{CH}_3)_2$), 26.82, 26.75, 25.79, 23.05, 21.42, 14.35 ($\text{C}(\text{CH}_3)_2$, $\text{C}(\text{CH}_3)_3$, CyCH_2), (CyH_2).

5.3.7 Preparation of $(\text{xNON}^{\text{TCHP}})\text{K}(\text{18-c-6})\text{K}$, 48

A solution of $(\text{xNON}^{\text{TCHP}})\text{InK}(\text{Et}_2\text{O})_2(\text{THF})_2$ (62.6 mg, 0.050 mmol) in C_6D_6 was added to 18-crown-6 (13.2 mg, 0.050 mmol) under nitrogen at room temperature. The solution was heated at 60°C for 5 minutes before crystallisation began in the *J Youngs* NMR tube, giving light yellow/green crystals suitable for an X-ray diffraction experiment. Yield 47.1 mg, 70.6 %.

^1H NMR (500 MHz, C_6D_6) δ 7.29 (s, 4H, *ArH*), 6.21 (d, $J = 2.4$ Hz, 2H, *XA-p-CH*), 6.06 (d, $J = 2.4$ Hz, 2H, *XA-o-CH*), 3.45 (tt, $J = 11.9$, 3.3 Hz, 4H, *p-CyH*) 3.20 (s, 24H, (*18-c-6(H)*)), 2.70 (tt, $J = 11.9$, 3.4 Hz, 2H, *o-CyH*), 2.27 (d, $J = 12.0$ Hz, 4H, CyH_2), 2.18 (d, $J = 12.8$ Hz, 4H, CyH_2), 2.06 (d, $J = 11.4$ Hz, 6H, CyH_2), 1.97 (s, 6H, $\text{C}(\text{CH}_3)_2$), 1.85 – 1.69 (m, 21H, CyH_2), 1.55 – 1.43 (m, 4H, CyH_2), 1.39 (s, 18H, $\text{C}(\text{CH}_3)_3$).

^{13}C $\{^1\text{H}\}$ NMR (126 MHz, C_6D_6) δ 152.64, 150.04, 143.58, 140.55, 139.79, 137.89, 129.33, 125.70 (*Ar*), 122.59 (*ArC*), 106.10 (*XA-p-CH*), 98.20 (*XA-o-CH*), 45.56 (*o-CyC*), 39.9 (*18-c-6*), 38.70 (*p-CyC*), 36.11, 35.99, 35.61, 35.59, 35.12, 34.99, 34.61 ($\text{C}(\text{CH}_3)_2$, $\text{C}(\text{CH}_3)_3$, CyCH_2), 33.78 $\text{C}(\text{CH}_3)_2$, 32.58 ($\text{C}(\text{CH}_3)_3$), 31.67, 28.62, 28.21, 27.89, 27.52, 27.39, 21.43 ($\text{C}(\text{CH}_3)_2$, $\text{C}(\text{CH}_3)_3$, CyCH_2).

5.3.8 Preparation of $(\text{xNON}^{\text{TCHP}})\text{InI}_2(18\text{-c-6})\text{K}$, 49

A solution of $(\text{xNON}^{\text{TCHP}})\text{InK}(\text{Et}_2\text{O})_2(\text{THF})_2$ (43.7 mg, 0.031 mmol) in C_6D_6 was added to 18-crown-6 (8.8 mg, 0.033 mmol) under nitrogen at room temperature. The solution was heated at 60°C for 5 minutes before crystallisation began in the *J Youngs* NMR tube, giving light yellow/green crystals suitable for an X-ray diffraction experiment. Yield 13.4 mg, 25.8 %.

^1H NMR (500 MHz, C_6D_6) δ 7.29 (s, 4H, *Ar-H*), 6.71 (d, $J = 2.1$ Hz, 2H, *XA-p-CH*), 6.40 (d, $J = 2.0$ Hz, 2H, *XA-o-CH*), 3.68 (tt, $J = 11.7, 3.3$ Hz, 4H, *Cy-H*), 3.05 (s, 24H, (*18-c-6-H*)), 2.62 – 2.59 (m, 2H, *Cy-H*), 2.57 (d, $J = 3.5$ Hz, 4H, *Cy-H*₂), 2.24 (d, $J = 12.4$ Hz, 4H, *Cy-H*₂), 2.06 (d, $J = 12.9$ Hz, 4H, *Cy-H*₂), 1.93 (dt, $J = 12.9, 3.4$ Hz, 4H, *Cy-H*₂), 1.87 (dt, $J = 13.0, 3.2$ Hz, 5H, *Cy-H*₂), 1.82 – 1.74 (m, 9H, *Cy-H*₂), 1.72 (s, 6H, *CH*₃), 1.62 (qd, $J = 13.1, 3.3$ Hz, 6H, *Cy-H*₂), 1.50 (ddd, $J = 21.6, 11.1, 3.1$ Hz, 8H, *Cy-H*₂), 1.45 – 1.41 (m, 4H, *Cy-H*₂), 1.41 – 1.37 (m, 5H, *Cy-H*₂), 1.36 (s, 18H, $\text{CH}(\text{CH}_3)_3$), 1.34 – 1.25 (m, 7H, *Cy-H*₂), 1.23 (s, 4H, *Cy-H*₂).

$^{13}\text{C}\{^1\text{H}\}$ NMR (126 MHz, C_6D_6) δ 147.8, 145.5, 144.2, 143.2, 142.7, 139.0, 132.6 (*Ar*), 122.9 (*ArC*), 111.7 (*XA-p-CH*), 104.7 (*XA-o-CH*), 69.6 (*18-c-6*), 65.6 (*Cy*), 44.8 (*o-CyH*), 38.3 (*o-CyH*), 37.3, 36.7, 35.2, 34.7, 34.3 ($\text{C}(\text{CH}_3)_2$, $\text{C}(\text{CH}_3)_3$, CyCH_2), 31.7 ($\text{C}(\text{CH}_3)_3$), 27.4 ($\text{C}(\text{CH}_3)_2$, 27.0, 26.9, 26.9, 26.5, 22.8, 15.3, 14.1 ($\text{C}(\text{CH}_3)_2$, $\text{C}(\text{CH}_3)_3$, CyCH_2).

5.3.9 Preparation of $(\text{xNON}^{\text{TCHP}})\text{In}(18\text{-c-6})\text{K}$, 50

A solution of $[(\text{xNON}^{\text{TCHP}})\text{InI}_2][(18\text{-c-6})\text{K}]$ (13.4 mg, 0.008 mmol) in C_6D_6 was added to excess potassium metal and stirred for 48 hours under nitrogen at room temperature. The solution was filtered through celite, and washed with hexane, then reduced and left to crystallise at room temperature, giving bright yellow crystals suitable for an X-ray diffraction experiment. Yield 11.2 mg, 98.2 %.

^1H NMR (500 MHz, C_6D_6) δ 7.24 (s, 4H, *ArH*), 6.53 (d, $J = 2.2$ Hz, 2H, *XA-p-CH*), 6.09 (d, $J = 2.2$ Hz, 2H, *XA-o-CH*), 3.64 – 3.55 (m, 4H, *o-CyH*), 3.02 (s, 24H, (*18-c-6-H*)), 2.62 – 2.56 (m, 2H, *p-CyH*), 2.22 (dd, $J = 23.7, 12.2$ Hz, 8H, *CyH*₂), 2.07 (d, $J = 12.6$ Hz, 5H, *CyH*₂),

1.98 (d, $J = 14.8$ Hz, 4H, CyH_2), 1.87 (s, 6H, $\text{C}(\text{CH}_3)_2$), 1.82 (s, 6H, CyH_2), 1.76 (s, 4H, CyH_2), 1.74 (d, $J = 7.6$ Hz, 8H, CyH_2), 1.71 (s, 4H, CyH_2), 1.66 – 1.62 (m, 8H, CyH_2), 1.45 (dt, $J = 9.1, 3.5$ Hz, 13H, CyH_2), 1.41 (s, 4H, $\text{C}(\text{CH}_3)_3$).

^{13}C $\{^1\text{H}\}$ NMR (126 MHz, C_6D_6) δ 146.44, 145.23, 144.48, 139.32, 129.14 (ArC), 122.02 (TCHP–ArC), 107.23 (XA–*o*–CH), 101.24 (XA–*p*–CH), 69.80 ((18–*c*–6)C), 45.01 (*p*–CyC), 39.10 (*o*–CyC), 37.22, 35.63 ($\text{C}(\text{CH}_3)_2$), 35.32, 34.71 CyCH_2 , 32.22 ($\text{C}(\text{CH}_3)_3$), 31.72, 27.64, 27.25, 22.78, 15.30, 13.99 ($\text{C}(\text{CH}_3)_2$, $\text{C}(\text{CH}_3)_3$, CyCH_2).

5.3.10 Preparation of $[(\text{xNON}^{\text{TCHP}})\text{InCl}_2\text{K}]_2$, 52

A solution of $(\text{xNON}^{\text{TCHP}})\text{InK}(\text{Et}_2\text{O})_2(\text{THF})_2$ (114.4 mg, 0.087 mmol) in diethyl ether was added to SnCl_2 (16.6 mg, 0.087 mmol) and stirred for 24 hours under nitrogen at room temperature. The solution was filtered through celite, and reduced and left to crystallise at room temperature, giving pale orange crystals suitable for an X-ray diffraction experiment.

Due to the extreme insolubility in both coordinating and non-coordinating solvents at either room temperature or elevated temperatures we were unable to record solution state data for this compound.

5.3.11 Preparation of $(\text{xNON}^{\text{TCHP}})\text{InCl}_2\text{K}(\text{THF})_4$, 53

Dried crystals of $[(\text{xNON}^{\text{TCHP}})\text{InCl}_2\text{K}]_2$ was extracted into a 1:1 ratio of THF and toluene. The solution reduced and left to crystallise at room temperature, giving colourless crystals suitable for an X-ray diffraction experiment.

Due to the extreme insolubility in both coordinating and non-coordinating solvents at either room temperature or elevated temperatures we were unable to record solution state data for this compound.

5.3.12 Preparation of $(\text{xNON}^{\text{TCHP}})\text{InI}(\text{DMP-NC})$, 55

A solution of $(\text{xNON}^{\text{TCHP}})\text{InK}(\text{Et}_2\text{O})_2(\text{THF})_2$ (57.0 mg, 0.04 mmol) in C_6D_6 was added to 2,6-dimethyl phenyl isocyanide (5.8 mg, 0.04 mmol). The solution was filtered through celite, and washed with benzene, then dried and crystallised at room temperature in diethyl ether, giving light yellow crystals suitable for an X-ray diffraction experiment. Yield 25.4 mg, 40.9 %.

^1H NMR (500 MHz, C_6D_6) δ 7.25 (s, 4H, TCHP-ArH), 6.79 (d, $J = 2.0$ Hz, 2H, XA-*p*-CH), 6.61 (d, $J = 8.2$ Hz, 1H, Phen-*p*-CH), 6.55 (d, $J = 2.0$ Hz, 2H, XA-*o*-CH), 6.42 (d, $J = 7.7$ Hz, 2H, Phen-*m*-CH), 3.40 – 3.35 (m, 4H, *o*-CyH), 2.55 – 2.47 (m, 2H, *p*-CyH), 2.06 (d, $J = 13.5$ Hz, 5H, CyH₂), 1.96 (s, 6H, Phen-CH₃), 1.92 (s, 1H, CyH₂), 1.74 (s, 6H, C(CH₃)₂), 1.73 – 1.63 (m, 22H, CyH₂), 1.57 – 1.42 (m, 20H, CyH₂), 1.39 – 1.30 (m, 10H, CyH₂), 1.26 (s, 18H, C(CH₃)₃).

^{13}C { ^1H } NMR (126 MHz, C_6D_6) δ 147.26, 146.55, 144.72, 143.98, 141.84, 139.79, 136.99, 134.88, 133.73 (ArC), 130.53 (Phen-*p*-CH), 129.36 (ArC), 129.34 (Phen-*m*-CH), 123.59 (TCHP-ArH), 123.33 (ArC), 112.69 (XA-*o*-CH), 111.86, 108.56 (ArC), 106.61 (XA-*p*-CH), 65.92 ($\text{C}\equiv\text{N}$), 44.98 (*p*-CyH), 39.35 (*o*-CyH), 37.10, 35.02, 34.62 (C(CH₃)₃, CyCH₂), 31.78 C(CH₃)₃, 27.77 C(CH₃)₂, 27.46, 27.39, 27.36, (C(CH₃)₃, CyCH₂), 18.70 (CH₃), 14.35 (C(CH₃)₂).

References

- (1) L  gar  , M.-A.; Pranckevicius, C.; Braunschweig, H. *Chem. Rev* **2019**, *119* (14), 8231-8261.
- (2) Woods, W. G. An introduction to boron: history, sources, uses, and chemistry. *Environ Health Perspect* **1994**, *102 Suppl 7* (Suppl 7), 5-11.
- (3) Frank, W. B.; Haupin, W. E.; Vogt, H.; Bruno, M.; Thonstad, J.; Dawless, R. K.; Kvande, H.; Taiwo, O. A. Aluminium. *Ullmann's Encycl. Ind. Chem.* Wiley. 2000
- (4) Dill, H. G. *Earth-Sci. Rev* **2001**, *53* (1), 35-93.
- (5) Wilmot, R. D.; Young, B. *Proc. Geol. Assoc.* **1985**, *96* (1), 47-52.
- (6) Bag, P.; Porzelt, A.; Altmann, P. J.; Inoue, S. *J. Am. Chem. Soc.* **2017**, *139* (41), 14384-14387.
- (7) Ni, C.; Ma, X.; Yang, Z.; Roesky, H. W. *Eur. J. Inorg. Chem.* **2022**, *2022* (10).
- (8) Exley, C. *Coord. Chem. Rev.* **2012**, *256* (19), 2142-2146.
- (9) Barron, A. R. Chemistry of the Main Group Elements. **2020**.
- (10) Tolcin, A. C. **2011**.
- (11) Galv  n-Arzate, S.; Santamar  a, A. *Toxicol Lett.* **1998**, *99* (1), 1-13.
- (12) Cvjetko, P.; Cvjetko, I.; Pavlica, M. *Arhiv za higijenu rada i toksikologiju.* **2010**, *61* (1), 111-118.
- (13) Hammond, C. The elements. *Handb. Chem. Phys.* **2000**, *81*.
- (14) Schwerdtfeger, P.; Heath, G. A.; Dolg, M.; Bennett, M. *J. Am. Chem. Soc.* **1992**, *114* (19), 7518-7527.
- (15) Atwood, D. A. *Coord. Chem. Rev.* **1998**, *176* (1), 407-430.
- (16) Oganov, A. R.; Solozhenko, V. L. *J. Superhard Mater.* **2009**, *31* (5), 285-291.
- (17) Bola  os, L.; Lukaszewski, K.; Bonilla, I.; Blevins, D. *Plant Physiol. Biochem.* **2004**, *42* (11), 907-912.
- (18) Zhang, Z.; Penev, E. S.; Yakobson, B. I. *Chem. Soc. Rev.* **2017**, *46* (22), 6746-6763.
- (19) Wade, K.; Banister, A. J. **2016**.
- (20) Drago, R. S. *J. Phys. Chem.* **1958**, *62* (3), 353-357.
- (21) Timoshkin, A. Y.; Frenking, G. *J. Am. Chem. Soc.* **2002**, *124* (24), 7240-7248.
- (22) Frenking, G.; Fr  hlich, N. *Chem. Rev* **2000**, *100* (2), 717-774.
- (23) Gemel, C.; Steinke, T.; Cokoja, M.; Kemptner, A.; Fischer, Roland A. *Eur. J. Inorg. Chem.* **2004**, *2004* (21), 4161-4176.
- (24) Macdonald, C. L. B.; Ellis, B. D.; Swidan, A. a. Low-Oxidation-State Main Group Compounds Update based on the original article by Charles L. B. Macdonald and Bobby D. Ellis, Encyclopedia of Inorganic Chemistry Second Edition,    2005, John Wiley & Sons, Ltd. *EIBC*. **2005**.
- (25) Schulz, S. *Chem. Eur. J.* **2010**, *16* (22), 6416-6428.
- (26) Dagorne, S.; Atwood, D. A. *Chem. Rev.* **2008**, *108* (10), 4037-4071.
- (27) Ghosh, B.; Phukan, A. K. *Inorg. Chem.* **2022**, *61* (37), 14606-14615.
- (28) Asay, M.; Jones, C.; Driess, M. *Chem. Rev.* **2011**, *111* (2), 354-396.
- (29) Dohmeier, C.; Robl, C.; Tacke, M.; Schn  ckel, H. *Angew. Chem., Int. Ed. Engl.* **1991**, *30* (5), 564-565.
- (30) Loos, D.; Baum, E.; Ecker, A.; Schn  ckel, H.; *Angew. Chem., Int. Ed. Engl.* **1997**, *36* (8), 860-862.
- (31) Beachley, O. T.; Churchill, M. R.; Fettingner, J. C.; Pazik, J. C.; Victoriano, L. *J. Am. Chem. Soc.* **1986**, *108* (15), 4666-4668.
- (32) Queen, J. D.; Lehmann, A.; Fettingner, J. C.; Tuononen, H. M.; Power, P. P. *J. Am. Chem. Soc.* **2020**, *142* (49), 20554-20559.

- (33) Zhu, Z.; Fischer, R. C.; Ellis, B. D.; Rivard, E.; Merrill, W. A.; Olmstead, M. M.; Power, P. P.; Guo, J. D.; Nagase, S.; Pu, L. *Chem. Eur. J.* **2009**, *15* (21), 5263-5272.
- (34) Hill, M. S.; Hitchcock, P. B.; Pongtavornpinyo, R. *Dalton Transactions* **2005**, (2), 273-277.
- (35) Cui, C.; Roesky, H. W.; Schmidt, H.-G.; Noltemeyer, M.; Hao, H.; Cimpoesu, F. *Angew. Chem. Int. Ed.* **2000**, *39* (23), 4274-4276.
- (36) Knabel, K.; Krossing, I.; Nöth, H.; Schwenk-Kircher, H.; Schmidt-Amelunxen, M.; Seifert, T. *Eur. J. Inorg. Chem.* **1998**, 1998 (8), 1095-1114.
- (37) Arduengo, A. J., III; Harlow, R. L.; Kline, M. *J. Am. Chem. Soc.* **1991**, *113* (1), 361-363.
- (38) Liu, Y.; Li, J.; Ma, X.; Yang, Z.; Roesky, H. W. *Coord. Chem. Rev.* **2018**, *374*, 387-415.
- (39) Hardman, N. J.; Eichler, B. E.; Power, P. P. *Chem comm.* **2000**, (20), 1991-1992.
- (40) Bollermann, T.; Cadenbach, T.; Gemel, C.; Freitag, K.; Molon, M.; Gwildies, V.; Fischer, R. A. *Inorg. Chem.* **2011**, *50* (12), 5808-5814.
- (41) Hardman, N. J.; Cui, C.; Roesky, H. W.; Fink, W. H.; Power, P. P. *Angew. Chem. Int. Ed.* **2001**, *40* (11), 2172-2174.
- (42) Adamczyk, T.; Li, G.-M.; Linti, G.; Pritzkow, H.; Seifert, A.; Zessin, T. *Eur. J. Inorg. Chem.* **2011** (23), 3480-3492.
- (43) Hill, M. S.; Hitchcock, P. B. *Chem comm.* **2004**, (16), 1818-1819.
- (44) Hopkinson, M. N.; Richter, C.; Schedler, M.; Glorius, F. *Nature* **2014**, *510* (7506), 485-496.
- (45) Jahnke, M. C.; Hahn, F. E. CHAPTER 1 Introduction to N-Heterocyclic Carbenes: Synthesis and Stereoelectronic Parameters. *The Royal Society of Chemistry*. **2017**; pp 1-45.
- (46) Huynh, H. V. *Chem. Rev* **2018**, *118* (19), 9457-9492.
- (47) Bourissou, D.; Guerret, O.; Gabbai, F. P.; Bertrand, G. *Chem. Rev* **2000**, *100* (1), 39-92.
- (48) de Frémont, P.; Marion, N.; Nolan, S. P. *Coord. Chem. Rev.* **2009**, *253* (7), 862-892.
- (49) De Sarkar, S.; Studer, A. *Org. Lett.* **2010**, *12* (9), 1992-1995.
- (50) Heinemann, C.; Müller, T.; Apeloig, Y.; Schwarz, H. *J. Am. Chem. Soc.* **1996**, *118* (8), 2023-2038.
- (51) Jacobsen, H.; Correa, A.; Poater, A.; Costabile, C.; Cavallo, L. *Coord. Chem. Rev.* **2009**, *253* (5), 687-703.
- (52) Crudden, C. M.; Allen, D. P. *Coord. Chem. Rev.* **2004**, *248* (21), 2247-2273.
- (53) Melaimi, M.; Soleilhavoup, M.; Bertrand, G. *Angew. Chem. Int. Ed.* **2010**, *49* (47), 8810-8849.
- (54) Hameury, S.; de Frémont, P.; Braunstein, P. *Chem. Soc. Rev.* **2017**, *46* (3), 632-733.
- (55) Yadav, S.; Deka, R.; Singh, H. B. *Chem. Lett.* **2019**, *48* (2), 65-79.
- (56) Schulz, S., D. M. P., Crabtree, R. H. Eds.; Elsevier, *COMC-III*. 2007; pp 287-342.
- (57) Schmidt, E. S.; Jockisch, A.; Schmidbaur, H. *J. Am. Chem. Soc.* **1999**, *121* (41), 9758-9759.
- (58) Sundermann, A.; Reiher, M.; Schoeller, W. W. *Eur. J. Inorg. Chem.* **1998**, 1998 (3), 305-310.
- (59) Qin, B.; Schneider, U. *J. Am. Chem. Soc.* **2016**, *138* (40), 13119-13122.
- (60) Weetman, C. *EIBC*. **2021**, pp 1-27.
- (61) Weber, L.; Domke, I.; Greschner, W.; Miqueu, K.; Chrostowska, A.; Baylère, P. *Organometallics* **2005**, *24* (22), 5455-5463.
- (62) Segawa, Y.; Yamashita, M.; Nozaki, K. *Science* **2006**, *314* (5796), 113-115.
- (63) Metzler-Nolte, N. *New J Chem* **1998**, *22* (8), 793-795.

- (64) Segawa, Y.; Suzuki, Y.; Yamashita, M.; Nozaki, K. *J. Am. Chem. Soc.* **2008**, *130* (47), 16069-16079.
- (65) Dettenrieder, N.; Schädle, C.; Maichle-Mössmer, C.; Anwander, R. *Dalton Transactions* **2014**, *43* (42), 15760-15770.
- (66) Schwamm, R. J.; Anker, M. D.; Lein, M.; Coles, M. P.; Fitchett, C. M. *Angew. Chem. Int. Ed.* **2018**, *57* (20), 5885-5887.
- (67) Anker, M. D.; Lein, M.; Coles, M. P. *Chem. Sci.* **2019**, *10* (4), 1212-1218.
- (68) Anker, M. D.; Altaf, Y.; Lein, M.; Coles, M. P. *Dalton Transactions* **2019**, *48* (44), 16588-16594.
- (69) Pyykkö, P.; Atsumi, M. *Chem. Eur. J.* **2009**, *15* (1), 186-197.
- (70) Yamamoto, H.; Oshima, K. *Main group metals in organic synthesis*; John Wiley & Sons, **2006**.
- (71) Hill, M. S. *The Lightest Metals: Science and Technology from Lithium to Calcium* **2015**, 409.
- (72) Hicks, J.; Vasko, P.; Goicoechea, J. M.; Aldridge, S. *Nature* **2018**, *557* (7703), 92-95.
- (73) Weetman, C. Low valent main group compounds in small molecule activation. *EIBC* **2021**.
- (74) Cordero, B.; Gómez, V.; Platero-Prats, A. E.; Revés, M.; Echeverría, J.; Cremades, E.; Barragán, F.; Alvarez, S. *Dalton Transactions* **2008**, (21), 2832-2838.
- (75) Schwamm, R. J.; Anker, M. D.; Lein, M.; Coles, M. P. *Angew. Chem. Int. Ed.* **2019**, *58* (5), 1489-1493.
- (76) Uhl, W. **2004**, *51*, 53-108.
- (77) Roy, K.; Kar, S.; Das, R. N. Understanding the Basics of QSAR for Applications in Pharmaceutical Sciences and Risk Assessment. *AP.* **2015**, pp 1-46.
- (78) Kurumada, S.; Takamori, S.; Yamashita, M. **2020**, *12* (1), 36-39.
- (79) Schwamm, R. J.; Hill, M. S.; Liu, H.-Y.; Mahon, M. F.; McMullin, C. L.; Rajabi, N. A. *Chem. Eur. J.* **2021**, *27* (60), 14971-14980.
- (80) Koshino, K.; Kinjo, R. *J. Am. Chem. Soc.* **2020**, *142* (19), 9057-9062.
- (81) Hicks, J.; Vasko, P.; Goicoechea, J. M.; Aldridge, S. *J. Am. Chem. Soc.* **2019**, *141* (28), 11000-11003.
- (82) Bakewell, C.; Ward, B. J.; White, A. J. P.; Crimmin, M. R. *Chem. Sci.* **2018**, *9* (8), 2348-2356.
- (83) Anker, M. D.; Coles, M. P. *Angew. Chem. Int. Ed.* **2019**, *58* (38), 13452-13455.
- (84) Schwamm, R. J.; Coles, M. P.; Hill, M. S.; Mahon, M. F.; McMullin, C. L.; Rajabi, N. A.; Wilson, A. S. S. *Angew. Chem. Int. Ed.* **2020**, *59* (10), 3928-3932.
- (85) Hicks, J.; Mansikkamäki, A.; Vasko, P.; Goicoechea, J. M.; Aldridge, S. *Nat. Chem.* **2019**, *11* (3), 237-241.
- (86) Sugita, K.; Yamashita, M. *Chem. Eur. J.* **2020**, *26* (20), 4520-4523.
- (87) Sugita, K.; Nakano, R.; Yamashita, M. *Chem. Eur. J.* **2020**, *26* (10), 2174-2177.
- (88) Heilmann, A.; Hicks, J.; Vasko, P.; Goicoechea, J. M.; Aldridge, S. *Angew. Chem. Int. Ed.* **2020**, *59* (12), 4897-4901.
- (89) Anker, M. D.; McMullin, C. L.; Rajabi, N. A.; Coles, M. P. *Angew. Chem. Int. Ed.* **2020**, *59* (31), 12806-12810.
- (90) Hicks, J.; Heilmann, A.; Vasko, P.; Goicoechea, J. M.; Aldridge, S. *Angew. Chem. Int. Ed.* **2019**, *58* (48), 17265-17268.
- (91) Anker, M. D.; Coles, M. P. *Angew. Chem. Int. Ed.* **2019**, *58* (50), 18261-18265.
- (92) Anker, M. D.; Schwamm, R. J.; Coles, M. P. *Chem comm.* **2020**, *56* (15), 2288-2291.
- (93) Savka, R.; Plenio, H. *Eur. J. Inorg. Chem.* **2014**, *2014* (36), 6246-6253.
- (94) Cruz, C. A.; Emslie, D. J. H.; Harrington, L. E.; Britten, J. F.; Robertson, C. M. *Organometallics*. **2007**, *26* (3), 692-701.

- (95) Rahm, M.; Hoffmann, R.; Ashcroft, N. W. *Chem. Eur. J.* **2016**, 22 (41), 14625-14632.
- (96) Hicks, J.; Vasko, P.; Heilmann, A.; Goicoechea, J. M.; Aldridge, S. *Angew Chem Int Ed Engl.* **2020**, 59 (46), 20376-20380.
- (97) Grams, S.; Mai, J.; Langer, J.; Harder, S. *Dalton Transactions.* **2022**, 51 (33), 12476-12483.
- (98) Evans, M. J.; Anker, M. D.; Gardiner, M. G.; McMullin, C. L.; Coles, M. P. *Inorg. Chem.* **2021**, 60 (23), 18423-18431.
- (99) Evans, M. J.; Anker, M. D.; McMullin, C. L.; Neale, S. E.; Coles, M. P. *Angew. Chem. Int. Ed.* **2021**, 60 (41), 22289-22292.
- (100) Yan, C.; Kinjo, R. *Angew. Chem. Int. Ed.* **2022**, 61 (42).
- (101) Gentner, T. X.; Evans, M. J.; Kennedy, A. R.; Neale, S. E.; McMullin, C. L.; Coles, M. P.; Mulvey, R. E. *Chem comm.* **2022**, 58 (9), 1390-1393.
- (102) Buschmann, H.-J. **1992**, 195 (1), 51-60.
- (103) Evans, M. J.; Anker, M. D.; Gardiner, M. G.; McMullin, C. L.; Coles, M. P. *Inorg. Chem.* **2021**, 60 (23), 18423-18431.
- (104) Heyden, Y. V.; Mangelings, D.; Matthijs, N.; Perrin, C. *Separation Science and Technology*, Ahuja, S., Dong, M. W. Eds.; Vol. 6; *AP*, **2005**; pp 447-498.
- (105) Menon, S. K.; Hirpara, S. V.; Harikrishnan, U. *Rev. Anal. Chem.* **2004**, 23 (4), 233-268.
- (106) Endicott, C.; Strauss, H. L. *J. Phys. Chem. A* **2007**, 111 (7), 1236-1244.
- (107) Bradshaw, J. S.; Izatt, R. M. *Acc. Chem. Res.* **1997**, 30 (8), 338-345.
- (108) Liou, C.-C.; Brodbelt, J. S. *JASMS.* **1992**, 3 (5), 543-548.
- (109) Stern, K. H.; Amis, E. S. Ionic size. *Chem. Rev* **1959**, 59 (1), 1-64.
- (110) Evans, M. J.; Anker, M. D.; McMullin, C. L.; Coles, M. P. *Chem Sci.* **2023**, 14 (23), 6278-6288.
- (111) Chen, W.; Zhao, Y.; Xu, W.; Su, J.-H.; Shen, L.; Liu, L.; Wu, B.; Yang, X.-J. *Chem comm.* **2019**, 55 (64), 9452-9455.
- (112) Mukhopadhyay, S.; Patro, A. G.; Vadavi, R. S.; Nembenna, S. *Eur. J. Inorg. Chem.* **2022**, 2022 (31).
- (113) Evans, M. J.; Anker, M. D.; McMullin, C. L.; Coles, M. P. *Chem. Sci.* **2023**, 14 (23), 6278-6288.
- (114) Brockway, L. *J. Am. Chem. Soc.* **1936**, 58 (12), 2516-2518.
- (115) Brinson, R. G. *Molecules* **2021**, 26 (23).
- (116) Singh, M. K.; Singh, A. *Characterization of Polymers and Fibres*, Singh, M. K., Singh, A. Eds.; Woodhead Publishing, **2022**; pp 321-339.
- (117) Patching, S. G. *J. Diagn. Imaging Ther.* **2016**, 3, 7-48.
- (118) Massa, W. *Springer.* **2004**.
- (119) Bashir, S.; Liu, J. In *Advanced Nanomaterials and their Applications in Renewable Energy*. Elsevier, **2015**; pp 117-180.